INFORMATION TO USERS

This manuscript has been reproduced from the microfilm master. UMI films the text directly from the original or copy submitted. Thus, some thesis and dissertation copies are in typewriter face, while others may be from any type of computer printer.

The quality of this reproduction is dependent upon the quality of the copy submitted. Broken or indistinct print, colored or poor quality illustrations and photographs, print bleedthrough, substandard margins, and improper alignment can adversely affect reproduction.

In the unlikely event that the author did not send UMI a complete manuscript and there are missing pages, these will be noted. Also, if unauthorized copyright material had to be removed, a note will indicate the deletion.

Oversize materials (e.g., maps, drawings, charts) are reproduced by sectioning the original, beginning at the upper left-hand corner and continuing from left to right in equal sections with small overlaps.

Photographs included in the original manuscript have been reproduced xerographically in this copy. Higher quality 6" x 9" black and white photographic prints are available for any photographs or illustrations appearing in this copy for an additional charge. Contact UMI directly to order.

ProQuest Information and Learning
300 North Zeeb Road, Ann Arbor, MI 48106-1346 USA
800-521-0600

SPECIATION AND SORPTION MECHANISMS OF METALS IN SOILS USING BULK AND MICRO-FOCUSED SPECTROSCOPIC AND MICROSCOPIC TECHNIQUES

by

Darryl R. Roberts

A dissertation submitted to the Faculty of the University of Delaware in partial fulfillment of the requirements for the degree of Doctor of Philosophy in Plant and Soil Sciences

Summer 2001

SPECIATION AND SORPTION MECHANISMS OF METALS IN SOILS USING BULK AND MICRO-FOCUSSED SPECTROSCOPIC AND MICROSOPIC TECHNIQUES

by

Darryl R. Roberts

Approved: Donald L. Sparks

Donald L. Sparks, Ph.D.
Chair of the Department of Plant and Soil Sciences

Approved: Robin W. Morgan

Robin W. Morgan, Ph.D.
Acting Dean of the College of Agriculture and Natural Resources

Approved:

Conrado M. Gempesaw II, Ph.D.
Vice Provost for Academic Programs and Planning

I certify that I have read this dissertation and that in my opinion it meets the academic and professional standard required by the University as a dissertation for the degree of Doctor of Philosophy.

Signed: _____

Donald L. Sparks, Ph.D.
Professor in charge of dissertation

I certify that I have read this dissertation and that in my opinion it meets the academic and professional standard required by the University as a dissertation for the degree of Doctor of Philosophy.

Signed: _____

Herbert E. Allen, Ph.D.
Member of dissertation committee

I certify that I have read this dissertation and that in my opinion it meets the academic and professional standard required by the University as a dissertation for the degree of Doctor of Philosophy.

Signed: _____

Steven K. Dentel, Ph.D.
Member of dissertation committee

I certify that I have read this dissertation and that in my opinion it meets the academic and professional standard required by the University as a dissertation for the degree of Doctor of Philosophy.

Signed: _____

Yan Jin, Ph.D.
Member of dissertation committee

ACKNOWLEDGMENTS

While at the University of Delaware several people made my journey extremely interesting and rewarding. First and foremost I wish to thank Dr. Donald L. Sparks for giving me the opportunity to do this research and for providing me with a positive and fruitful academic environment. Thanks to "Uncle" Jerry Hendricks for his support, late nights at the beamlines and for his friendship. Thanks to Drs. Andreas Scheinost, Andre Scheidegger, and Robert Ford for their knowledge, assistance and inspiration during my graduate work. Thanks to the members of the UDel Environmental Soil Chemistry Research group for making the working environment both fun and interesting. Without them my career at the University of Delaware would not be as remarkable. Thanks to the members of my dissertation committee for giving me insights from their own perspective.

Several people have been involved with helping me gather and understand my data. I have taken numerous trips to the National Synchrotron Light Source and the X-11A and X-26a beamline staffs were critical in the data acquisition process. This included Tony Lanzarotti, Kumi Pandya, and Larry Ferraeri. Steve Sutton, Matt Newville and Nancy Lazarus provided an enjoyable experience at Argonne National Lab for collection of micro-EXAFS data. Geraldine Lamble assisted with data acquisition while at Berkeley National Lab. Thanks to Brian McCandless of the IEC and Raol Lobo of the University of Delaware for allowing me to collect XRD data on their instruments. Thanks to Ken Levy at Johns Hopkins University and Giorgio Senesi for assistancewith electron microprobe data collection and interpretation. Thanks to Carolyn Golt and Cathy Olsen and for ICP and AAS analyses.

While at Delaware I met Mary Jane. An amazing twist of fate and icing to an already great life experience. She amazed in here ability to make me smile. have confidence in me. and for reminding me that life is meant to be lived. And last. but certainly not least. a big old heart-felt thank you to all of my family and friends in California. Mom. dad. Scotty. Holly. Kim. Nate and everyone else - I really appreciate your love and unending support.

TABLE OF CONTENTS

LIST OF TABLES

LIST OF FIGURES

ABSTRACT

Due to anthropogenic processes, including metal smelting and refining, land application of biosolids, and other industrial processes, heavy metals are often found in very high concentrations in soils. Elevated levels of heavy metals in soils can cause phytotoxicity and can ultimately result in pronounced environmental degradation. The mobility and ultimate fate of metals in the environment is greatly dependent on reactions occurring at the interface between solid surfaces found in soils soil solutions. Understanding these reactions is of crucial importance for predicting the long term fate of metals in surface and subsurface environments. In this study, metal sorption mechanisms to several solid phases was investigated using an array of analytical techniques so that direct identification of mechanisms could be achieved.

The kinetics and mechanisms of Ni sorption on a Delaware soil and soil clay mineral fraction were monitored using X-ray absorption fine structure (XAFS) spectroscopy. Above a pH value of 6.8, formation of Ni-Al layer double hydroxide (Ni-Al LDH) phases was a major mechanisms for Ni removal from solution. This is one of the first studies to have identified LDH phases in soils. Ni in precipitated LDH phases was more resistant to desorption compared to systems in which no precipitation occurred. Moreover, an increased aging time had a stabilizing effect on Ni-Al LDH phases.

Zinc may also forms Zn-Al LDH phases upon sorption to clay minerals and oxides. To assess this, Zn sorption kinetics and mechanisms on amorphous silica and gibbsite were monitored using XAFS spectroscopy. In the presence of amorphous silica, Zn did not favor precipitate formation and was present mostly as inner-sphere sorption complexes bound to silica tetrahedra in a tetrahderal geometry. Only at

increased values of Zn on the silica surface did evidence of a precipitate phase occur. In the case of high surface area gibbsite, Zn formed inner-sphere sorption complexes to alumina octahedra in a distorted octahedral geometry. In the case of low surface area gibbsite a Zn-Al LDH phase formed at pH 7.5. The results indicate Zn has variable speciation when adsorbed to the two metal oxide phases.

Using the spectroscopic information gleaned for Ni and Zn sorption to laboratory-contaminated systems, direct identification of Zn species in a contaminated soil was investigated. The soils of the Blue Mountain operable unit near the former Zn smelter at Palmerton, PA are devegetated due to elevated levels of heavy metals. In the surface soil XAFS was used to directly identify $ZnFe_2O_4$ (franklinite) and ZnS (sphalerite), mineral phases introduced to the soils as a result of the smelting operations. Results indicated that upon their dissolution, Zn re-mobilized and repartitioned in the subsurface soil, binding to Al, Fe, and Mn oxide minerals. Micro-XAFS was employed to determine the micro-scale heterogeneity in this complicated system. Zn was found to be more bound to Al-bearing minerals relative to Mn and Fe minerals. Zinc was more labile in the subsurface soil where it was found to occur in both outer- and inner- sphere sorption complexes.

Chapter 1

INTRODUCTION

1.1 Research Motivation

Contamination of surface and subsurface environments via anthropogenic inputs has established the need to understand metal-soil interactions. Heavy metals may enter soil and aquatic environments via application of sewage sludge, municipal composts, mine wastes, dredged materials, fly ash, and atmospheric deposits (Förstner, 1995). Of the 1000 superfund sites named in the United States' National Priority List of 1986, 40% were reported to have metal problems (EPA, 1986). The fate and mobility of these metals in soils and sediments is of concern because of potential bioaccumulation, food chain magnification, and human exposure (Hering, 1995). Thus, remediation of contaminated soils and sediments containing excessive amounts of heavy metals is of utmost importance to ensure environmental quality. Before any remediation strategy can be attempted one must first determine and understand the interaction of metal ions with soils and soil constituents.

The multiple sorbents in soils include clay minerals, metal oxides, and organic material. Metals can potentially bind to these sorbents by a number of sorption processes, including adsorption and precipitation. The degree to which metals partition

to these sorbents ultimately controls their fate and bioavailability in the environment. The heterogeneous nature of soils has made it difficult to determine the exact mechanisms by which divalent metals sorb to soil materials and most studies concerned with metal sorption behavior in soils have relied solely on macroscopic approaches. To help alleviate this difficulty numerous metal sorption studies have used single component systems including reference clay minerals, metal oxides and organic materials. When coupled with advanced microscopic and spectroscopic techniques, these single component studies may elucidate metal sorption and desorption reaction mechanisms. However, while metal sorption studies on isolated mineral and oxide phases may help discern sorption mechanisms in these specific cases, it can be difficult to apply these findings to actual soil environments.

One of the major limitations in identifying metal sorption mechanisms in soils has been the lack of sophisticated analytical tools capable of probing the local chemical environment of a specific contaminant (i.e., metal, oxyanion, organic compound). To overcome these limitations several soil-metal sorption studies have relied on indirect approaches. For example, chemical extraction techniques estimate the soil component(s) with which a particular contaminant is partitioned. Another approach has been to model metal sorption data based on 24 hour equilibrium-based studies and make assessments about sorption mechanisms depending on the slope or shape of an isotherm. While these types of studies may be useful to make general comparisons between metal sorption studies, one should not rely on results from these studies to define sorption mechanisms.

The advent of cutting-edge analytical tools and their application to geochemical and earth science studies has enabled researchers to elucidate sorption mechanisms on materials typically found in soil environments. By probing a particular element on the molecular level it is possible to directly identify sorption complexes and gain information on chemical speciation. As previously stated, most studies using advanced molecular-level techniques have investigated systems composed of individual reference sorbents (ie, carbonates, metal oxides, aluminosilicates) and individual sorbates. While such studies are the essential first step in understanding the behavior of contaminants in the soil environment, one is unlikely to find such isolated systems in nature. As techniques evolve and are combined, more complex sorption systems may be studied and predictions about contaminants in subsurface environments may improve.

There remains a need to extend our findings of metal sorption behavior on model mineral and clay systems using advanced analytical techniques to more real-world natural settings. When attempting to undertake such an arduous challenge one should be aware of possible shortcomings of each technique and be prudent in making assessments about metal sorption mechanisms and speciation. Additionally, one should not rely too heavily on one technique as each has their shortcomings in addition to their strengths. The research presented here will attempt to better understand metal ion behavior in soil systems by 1) studying a range of reaction conditions, 2) combining several analytical techniques, and 3) investigating homogeneous systems in addition to heterogeneous ones.

The application of spectroscopic and microscopic tools to study metal sorption studies has prompted some researchers to reevaluate some of the results attained from macroscopic sorption experiments. An example of this is the use of X-ray absorption fine structure (XAFS) spectroscopy to monitor the sorption of heavy metal ions onto clay minerals and metal oxides. It has traditionally been thought that the primary mechanism for metal removal from solution in the presence of soils and soil materials was an adsorption phenomenon, or a two-dimensional accumulation at the mineral surface. The adsorption complex formed can vary from mono- to bidentate or inner- vs. outersphere. Only after long sorption periods (months-years) and with high concentrations of metal ions (i.e., above the solubility limit of the metal-hydroxide phase) was the phenomenon of metal precipitate formation thought to be of much importance. Recent XAFS studies have shown the formation of precipitates during metal sorption to mineral and oxide surfaces over rapid time scales, at pH levels undersaturated with respect to pure metal hydroxide solubility, and at metal surface coverages below a theoretical monolayer coverage (Charlet and Manceau, 1992; Chisholm-Brause et al., 1990; Fendorf et al., 1994a; O'Day et al., 1994a; O'Day et al., 1996; Scheidegger et al., 1996b; Towle et al., 1997; Weesner and Bleam, 1997; Xia et al., 1997). The formation of such precipitates may result in stabilization of metals in soil environments and merits further investigation. These results demonstrate the importance of using advanced analytical techniques to investigate metal sorption behavior in soil environments.

While it has been shown that the formation of metal surface precipitate phases are important in "pure" systems in which individual sorption phases are present, the question still remains as to the likelihood of such phases forming in actual soil environments. Unlike pure mineral/oxide studies of metal sorption under a limited reaction range, soil environments are characterized by a variety of potentially competitive sorption sites (including different inorganic and organic phases), a range of pH and metal concentration values, competing metal ions, a range of ionic strength levels, various anions, variable temperatures, wetting and drying cycles, and long periods in which the contaminant is in contact with sorbents. The complexity of soil has also made it exceedingly difficult to apply many advanced analytical techniques, leading to studies on more model systems. One approach would be to gradually increase the complexity of the sorbent phase so it is more heterogeneous than individual mineral phases, but not too complex as to make it difficult to apply spectroscopic and microscopic tools. In order to achieve this it is necessary to use an array of techniques that may complement each other, ensure that the sorbent phases are thoroughly characterized, couple the molecular-scale studies with macroscopic approaches. While it may be an arduous task to look at a broad array of reaction conditions, solid surfaces, and a range of time scales, it is crucial to undertake this task if one wants to definitively determine the likelihood of metal precipitates forming in complex soil environments.

In addition to using analytical techniques to understand metal sorption behavior in studies, it is also useful to monitor the sorption kinetics to better understand the changes that may occur in the structure of a sorption phase over time. Several studies

have assumed a thermodynamic-based situation in soils whereby it was thought the sorbate phase was in equilibrium with the sorbent after sorption times as short as 24 hours. While this may appear to be true since the majority of the metal is removed from solution in this time. slow sorption processes via various mechanisms may occur and the metal-solid phase that initially formed over short times may change or become more stable over longer times. Considering the length of time metal contaminants may be in contact with sorbent phases in actual soil environments, it is critical to investigate sorption phenomena over long reaction times to more accurately describe the fate and mobility of metals in subsurface environments.

The proposed research will attempt to better understand the conditions that control Ni and Zn sorption reactions in soil environments. specifically the formation of metal precipitates. The approach here will be to combine macroscopic methods with molecular-level investigations. A range of time scales and reaction conditions will be used to help simulate actual soil environments. In addition. the release of Ni and Zn from sorbent phases will be studied to aid in understanding the factors that control their mobility and availability in the environment. By combining analytical techniques and carefully monitoring sorption kinetics it may be possible to understand metal precipitate formation mechanisms in soil environments. This information may be useful to incorporate into models that seek to predict the fate of heavy metals in the surface and subsurface environment.

1.2 Metal Sorption Mechanisms

The removal of metals from soil solutions by inorganic and organic phases is a process by which toxic metals can be sequestered, potentially alleviating deleterious environmental effects. The importance of metal partitioning to soil components (clay minerals, metal oxides, organic material, microorganisms) has lead to numerous studies intent on identifying the processes that control the sequestration of heavy metals (As, Cd, Co, Cu, Ni, Pb, Zn, Cr) by these soil components. The multitude of reactive sites which are found in soils such as organic material, oxides of Al, Fe, and Mn, and silicate mineral edge, planar and interlayer sites, make the study of metal sorption on soils difficult, especially when one tries to determine reaction and sorption mechanisms. The studies performed in the literature on metal sorption range from whole soil studies to individual soil component studies such as metal oxides, phyllosilicates, and organic materials and have investigated a wide variety of reaction conditions (Mattigod et al., 1979; Puls et al., 1991; Spark et al., 1995; Theis and Richter, 1980; Tiller et al., 1984a; Traina and Doner, 1985; Yin et al., 1996).

The mechanism of metal removal from solution onto a solid material is dependent on several factors including the type of metal ion, the sorbent phase, solution pH, ionic strength, metal concentration and the length of the reaction. It is possible that several mechanisms may contribute to the removal of a metal ion from solution concurrently. The broad classification given to the removal of chemical species from solution is termed sorption. Sorption is a general term used when the retention mechanism of a chemical species at a solid interface is unknown (Sparks, 1995a). This

broad classification includes a variety of mechanisms that will be discussed in the following sections. The metal sorption mechanism is dependent on the several parameters listed above and these will be briefly discussed in the subsequent sections. The research review below will discuss the various metal sorption mechanisms possible in soils with an emphasis placed on precipitate formation

1.2.1 Metal Cation Adsorption

Adsorption is defined as the net accumulation of matter at the interface between a solid phase and an aqueous solution phase (Sposito. 1989). This term is limited to the formation of two-dimensional molecular arrangements and does not include the formation of three-dimensional phases or diffusion phenomena (Scheidegger and Sparks. 1996a). There are essentially three mechanisms by which a metal ion can adsorb to a soil surface. These mechanisms include inner-sphere complex formation. outer-sphere complex formation. and a diffuse-ion association whereby the ion does not form a complex with a surface functional group (Sposito. 1989). Outer-sphere complexes and diffuse ion swarms are considered weak. physical interactions while inner-sphere complexes are considered to be strong. chemical interactions (Scheidegger and Sparks. 1996a).

Adsorption isotherms have often been used by researchers to describe metal ion sorption behavior on soils and soil constituents. These involve the adsorption of the metal from solution at constant pH as a function of metal ion concentration (McBride.

1994). Most studies of this nature were carried out for 24 hours because it was assumed the reaction reached completion. The data generated are then described by one of many equilibrium-based adsorption isotherms with the notion that the sorption mechanism can be gleaned. However, field soils are rarely at equilibrium and adsorption isotherms are purely descriptions of macroscopic data and do not definitively prove a reaction mechanism (Sparks, 1995a). Sorption mechanisms may be identified using molecular-level spectroscopic and microscopic techniques that will be described later.

1.2.2 Specific Adsorption Phenomena

Inner-sphere complexation (i.e., chemisorption, specific adsorption) may involve ionic as well as covalent bonding (Sposito, 1989). This adsorption mechanism occurs when an adsorbing metal ion bonds directly to oxygen atom(s) at a solid surface with no water molecules present between the ion and the surface group (McBride, 1994; Sparks, 1995a). Noncrystalline aluminosilicates (allophanes), oxides, and hydroxides of Fe, Al, and Mn, and even the edges of layer silicate clays to a lesser extent provide surface sites for the specific adsorption of transition and heavy metals (McBride, 1994). An adsorptive site is a valence-unsatisfied OH^- or H_20 ligand bound to a metal ion (Fe, Al, or Mn). Inner-sphere complexes can be monodentate (metal bound to one oxygen) or bidentate (metal bound to two oxygen atoms) (Sparks, 1995a). These types of complexes are relatively strong and a metal that is chemically adsorbed in this manner can be considered non-exchangeable. Adsorption by this mechanism is usually independent of ionic strength and in general metals become increasingly non-

exchangeable as the pH is raised (McBride, 1994; Sparks, 1995a). In general >Al-OH groups chemisorb metals more effectively than >Si-OH groups on the basis of the ratio of metal valence to coordination number (McBride, 1994).

Several researchers have used molecular-level techniques to demonstrate the importance of inner-sphere complex formation between metal ions and soil constituents. Grossl et al. (1994) used pressure-jump relaxation technique to identify the formation of a monodentate inner-sphere complex at the Cu/goethite interface. Bergaoui et al. (1995) investigated Cu sorption on Al-pillared montmorillonite using EPR spectroscopy to distinguish between different adsorption mechanisms. They found that at low concentrations, Cu adsorbed on the Al pillared clay through an inner-sphere mechanism. Papelis and Hayes (1996) investigated Co sorption on montmorillonite as a function of pH and Na ion concentration. Using XAFS spectroscopy they identified inner-sphere sorption complexes with increasing pH and Na ion concentration. The potentially strong inner-sphere complex formed between a metal cation and a sorbent can provide a way to immobilize metals in surface and subsurface environments. One should be aware that as a system becomes more complicated, i.e., competing sorbent phases or anions are introduced, it becomes increasingly difficult to identify these types of complexes.

1.2.3 Non-Specific Adsorption Phenomena

Outer-sphere complexation and diffuse-ion association fall under the category of non-specific adsorption (Sposito, 1989). Partitioning of metals to soil surfaces and ion

exchange reactions are considered examples of non-specific adsorption (Sparks, 1995a). The physical forces involved in these types of complexes are generally weaker than those involved in specific adsorption complexes. A strong dependence on ionic strength is typical for an outer-sphere complex due to the weak nature of the electrostatic bond between the metal ion and the surface (Stumm, 1992). Adsorption of ions via outer-sphere complexation occurs only on surfaces that are of opposite charge to the adsorbate (Sparks, 1995a). In the case of nonspecific adsorption there is little dependence on the electron configuration of the surface group and adsorbed ion to be expected for the interaction of solvated species (Sposito, 1989).

The sorption of metal cations to soil constituents via non-specific adsorption mechanisms has been demonstrated by several researchers. Koppelman and Dillard (1977) examined Ni adsorption on kaolinite, chlorite, and illite. Using X-ray photoelectron spectroscopy (XPS) they concluded that at pH = 6 Ni was adsorbed as an aquated species, suggesting an outer-sphere adsorption mechanism. Baeyens and Bradbury (1995) extensively investigated Ni and Zn sorption on montmorillonite over a range of reaction conditions. They concluded that non-specific adsorption was characterized by a linear adsorption behavior and independent of pH but strongly dependent on ionic strength. Bargar et al. (1996) used grazing-incidence X-ray absorption fine structure (GI-XAFS) to monitor the sorption of Pb on α-Al_2O_3. They found that the Pb ions adsorbed as structurally well-defined outer-sphere complexes at specific sites on the α-Al_2O_3 single crystal surface.

1.2.4 Diffusion

Diffusion is a physical process whereby a substance can be removed from the bathing solution around a mineral phase and therefore falls under the broad classification of sorption. Soils are porous materials consisting of both macropores (>2nm) and micropores (<2nm) making diffusion a major mechanism of metal sorption, especially over long time scales found in natural settings (Sparks et al., 1999). For a metal ion to reach all potential sorption sites it must be transported through the bulk solution, travel through the liquid film on the solid surface (film diffusion), traverse pores within an individual particle (intra-particle pore diffusion) or pores between particles (inter-particle pore diffusion), and penetrate into the solid matrix (Pignatello and Xing, 1996; Sparks et al., 1999). Pore diffusion and matrix diffusion are considered as likely transport-limiting processes (Sparks et al., 1999). Most research attributes slow sorption kinetics of metal ions and organic contaminants to some sort of diffusion limitation due to the porous nature of soil particles and because diffusive constraints are imminent throughout any sorption experiment (Pignatello and Xing, 1996).

There are several examples in the literature that ascribe slow metal sorption and desorption behavior to diffusion processes. The kinetics of Ni, Zn, and Cd adsorption and desorption by goethite were investigated by Bruemmer et al. (1988). The desorption hysteresis they observed was explained by diffusion-dependent adsorption and fixation processes of the metal cations inside the goethite structure. Lo and Leckie (1993) monitored the kinetics of Zn and Cd sorption and desorption onto an amorphous

aluminum oxide assuming a two-domain pore size distribution. Their results showed a fairly rapid sorption stage whereby Zn and Cd were subject to film diffusion and some internal diffusion followed by a second, slower sorption stage resulting from internal mass transport of the metal ions. Similar observations involving Cd and Se adsorption on porous aluminum oxides were made by Papelis (1995). XPS results verified the hypothesis that adsorbate intra-particle diffusion followed by sorption was the predominant Cd and Se uptake mechanism. Coughlin and Stone (1995) proposed the nonreversible adsorption of several divalent metal cations sorbed on goethite was due to slow pore diffusion.

1.2.5 Precipitation

Precipitation is a general term that is defined as an accumulation of a substance to form a new bulk solid phase. In pure solutions this is a fairly simple phenomenon to study since the solubility product of a new solid phase must be exceeded prior to nucleation of a new phase (McBride, 1994). In solutions where a solid phase such as a clay mineral or metal oxide is present, this scenario increases in complexity since the solid phase may effect the formation of a new secondary phase. An array of nucleation processes in soil environments is possible, including: polymer sorption or formation on a solid surface; coprecipitation with dissolved co-ions derived from the sorbent; and precipitation on a surface composed of ions from the bulk solution (Sparks et al., 1999). In soil solutions, the array of solid phases present may reduce the energy barrier for a

new crystal to nucleate, especially when there is crystallographic similarity between the surface and the precipitate (McBride, 1994).

In soil solutions and natural waters heterogeneous nucleation, or formation of crystal nuclei at surfaces of a different solid that is present before the initiation of precipitation, is much more likely to occur than homogeneous nucleation. Heterogeneous nucleation may take place at a lower saturation ratio on a solid substrate surface than in solution (Stumm, 1992). This may explain why many researchers have observed the formation of metal surface precipitates on mineral and oxide surfaces at pH values well below the pH where the formation of metal hydroxide precipitates form in solution (Charlet and Manceau, 1992; d'Espinose de la Callerie et al., 1995; Fendorf et al., 1994a; O'Day et al., 1994; Scheidegger et al., 1997; Scheidegger et al., 1998). There are still questions remaining as to the exact mechanism of formation of these types of surface precipitates and the role the solid surface has in their formation. Current research using molecular level techniques is beginning to answer some of these questions.

Prior to the formation of a surface precipitate, surface complexation of the adsorbing metal at the surface is necessary (Sparks, 1995a). At low surface coverages surface complexation dominates, leading to nucleation as surface coverage increases more, and finally surface precipitation becomes the dominant mechanism at the highest surface loadings. However, the critical surface coverage loading necessary for nucleation is vague and there is clearly a continuum from pure adsorption processes to the formation of a precipitate. The term "surface induced precipitation" has been used

to describe the formation of a precipitate under solution conditions that would, in the absence of the substrate solid, be undersaturated with respect to any known solid phase (Towle et al., 1997). Several hypotheses explaining this "surface-induced" precipitate formation have been suggested including: formation of a non-uniform coprecipitate of dissolved ions and sorbate ions resulting in a solid phase with activity below a pure crystal (Farley et al., 1985); the solid substrate reduces the energy barrier for nucleation by providing a sterically similar, yet chemically foreign, surface for nucleation (McBride, 1989); and a lowering of the solubility of the precipitate due to the lowering of the dielectric constant of the solution near the surface (O'Day et al., 1994).

Regardless of the mechanism by which a heterogeneous surface precipitate forms it is necessary that the surface undergo dissolution to release the co-ions that are incorporated into the newly formed solid-solution phase. This mineral dissolution may be the rate-controlling step in the formation of mixed precipitate phases (McBride, 1989). McBride (1994) suggested that the measurement of the concentration of silicon in a soil solution is essential if the sorption of metal by a soil is under investigation, since the precipitation of an metal through the incongruent dissolution of aluminosilicates is accompanied by the release of silicon. Also, the Al concentration in solution may be measured to assess the degree of mineral dissolution although concentration levels may be too low to detect, especially if Al is immediately incorporated into a new phase. The work of Scheidegger et al. (1997) demonstrated the enhanced dissolution of the clay minerals pyrophyllite and kaolinite as a mixed Ni-Al hydroxide phase formed. They saw a correlation between the removal of Ni from

solution and the release of Si into solution from the mineral surface. A similar study by O'Day et al. (1994) suggested the formation of a $Co(OH)_2$-like precipitate phase upon Co sorption to kaolinite was the main sorption mechanism. While they did not directly measure the dissolution products of kaolinite they did hypothesize that dissolution of the kaolinite substrate was most likely occurring.

Because the onset of metal chemisorption and the beginning of metal hydroxide precipiation are not often separated by a wide margin of pH, metal coverage, or reaction time, macroscopic sorption data alone cannot be use to make distinctions between these mechanims (McBride, 1994). One must use microscopic and spectroscopic techniques coupled with macroscopic metal sorption studies to reveal molecular and mechanistic information (Sparks, 1995a). Several studies of metal cation sorption on soil minerals and oxides have employed EXAFS spectroscopy to show a distinction between adsorption and precipitation (Charlet and Manceau, 1992; Cheah et al., 1998; Chisholm-Brause et al., 1990; Fendorf et al., 1994a; O'Day et al., 1994a; O'Day et al., 1996; Scheidegger et al., 1996c; Scheidegger et al., 1997; Thompson, 1998; Towle et al., 1997; Xia et al., 1997; d'Espinose de la Callerie et al., 1995). For example, Chisholm-Brause et al. (1990) studied the sorption of divalent Co on the surfaces of aluminum oxide, rutile (TiO_2), and kaolinite at pH values selected to achieve ~95% Co removal from solution. After equilibrating for 16-28 h, EXAFS analysis revealed the formation of multinuclear sorption complexes at surface coverages below one monolayer of Co(II) atoms. Fendorf et al. (1994) investigated the sorption of Cr(III) on silica using EXAFS analysis to discern the local structural environment of the Cr(III). The authors found

that at pH 6 surface nucleation of the γ-CrOOH-type structure occurred prior to monolayer coverage and under conditions where solution precipitation was not observed. These advances in identifying the formation of mixed metal surface precipitates on soil constituents opens a new area of study in that the new phases may cause a more stable form of the metal in natural settings.

The above studies and others demonstrate the fact that surface precipitation can be a significant mode of sorption even at low metal loading levels and at field pH ranges. However, the majority of the experiments investigating metal precipitate formation in the presence of clay minerals and oxides have involved fairly "clean" systems in which only one sorbent phase is present or a limited range of experimental conditions (pH, I.S., metal concentration) are used. To address the lack of research investigating metal precipitate formation in mixed mineral systems, Elzinga and Sparks (1999) used XAFS as a tool to characterize Ni sorption in a clay mixture of pyrophyllite and montmorillonite. Under the time scale investigated (within 40 minutes) it was established that adsorption was the major Ni uptake mechanism in a single montmorillonite system and surface precipitation in the pyrophyllite system. When the clay minerals were mixed together prior to Ni addition, both adsorption and surface precipitation were important mechanisms in the overall Ni uptake, and neither sorption mechanism truly out-competed the other over a reaction time of 40 minutes. Elzinga and Sparks (1999) concluded that both mechanisms should be considered when modeling Ni sorption in similar systems.

The formation of metal precipitates on clay minerals and oxides has been demonstrated in the above studies, but questions still remain as to the stability of these structures. In natural settings metal contaminants may have contact with sorbent phases on the order of several years and reaction conditions such as pH may change dramatically. Therefore, it is important to consider the effect of residence time, pH and desorptive agent on metal precipitate dissolution. A study by Scheckel and Sparks (1999) investigated the dissolution of Ni precipitates from several sorbent phases under a range of reaction conditions using XAFS spectroscopy. Several observations were made including, 1) mixed Ni-Al hydroxide precipitates appeared to be more stable relative to $Ni(OH)_2$ precipitates, 2) ligands (EDTA, oxalate, acetylacetone) were more aggressive in their dissolution of Ni precipitates relative to proton promoted dissolution (HNO_3 at pH 4 and 6), and 3) with increased residence time the stability of the Ni precipitates increased, with differences occurring even between 1 year and 2 year aged samples.

The reasons for the increased stability of Ni precipitates on the surface of pyrophyllite was investigated by Ford et al. (1999). They showed a solid-state transformation of a Ni precipitate formed at the surface of pyrophyllite that resulted in a dramatic stabilization of sorbed Ni after aging for 1 year. Time-resolved characterization of the surface precipitate via XAFS and diffuse reflectance spectroscopies and high resolution thermal gravimetric analysis (HRTGA) indicated that stabilization occurred during stepwise transformation of an initial Ni-Al hydroxide to a precursor Ni-Al phyllosilicate phase. They hypothesized that the observed

stabilization is realized through exchange of silicate for nitrate within the Ni-Al layered double hydroxide (LDH) interlayer leading to formation of a precursor Ni-Al phyllosilicate. They concluded that Ni sorption to the pyrophyllite surface proceeds via at least two steps: 1) initial formation of a Ni-Al LDH precipitate where Al is derived from the pyrophyllite structure and 2) the ultimate formation of a Ni-Al phyllosilicate due to incorporation of Si (derived from the pyrophyllite) into the Ni-Al LDH interlayer.

Surface precipitation is not necessarily limited to laboratory systems since natural environments too will often have near-saturation concentrations of relatively insoluble ions such as Al(III) which may be incorporated into a coprecipitate with a range of metal cations such as Cd, Cr, Cu, Co, Ni, Pb, and Zn (Towle et al., 1997). In order to make the progression from these fairly simple systems to complex soil environments a range of analytical techniques capable of discerning reaction mechanisms must be used.

1.3 Metal Desorption/Dissolution From Soils and Soil Components

The majority of studies investigating the reactions between metal cations and soils or soil constituents (clay minerals, oxides, organic material) have focused on the removal of the metal from the solution rather than the release of the sorbed metal from the sorbent. The processes of metal desorption (in the case of adsorption) and dissolution (in the case of surface precipitation) are extremely important in surface and subsurface environments considering that in most field scale situations the soils have

been contaminated for some time and the majority of the metal may already be sequestered by a sorbent phase. To predict the fate and mobility of metals in contaminated soils information on desorption/dissolution is required (Sparks. 1995a).

It is a common observation among researchers that sorption is often an irreversible process (Sparks. 1995a). The hysteretic effect of metal sorption is indicated when the desorption isotherm does not follow the adsorption isotherm. This effect is even more pronounced as the aging time of the metal-solid complex increases. Several physical and chemical reasons for this phenomenon have been proposed. however most research dealing with this topic has been purely macroscopic and differences exist depending on the metal and sorbent investigated. For example. Ainsworth et al. (1994) aged a hydrous ferric oxide in the presence of Co. Cd. and Pb and then followed this with desorption of the metals. Their results indicated that Pb adsorption was completely reversible but Cd and Co adsorption were substantially non-reversible. They explained this by suggesting Cd and Co were incorporated into the metal oxides structure. while Pb was not. Considering that the ionic radii for Cd and Co are similar to that of Fe while the ionic radii of Pb is much larger than all these metals. their results are reasonable. Similar results were presented in the work of McLaren et al. (1998) for Cd and Co desorption from soil clays. They found that an increased sorption period was accompanied by substantial decreases in the proportions of sorbed metal desorbed and increasing the contact period between metal and clay material resulted in decreased rates of metal desorption. Other metal sorption-desorption studies from soils and soil

components show similar hysteretic behavior with increased adsorption time (Backes et al., 1995; Gray et al., 1998; Jenne, 1995; Lehmann and Harter, 1984).

The complex and heterogeneous array of mineral sorption sites, organic materials, metal oxides, macro- and micro- pores, and microorganisms in soils provide a matrix that may strongly sequester metal ions. Fixation, hysteresis, and irreversibility are all terms reflecting the tendency of metals to be desorbed from soils more slowly than they are adsorbed because of the smaller driving force during desorption (Jenne, 1995). Yin et al. (1997) examined Hg(II) desorption from a soil and observed that the rate coefficients of adsorption and desorption were inversely correlated with the soil organic C content. They contended that diffusion of Hg through intraparticle micropores of soil organic matter may have been responsible for the irreversibility of Hg adsorption. Other studies have shown a correlation between organic matter and the amount and rate of metal release from soils (Sheppard and Thibault, 1992; Wu et al., 1999). Iron oxides in soils have also been recognized as contributing to the strong fixation of metal cations (Cavallaro and McBride, 1984; McLaren et al., 1986).

In addition to physical and diffusion processes accounting for the reduction of reversibility of metals partitioned from solution, modifications in surface complex structure may cause hysteretic effects. Coughlin and Stone (1995) have shown increased sorption of Co, Ni, and Cu onto the surface of goethite coupled to the introduction of aqueous Fe(II). They proposed that the microscale formation of metal spinels (Me^{2+}, Fe^{2+})$Fe^{3+}{}_2O_4$, at the goethite surface may have caused a decrease in the ability to desorb partitioned metals. The differences in stability of discrete Cr(III)

surface precipitate clusters vs. evenly distributed Cr(III) surface precipitates was investigated by Fendorf et al. (1996). Based on oxalate-induced extractions they found a greater dissolution rate for Cr(III) precipitates formed on silica (discrete clusters) than for Cr(III) precipitates formed on goethite (evenly distributed). This suggests surface morphology and distribution is an important factor in surface precipitate stability. A study by Scheidegger and Sparks (1996b) displayed slow Ni detachment from a Ni-reacted pyrophyllite surface which they attributed to the formation and dissolution of a mixed Ni-Al-hydroxide phase. This is a significant finding since the co-precipitate formed upon Ni sorption and pyrophyllite dissolution may be more stable than a crystalline $Ni(OH)_2$ phase indicating its potential effectiveness as a sink for metals in soil environments.

1.4 Time Scales and Kinetics of Metal Sorption Reactions

As outlined above there are a multitude of mechanisms responsible for the uptake of metal ions from soil solutions. With this range of mechanisms also comes a large range of reaction times from extremely rapid (microseconds) to slow (months-years), depending on the sorbate/sorbent system (Sparks et al., 1999). Cation exchange reactions on clays without narrow interlayer regions such as kaolinites and dispersed smectites are usually instantaneous compared to very slow exchange reactions on partially collapsed 2:1 clays (McBride, 1994). Sparks and Jardine (1984) studied K-Ca exchange on kaolinite, montmorillonite, and vermiculite. The apparent K adsorption rate coefficients were in the order kaolinite > montmorillonite > vermiculite. The

process of cation exchange and the formation of other complexes involving electrostatic interactions (i.e., non-specific adsorption) are usually quite rapid and difficult to measure using conventional methods (McBride, 1994; Sparks, 1995a).

The kinetics of heavy metal sorption on soil and soil constituents is typically rapid initially, followed by a slower reaction may continue for days or weeks (Scheidegger and Sparks, 1996a). The rapid sorption step is generally attributed to an adsorption mechanism, i.e., inner-sphere or outer-sphere complex formation and/or film-diffusion processes (Scheidegger and Sparks, 1996a). For example, the rapid kinetics of Cu adsorption and desorption on goethite was evaluated using the pressure-jump relaxation technique (Grossl et al., 1994). The authors concluded the sorption mechanism was the formation of a monodentate innersphere Cu/goethite surface complex. The half-lives for Pb^{2+}, Cu^{2+}, and Zn^{2+} sorption on peat ranged from 5 to 15 s (Bunzl et al., 1976).

The slow second stage of metal adsorption to soil clay minerals, hydr(oxides), and soils has been attributed to 1) adsorption onto sites of lower reactivity (Benjamin and Leckie, 1981), 2) diffusion of the sorbate into the adsorbent (Bruemmer et al., 1988) and 3) a precipitation reaction (Scheidegger and Sparks, 1996b). All three of the proposed mechanisms may occur separately or concurrently, however discerning between them is not possible by using a macroscopic approach alone. McBride (1982) used EPR to study Cu sorption on an aluminum oxide. He saw a biphasic sorption behavior and attributed the initial rapid step to sorption on high-energy sites and the slow second step to sorption on less energetic sites. Similarly, Strawn et al. (1998)

observed a biphasic sorption kinetics in the case of Pb^{2+} on an aluminum oxide. They attributed the initially fast sorption kinetics to the formation of an inner-sphere bidentate complex and the slow sorption kinetics to diffusion through micropores. Scheidegger et al. (1997) studied the sorption of Ni on pyrophyllite, gibbsite, and montmorillonite at pH 7.5. Ni sorption reactions were initially fast followed by a significantly slower rate. EXAFS analysis revealed the slow reaction stage was attributed to nucleation processes on the mineral surfaces. In the Ni/pyrophyllite and Ni/gibbsite systems, the appearance of multinuclear Ni complexes occurred after a reaction time of just minutes. In contrast, for the Ni/montmorillonite system, Ni complexes were not observed until a reaction time of 48 hours. It was established that kinetics and sorption mechanisms were greatly dependent on the type of sorbent studied.

In heterogeneous soil systems mass transfer and transport predominate, so only apparent rate laws can be measured (i.e., not chemical kinetics) (Sparks, 1995b). Although the soil is a complex medium and attributing certain sorption mechanisms based on kinetic data is difficult, it is still important to study a range of metal reaction times since temporal and structural changes of a metal complex may be time-dependent. It is especially essential to vary sorption times if one is studying metal desorption/dissolution behavior as evidenced by the several examples of the dependence of sorption time on metal release. Ideally one would also couple spectroscopic and microscopic techniques with sorption/desorption studies to glean mechanistic information. Examples of such techniques are presented in the next section.

1.5 Use of Analytical Techniques to Identify Metal Surface Precipitates

It is nearly impossible to distinguish a precipitate phase from an adsorption complex based on macroscopic data alone. The identification of a new phase is necessary to confidently claim a metal surface precipitate accounts for the removal of a metal ion from solution. In recent years, the application of advanced spectroscopic and microscopic tools has helped define the mechanisms controlling contaminant reactions in soils and aquatic environments (Bertsch and Hunter, 1998; Brown Jr. et al., 1995). Since no single characterization method gives a complete description of surface structure or the geometric details of sorption complexes, it is important to employ a variety of methods that provide complementary information (Brown Jr., 1990). This is the approach to be taken in this research project to ascertain the importance of metal surface precipitate formation in controlling the mobility and availability of Ni and Zn in soils.

1.5.1 Spectroscopic Techniques

Spectroscopy offers researchers a way to probe molecular and atomic structures and determine details of a local coordination environment around a central atom of interest. One popular spectroscopy used in soil and geochemical sciences is X-ray absorption fine structure (XAFS) spectroscopy. With XAFS the local environment of an element is probed, allowing its application to the study of solution species and

amorphous materials that may be found in soils (Fendorf et al., 1994b). XAFS is an ideal technique to study reactions at mineral-water interfaces since it is element specific and samples can be analyzed in-situ (i.e., as wet pastes) (Brown Jr. et al., 1998). Bond distances, coordination numbers, and identification of neighboring atoms can be discerned using this technique. One should realize that XAFS spectra do not provide precise measurements of an atom's local environment, but averages from all atoms within the sample (O'Day et al., 1994).

Several researchers have used XAFS to characterize metal sorption mechanisms and to identify complex formation of metals sorbed to oxides, clay minerals, and soils (Bargar et al., 1997a; Bargar et al., 1997b; Charlet and Manceau, 1992; Chisholm-Brause et al., 1990; Fendorf et al., 1994a; Hesterberg et al., 1997; O'Day et al., 1996; Papelis and Hayes, 1996; Scheidegger et al., 1997; Spadini et al., 1994; Towle et al., 1997). For example, Scheidegger et al. (1997) used XAFS to identify the formation of a mixed Ni-Al hydroxide precipitate upon Ni sorption to several clay minerals and aluminum oxides. This technique is quite useful to identify metal precipitates in sorption studies since a strong backscattering signal from a neighboring metal atom (i.e., Ni or Zn) around the central atom would indicate a precipitate phase has formed.

Another useful spectroscopic technique used in metal-mineral studies is diffuse reflectance spectroscopy (DRS). DRS is the study of light as a function of wavelength that has been reflected or scattered from a solid, liquid, or gas (Clark, 1995). This technique is sensitive to elements in minerals that have unfilled electron shells. This makes DRS useful to investigate Ni precipitates since Ni^{2+} has an unfilled d orbital.

This technique would not be useful in the case of identifying Zn^{2+} precipitates since this element has no unfilled electron orbital. The usefulness in using DRS to identify Ni hydroxide precipitates is due to the sensitivity of this technique to OH absorption bands. DRS is capable of distinguishing kaolinite from halloysite and montmorillonite from illite which is difficult using XRD alone (Clark et al., 1990). Scheinost et al. (1999) demonstrated the usefulness of DRS in differentiating $Ni(OH)_2$ from a Ni-Al layered double hydroxide phases. This task would be difficult using XAFS alone since Al is a fairly weak backscattering atom and would most likely be drowned out by the Ni signal.

1.5.2 Microscopic Techniques

An array of microscopic techniques that can be applied to soil systems have become increasingly available in the last several years. Arguably, it has been the introduction and application of scanning probe microscopy (SPM) that has had of the greatest impacts on advancing research in soil and environmental chemistry (Bertsch and Hunter, 1998). SPM represents a class of microscopic techniques that provide high resolution multidimensional images of solid surfaces by monitoring the interactions between sharp tips and the surface (Bertsch and Hunter, 1998). SPM includes scanning tunneling microscopy (STM), atomic force microscopy (AFM), magnetic force microscopy (MFM) and chemical force microscopy (CFM). AFM, CFM, and MFM are all types of scanning force microscopies (SFM). SFM techniques are advantageous in that they are relatively low cost and the samples may be run in-situ.

SFM is a powerful microscopic technique capable of imaging mineral surfaces immersed in aqueous solution over the course of precipitation and heterogeneous nucleation (Maurice, 1998). Fendorf et al. (1996) studied the kinetics of Cr(III) sorption reactions on goethite and silica using a flow cell mounted in a SFM. Scanning force micrographs revealed the formation of a Cr(III) precipitate that was distributed over the entire surface of goethite while discrete surface clusters were observed on the SiO_2 surface. A study by Thompson et al. (1998) utilized high resolution tunneling electron microscopy (HRTEM) to observe a kaolinite surface reacted with Co for several hours. Co was spatially associated with Al and Si, suggesting an association with kaolinite.

1.6 Nickel and Zinc Sorption Behavior and Chemistry

Researchers have clearly established that the mechanism for metal ion sorption on clay minerals, metal oxides, and whole soils is dependent on several parameters including: (1) metal concentration, (2) identity of the sorbent phase, (3) reaction time, (4), ionic strength, and (5) pH. All of these reaction variables may have pronounced effects on one another, providing quite complex sorption behavior even in relatively pure systems. This study will investigate both Ni and Zn as the metal ions of study since both have been demonstrated to form mixed metal-Al layered double hydroxide phases upon sorption to Al-bearing clay minerals and metal oxides (Ford and Sparks, 2000; Scheckel et al., 2000; Scheidegger et al., 1998; Scheinost et al., 1999; Trainor et al., 2000). In addition, both Ni and Zn have been demonstrated to have variable

reaction sorption mechanisms in both soil and mineral studies, including: ion exchange; inner- and outer- sphere sorption complexation; substitution into mineral phases; diffusion into metal oxides; formation of solid solutions and formation of ternary sorption complexes. The several studies investigating Ni and Zn sorption onto clay minerals and oxides using XAFS makes these metal ions good candidates for investigations of their behavior in more complex systems.

1.6.1 Nickel

The element nickel is a Group VIII metal that is part of the first transition series on the periodic table. Its ionic radius is 70 pm, comparable to Mg (72 pm), Al (53 pm), and several trace metal cations. The outer sphere electron configuration for nickel is $3d^8$ $4s^2$ which readily yields the 4s electrons to give the divalent ion Ni^{2+}, or the nickelous ion (Theis and Richter, 1980). The most common oxidation state of nickel is II, although I, III and IV states can exist under certain conditions. In natural aquatic systems, only the II oxidation state is of importance as the I, III, and IV states are not stable in aqueous solution. Most nickel found in soils is distributed between the insoluble organic and inorganic phases, with approximately 0.001% of the total Ni found in the soil solution (Uren, 1992). Therefore, understanding the mechanisms by which nickel is bound to these phases is of crucial importance as they dictate the mobility and availability of Ni in soil.

In aqueous systems with acidic to neutral pH values, nickel is octahedrally coordinated as $Ni(H_2O)_6^{2+}$. Because Ni has the highest crystal field stabilization energy

of the common divalent metals, it has the highest octahedral site preference (Uren, 1992). At higher pH values, the activity of various ligands in soil solution tends to increase and nickel may form various complexes. The formation of complexes follows the trend (most common to least common): $OH^- > SO_4^{2-} > Cl^-$ (Theis and Richter, 1980). The stability of such complexes depends on the ligand with which nickel is associated. In general, nickel forms weak complexes with common inorganic ligands and more stable complexes with many organic ligands, namely sulfate, citrate, glycine, and cyanide (Theis and Richter, 1980).

Nickel is a heavy metal that has received much attention recently due to its increased introduction into soil and aquatic environments. There are several sources that have the potential to contaminate soil with nickel. The sources and average concentration of nickel in each source are as follows: fertilizer, 30 ppm; sewage sludge, 80 ppm; municipal compost, 120 ppm; fuel ash, 270 ppm; and atmospheric fallout; 703 ppm (Förstner, 1995). While nickel is essential to plants, animals and microorganisms at low concentrations, higher concentrations of nickel can be toxic. The major industrial sources of nickel are metal plating and finishing, combustion of fossil fuels, and nickel mining and refining.

The natural concentration of nickel in soils varies greatly with the type of soil parent material. The primary source of nickel found in soil is igneous rocks such as serpentine and peridotite, which may have concentrations as high as 2000 ppm Ni (Förstner, 1995). Ni concentrations in uncontaminated soil range from 0.1 to 1520 mg/kg. As a result, the literature values for Ni contents in soils are quite variable

ranging anywhere from 1 ppm to 500 ppm and upwards of 5,000 ppm for soil derived from ultrabasic igneous rocks. However, much of this nickel is not readily extractable and a better indicator is the amount of nickel found in soil solution. The concentration of nickel in 68 "normal" soil solutions from California ranged from <0.01 to 0.20 ppm (Uren, 1992). Soils exposed to additional amounts of nickel in the form of sewage sludge or fertilizers may have values 100 times greater than the concentration for normal soil solutions.

Sorption and release studies of nickel have traditionally been done using hydrous oxides (Bruemmer et al., 1988; Kinniburgh et al., 1976; Schulthess and Huang, 1990; Theis and Richter, 1980), purer layer silicate minerals (Bowman et al., 1981; Koppelman and Dillard, 1977; Puls and Bohn, 1988) and whole soils (Harter, 1983; Sadiq and Enfield, 1984; Tiller et al., 1984a). With the exception of the work of Traina and Doner (1985), few studies have looked at mixtures of clay minerals and oxides which are more indicative of field conditions though less complicated than whole soils allowing for easier interpretation of molecular-level data. Moreover, with the exception of a few studies, application of spectroscopic and microscopic techniques to such systems has been limited, however, they are necessary in identifying any reaction mechanisms (Scheidegger et al., 1996a; Scheidegger et al., 1996b; Scheidegger et al., 1996c; Scheidegger and Sparks, 1996b). There is ample evidence that mixed Ni-Al layer double hydroxide phases (surface precipitates) form upon Ni sorption to a range of clay minerals and Al-oxides (Scheidegger and Sparks, 1996b). Ni sorption studies have also been traditionally unrealistically brief (several minutes to hours) relative to soil

processes (Uren, 1992). Therefore, there is a need to study the kinetics and mechanisms of nickel sorption/release reactions in soils and soil components using advanced spectroscopic and microscopic techniques, paying particular attention to precipitate formation.

1.6.2 Zinc

Under acidic, oxidizing conditions, Zn is one of the most soluble and mobile of the trace metal cations. It does not complex tightly with organic matter at low pH and acid-leached soils often have Zn deficiencies because of depletion of this element in the surface layer. Toxicity of Zn to plants is most likely to appear in acid soils that have not been subjected to prolonged acid leaching. The high potential solubility of Zn in acid soils, and that the fact that Zn is typically a high-concentration pollutant of industrial wastes and sewage sludges, combine to create a significant potential for phytoxicity from land application of wastes (McBride, 1994).

The element zinc is a metal that is part of the first transition series on the periodic table. The outer sphere electron configuration for Zn is $3d^{10}\ 4s^2$, so its orbitals are completed filled. As a result, Zn(II) can be 4-coordinate (tetrahedral) or 6-coordinate (octahedral). The ionic radius of tetrahedral Zn is 74 pm and the ionic radius of octahedral Zn is 88 pm. The most common oxidation state of zinc is II. In aqueous systems with acidic to neutral pH values zinc can be octahedrally or tetrahedrally coordinated since it gains no crystal field stabilization energy from either configuration.

As a result, the coordination environment of Zn is variable and it can be useful to determine the form of Zn found in soils.

Zinc is considered a trace element in soils with typical concentration values ranging from 10 to 300 ppm (Förstner, 1995). In the vicinity of mining districts Zn concentrations can be on the order of several thousand ppm (Henderson et al., 1998; Lin and Herbert Jr., 1997; O'Day et al., 1998). Sadiq (1991) contended that instead of adsorption, precipitation was playing a major role in determining solubility relationships of Zn in soils. Zinc sorption phenomena have been extensively studied in relatively pure systems (Baeyens and Bradbury, 1995; Benjamin and Leckie, 1981; Micera et al., 1986; Xu et al., 1994) and more complex whole soil systems (Bruemmer et al., 1983; Hinz and Selim, 1999; Tiller et al., 1984a; Tiller et al., 1984b; Zhang et al., 1997).

The formation of Zn precipitates in soils and on soil constituents has been established (Roberts et al., 1999). A XAFS study of a zinc contaminated groundwater aquifer indicated Zn sulfides were the dominant mineral phases present and were a significant sink for Zn in this system (Hesterberg et al., 1997). Another XAFS study of a Zn-contaminated sediment revealed the presence of Zn hydroxide and/or zinc-iron oxyhydroxide phases, depending on the total amount of Fe in the system (O'Day et al., 1998). Zinc was found to be associated with a secondary Cu-phase and zinc sulfates in a mine rock dump as verified by SEM and extraction techniques (Lin and Herbert Jr., 1997). Based on thermodynamic calculations, Lindsay theorized the formation of franklinite ($ZnFe_2O_4$) in soils (Lindsay, 1979). Sorption of Zn on hydroxyapatite

resulted in the formation of a Zn-Ca coprecipitate (Xu et al., 1994). The sorption of Zn to a calcite surface resulted in the formation of a precipitate resembling hydrozincite as verified by XPS and XRD (Zachara et al., 1989). Clearly the type of precipitate phase Zn found greatly depends on the conditions of the soil environment.

Using X-ray absorption fine structure (XAFS) spectroscopy to monitor zinc sorption to oxides under neutral to basic pH values, researchers have demonstrated that Zn can form both inner-sphere surface complexes and Zn hydrotalcite-like phases upon sorption to Al-bearing minerals (Ford and Sparks, 2000; Trainor et al., 2000); inner-sphere surface complexes upon sorption to goethite (Schlegel et al., 1997); and both innersphere and multinuclear hydroxo-complexes upon Zn sorption to manganite (Bochatay and Persson, 2000). By applying XAFS and electron microscopy to Zn-contaminated soils and sediments, Zn has been demonstrated to occur as ZnS in reduced environments, often followed by repartitioning into Zn hydroxide and/or ZnFe hydroxide phases upon oxidation (Hesterberg et al., 1997; O'Day et al., 1998; Webb et al., 2000). Manceau et al. (2000) used a variety of techniques, including XAFS and micro-focused XAFS to demonstrate that upon weathering of Zn-mineral phases, Zn was taken up by the formation of Zn-containing phyllosilicates and, to a lesser extent, by adsorption to Fe and Mn (oxyhydr)oxides. These studies demonstrate that in any given system, Zn may be present in one of several forms making direct identification of each species difficult using traditional approaches.

Several other studies have reported adsorption as the primary mechanism of Zn removal though few have been verified with molecular-level techniques (Dang et al.,

1994; Harter, 1983; Hinz and Selim, 1999; Ladonin, 1997; Maguire et al., 1981; Micera et al., 1986). The sorption mechanism of Zn seems to be greatly dependent on concentration levels, pH, the sorbent phases present, and time scales of sorption reactions.

1.7 Research Justification

The introduction of higher than natural levels of metals such as Zn and Ni into surface and subsurface environments has established the need to study their interactions with soils and soil materials. Most of the studies examining metal cation reactions in soils have relied on macroscopic data, relatively short sorption times, and have often neglected the reversibility of the reaction. Remediation strategies and soil management policies based on equilibrium-based models derived from macroscopic data may lead to mistakes and an unnecessary expenditure. In order to establish sound remediation strategies and techniques metal sorption studies over long time scales using analytical techniques capable of gleaning sorption mechanisms are necessary.

While many researchers have verified the formation of mixed metal surface precipitates with several metals (Cd, Co, Cr, Cu, Ni, Zn) in the presence of relatively pure clay minerals and metal oxides, the importance of this mechanism in soil environments has yet to be determined. In addition, most of the studies have relied on a limited range of reaction conditions (pH, ionic strength, metal concentration) while in soil environments these conditions are quite variable and can control sorption behavior of metals. Moreover, there is a lack of studies that have investigated the stability of

mixed metal surface precipitates. Determining the stability of these phases is necessary to establish their effects on the transport and bioavailability of metal contaminants in soils.

This research is an investigation of Ni and Zn precipitate formation and the factors affecting their formation. To meet this end, relatively simple laboratory systems will be investigated leading up to metal speciation in actual contaminated soils. This information will be useful to researchers and professionals seeking to develop sound remediation strategies and develop models capable of predicting metal behavior in soils. Investigators interested in preserving clean soil environments and cleaning up those sites already contaminated will take interest in this research.

1.8 Objectives of Research

In order to complete the goals outlined in the research justification, these objectives were established:

1) Monitor Ni(II) sorption kinetics on soil constituents over a range of reaction conditions (time, metal concentration, pH) to determine if mixed Ni-Al LDH phases are capable of forming in natural settings.

2) Assess the stability of Ni-Al LDH phases formed under a range of reaction conditions.

3) Compare the sorption behavior of Zn(II) on metal oxides to and assess the effects of reaction conditions on the type of surface complexes formed and determine if Zn hydroxide phases are playing a dominant role in Zn speciation.

4) Directly investigate the speciation of Zn in smelter-contaminated soils using a variety of analytical techniques and relate Zn speciation to bioavailability.

1.9 References

Ainsworth, C.C., J.L. Pilou, P.L. Gassman and W.G.V.D. Sluys. 1994. Cobalt, cadmium, and lead sorption to hydrous iron oxide: Residence time effect. *Soil Sci. Soc. Am. J.* **58:** 1615-1623.

Backes, C.A., R.G. McLaren, A.W. Rate and R.S. Swift. 1995. Kinetics of cadmium and cobalt desorption from iron and manganese oxides. *Soil Sci. Soc. Am. J.* **59:** 778-785.

Baeyens, B. and M.H. Bradbury. 1995. A quantitative mechanistic description of Zn, Ca and Ni sorption on Na-montmorillonite Part II: Sorption measurements. PSI Bericht Nr.95-10, Paul Scherrer Institut, Villagen, Switzerland and Nagra Technical Report NTB 95-04, Nagra, Wettingen, Switzerland, Paul Scherrer Institut.

Bargar, J.R., G.E. Brown Jr. and G.A. Parks. 1997a. Surface complexation of Pb(II) at oxide-water interfaces: I. XAFS and bond-valence determination on mononuclear and polynuclear and polynuclear Pb(II) sorption products on aluminum oxides. *Geochim. Cosmochim. Acta* **61:** 2617-2637.

Bargar, J.R., G.E. Brown Jr. and G.A. Parks. 1997b. Surface complexation of Pb(II) at oxide-water interfaces: II. XAFS and bond-valence determination on mononuclear and polynuclear Pb(II) sorption products and surface functional groups on iron oxides. *Geochim. Cosmochim. Acta* **61:** 2639-2652.

Bargar, J.R., S.N. Towle, G.E. Brown Jr. and G.E. Parks. 1996. Outer-sphere Pb(II) adsorbed at specific surface sites on single crystal γ-alumina. *Geochim. Cosmochim. Acta* **60:** 3541-3547.

Benjamin, M.M. and J.O. Leckie. 1981. Multi-site adsorption of Cd, Co, Zn, and Pb on amorphous iron oxyhydroxide. *J. Colloid Interface Sci.* **79:** 1999-2010.

Bergaoui, L., J.-F. Lambert, H. Suquet and M. Che. 1995. Cu^{II} on Al_{13}-Pillared saponite: Macroscopic adsorption measurements and EPR spectra. *J. Phys. Chem.* **99:** 2155-2161.

Bertsch, P.M. and D.B. Hunter. 1998. Elucidating fundamental mechanisms in soil and environmental chemistry: The role of advanced analytical spectroscopic, and microscopic methods. pp. 103-122. *In* P.M. Huang, D.L. Sparks and S.A. Boyd (eds.) Future of Soil Chemistry. Soil Sci. Soc. Am., Madison, WI.

Bochatay, L. and P. Persson. 2000. Metal ion coordination at the water-manganite (γ-MnOOH) interface II. An EXAFS study of zinc(II). *J. Colloid Interface Sci* **229:** 593-599.

Bowman, R.S., M.E. Essington and G.A. O'Connor. 1981. Soil sorption of nickel: influence of solution composition. *Soil Sci. Soc. Am. J.* **45:** 860-865.

Brown Jr., G.E. 1990. Spectroscopic studies of chemisorption reaction mechanisms at oxide-water interfaces. pp. 309-353. *In* M.F. Hochella and A.F. White (eds.) Mineral-Water Interface Geochemistry. Mineralogical Society of America, Washington, DC.

Brown Jr., G.E., G.A. Parks, J.R. Bargar and S.E. Towle. 1998. Use of X-ray absorption spectroscopy to study reaction mechanisms at metal oxide-water interfaces. *In* D.L. Sparks and T.J. Grundl (eds.) Mineral-water Interfacial Reactions: Kinetics and Mechanisms. ACS Symposium Series. Am. Chem. Soc., Washington, D.C.

Brown Jr., G.E., G.A. Parks and P.A. O'Day. 1995. Sorption at mineral-water interfaces: macroscopic and microscopic perspectives. pp. 129-183. *In* D.J. Vaughan and R.A.D. Pattrick (eds.) Mineral Surfaces. Chapman & Hall, London.

Bruemmer, G.W., J. Gerth and K.G. Tiller. 1988. Reaction kinetics of the adsorption and desorption of nickel, zinc and cadmium by goethite: I. Adsorption and diffusion of metals. *J. Soil Sci.* **39:** 37-52.

Bruemmer, G.W., K.G. Tiller, U. Herms and P.M. Clayton. 1983. Adsorption-desorption and/or precipitation-dissolution processes of Zn in soils. *Geoderma* **31**.

Bunzl, K., W. Schmidt and B. Sansoni. 1976. Kinetics of ion exchange in soil organic matter. IV. Adsorption and desorption of Pb^{2+}, Cu^{2+}, Zn^{2+}, and Ca^{2+} by peat. *J. Soil Sci.* **27:** 32-41.

Cavallaro, N. and M.B. McBride. 1984. Zinc and copper sorption and fixation by an acid soil clay: effect of selective dissolutions. *Soil. Sci. Soc. Am. J.* **48:** 1050-1054.

Charlet, L. and A. Manceau. 1992. X-ray absorption spectroscopic study of the sorption of Cr(III) at the oxide-water interface. II. Adsorption, coprecipitation, and surface precipitation on hydrous ferric oxide. *J. Colloid Interface Sci.* **148:** 443-458.

Chisholm-Brause, C.J., P.A. O'Day, G.E. Brown Jr. and G.A. Parks. 1990. Evidence for multinuclear metal-ion complexes at solid/water interfaces from X-ray absorption spectroscopy. *Nature* **348:** 528-531.

Clark, R.N. 1995. Reflectance Spectra. pp. 178-188. AGU Handbook of Physical Constants. Am. Geophys. Union. Washington D.C.

Clark, R.N., T.V.V. King, M. Klejwa, G. Swayze and N. Vergo. 1990. High spectral resolution reflectance spectroscopy of minerals. *J. Geophys. Res.* **95:** 12653-12680.

Coughlin, B.R. and A.T. Stone. 1995. Nonreversible adsorption of divalent ions (Mn^{II}, Co^{II}, Ni^{II}, Cu^{II}, and Pb^{II}) onto goethite: effects of acidification, Fe^{II} addition and picolinic acid addition. *Environ. Sci. Technol.* **29:** 2445-2455.

Dang, Y.P., R.C. Dalal, D.G. Edwards and K.G. Tiller. 1994. Kinetics of zinc desorption from Vertisols. *Soil Sci. Soc. Am. J.* **58:** 1392-1399.

d'Espinose de la Callerie, J.-B., M. Kermarec and O. Clause. 1995. Impregnation of γ-alumina with Ni(II) or Co(II) ions at neutral pH: hydrotalcite-type coprecipitate formation and characterization. *J. Am. Chem. Soc.* **117:** 11471-11481.

Elzinga, E.J. and D.L. Sparks. 1999. Nickel sorption mechanisms in a pyrophyllite-montmorillonite mixture. *J. Colloid Interface Sci.* **213:** 506-512.

EPA, U.S. 1986. National Priorities List Fact Book. H.W. 7.3. U.S. EPA. Washington D.C.

Farley, K.J., D.A. Dzombak and F.M. Morel. 1985. A surface precipitation model for the sorption of cations on metal oxides. *J. Colloid Interface Sci.* **106:** 226-242.

Fendorf, S.E., G.M. Lamble, M.G. Stapleton, M.J. Kelley and D.L. Sparks. 1994a. Mechanisms of chromium (III) sorption on silica: 1. Cr(III) surface structure derived by extended x-ray absorption fine structure spectroscopy. *Environ. Sci. Technol.* **28:** 284-289.

Fendorf, S.E., G. Li and M.E. Gunter. 1996. Micromorphologies and stabilities of chromium (III) surface precipitates elucidated by scanning force microscopy. *Soil Sci. Soc. Am. J.* **60:** 99-106.

Fendorf, S.E., D.L. Sparks, G.M. Lamble and M.J. Kelley. 1994b. Applications of X-ray absorption fine structure spectroscopy to soils. *Soil Sci. Soc. Am.* **58:** 1583-1595.

Ford, R.G., A.C. Scheinost, K.G. Scheckel and D.L. Sparks. 1999. The link between clay mineral weathering and structural transformation in Ni surface precipitates. *Environ. Sci. Technol.* **33:** 3140-3144.

Ford, R.G. and D.L. Sparks. 2000. The nature of Zn precipitates formed in the presence of pyrophyllite. *Environ. Sci. Technol.* **34:** 2479-2483.

Förstner, U. 1995. Land contamination by metals - global scope and magnitude of problem. pp. 1-24. *In* H.E. Allen, C.P. Huang and G.W. Bailey (eds.) Metal Speciation and Contamination of Soil. CRC Press, Boca Raton, FL.

Gray, C.W., R.G. McLaren, A.H.C. Roberts and L.M. Condron. 1998. Sorption and desorption of cadmium from some New Zealand soils: effect of pH and contact time. *Aust. J. Soil Res.* **36:** 199-216.

Grossl, P.R., D.L. Sparks and C.C. Ainsworth. 1994. Rapid kinetics of Cu (II) adsorption/desorption on goethite. *Environ. Sci. Technol.* **28:** 1422-1429.

Harter, R., D. 1983. Effect of soil pH on adsorption of lead, copper, zinc, and nickel. *Soil Sci. Soc. Am. J.* **47:** 47-51.

Henderson, P.J., I. McMartin, G.E. Hall, J.B. Percival and D.A. Walker. 1998. The chemical and physical characteristics of heavy metals in humus and till in the vicinity of the base metal smelter at Flin Flon, Manitoba, Canada. *Environ. Geol.* **34:** 39-58.

Hering, J.G. 1995. Implication of complexation, sorption and dissolution kinetics for metal transport in soils. pp. 59-86. *In* H.E. Allen, C.P. Huang and G.W. Bailey (eds.) Metal Speciation and Contamination of Soil. CRC Press, Boca Raton, FL.

Hesterberg, D., D.E. Sayers, W. Zhou, G.M. Plummer and W. Robarge. 1997. X-ray absorption spectroscopy of lead and zinc speciation in a contaminated groundwater aquifer. *Environ. Sci. Technol.* **31.**

Hinz, C. and H.M. Selim. 1999. Kinetics of Zn sorption-desorption using a thin disk flow method. *Soil Sci.* **164:** 92-100.

Jenne, E.A. 1995. Metal adsorption onto and desorption from sediments: I. Rates. *In* H.E. Allen (ed.) Metal contaminated Aquatic Systems. CRC Press, Boca Raton, FL.

Kinniburgh, D.G., M.L. Jackson and J.K. Syers. 1976. Adsorption of alkaline earth, transition, and heavy metal cations by hydrous oxide gels of iron and aluminum. *Soil Sci. Soc. Am. J.* **40:** 796-799.

Koppelman, M.H. and J.G. Dillard. 1977. A study of the adsorption of Ni(II) and Cu(II) by clay minerals. *Clays Clay Miner.* **25:** 457-462.

Ladonin, D.V. 1997. Specific adsorption of copper and zinc by some soil minerals. *Eurasian Soil Sci.* **30:** 1478-1485.

Lehmann, R.G. and R.D. Harter. 1984. Assessment of copper-soil bond strength by desorption kinetics. *Soil Sci. Soc. Am. J.* **48:** 769-772.

Lin, Z. and R.B. Herbert Jr. 1997. Heavy metal retention in secondary precipitates frm a mine rock dump and underlying soil, Dalarna, Sweden. *Environ. Geol.* **33:** 1-12.

Lindsay, W.L. 1979. Chemical Equilibria in Soils. John Wiley and Sons, New York.

Lo, K.S.L. and J.O. Leckie. 1993. Kinetic studies of adsorption-desorption of Cd and Zn onto Al_2O_3/solution interfaces. *Wat. Sci. Tech.* **28:** 39-45.

Maguire, M., J. Slavek, I. Vimpany, F.R. Higginson and W.F. Pickering. 1981. Influence of pH on copper and zinc uptake by soil clays. *Aust. J. Soil Res.* **19:** 217-229.

Manceau, A. et al. 2000. Quantitative Zn speciation in smelter-contaminated soils by EXAFS spectroscopy. *Am. J. Sci.* **300:** 289-343.

Mattigod, S.V., A.S. Gibali and A.L. Page. 1979. Effect of ionic strength and ion pair formation on the adsorption of nickel by kaolinite. *Clays Clay Miner.* **27:** 411-416.

Maurice, P.A. 1998. Scanning probe microscopy of environmental surfaces. pp. 109-153. *In* P.M. Huang, N. Senesi and J. Buffle (eds.) Structure and Surface Reactions of Soil Particles. John Wiley and Sons, New York.

McBride, M. 1989. Reactions controlling heavy metal solubility in soils. Adv. Soil Sci. Springer-Verlag, New York.

McBride, M.B. 1982. Cu^{2+} adsorption characteristics of aluminum hydroxide and hydroxides. *Clays Clay Miner.* **30:** 21-28.

McBride, M.B. 1994. Environmental Chemistry of Soils. Oxford University Press, New York.

McLaren, R.G., C.A. Backes, A.W. Rate and R.S. Swift. 1998. Cadmium and cobalt desorption kinetics from soil clays: effect of sorption period. *Soil Sci. Soc. Am. J.* **62:** 332-337.

McLaren, R.G., D.M. Lawson and R.S. Swift. 1986. Sorption and desorption of cobalt by soils and soil components. *J. Soil. Sci.* **37:** 413-426.

Micera, G. et al. 1986. Zinc(II) adsorption on aluminum hydroxide. *Colloids Surf.* **17:** 389-394.

O'Day, P.A., S.A. Carroll and G.A. Waychunas. 1998. Rock-water interactions controlling zinc, cadmium, and lead concentration in surface waters and sediments, U.S. tri-state mining district. 1. Molecular identification using x-ray absorption spectroscopy. *Environ. Sci. Technol.* **32:** 943-955.

O'Day, P.A., C.J. Chisholm-Brause, S.N. Towle, G.A. Parks and G.E. Brown Jr. 1996. X-ray absorption spectroscopy of Co(II) sorption complexes on quartz (α-SiO_2) and rutile (TiO_2). *Geochim. Cosmochim. Acta* **60:** 2515-2532.

O'Day, P.A., G.A. Parks and G.E. Brown Jr. 1994. Molecular structure and binding sites of cobalt(II) surface complexes on kaolinite from X-ray absorption spectroscopy. *Clays Clay Miner.* **42:** 337-355.

Papelis, C. 1995. X-ray photoelectron spectroscopic studies of cadmium and selenite adsorption on aluminum oxide. *Environ. Sci. Technol.* **29:** 1526-1533.

Papelis, C. and K.F. Hayes. 1996. Distinguishing between interlayer and external sorption sites of clay minerals using X-ray absorption spectroscopy. *Colloids Surf., A* **107:** 89-96.

Pignatello, J.J. and B. Xing. 1996. Mechanisms of slow sorption of organic chemicals to natural particles. *Environ. Sci. and Technol.* **30:** 1-11.

Puls, R.W. and H.L. Bohn. 1988. Sorption of cadmium, nickel and zinc by kaolinite and montmorillonite suspensions. *Soil Sci. Soc. Am. J.* **52:** 1289-1292.

Puls, R.W., R.M. Powell, D. Clark and C.J. Eldred. 1991. Effects of pH, solid/solution ration, ionic strength, and organic acids on Pb and Cd sorption on kaolinite. *Water, Air, Soil, Pollut.* **57-58:** 423-430.

Roberts, D.R., F. R.G. and D.L. Sparks. 1999. Role of sorbent phase on the formation of Zn surface precipitates. *In Preparation.*

Sadiq, M. 1991. Solubility and speciation of zinc in calcareous soils. *Water, Air, Soil Pollut.* **57-58:** 411-421.

Sadiq, M. and C.G. Enfield. 1984. Solid phase formation and solution chemistry of nickel in soils: 2. Experimental. *Soil Sci.* **138:** 335-340.

Scheckel, K.G., A.C. Scheinost, R.G. Ford and D.L. Sparks. 2000. Stability of layered Ni hydroxide surface precipitates - a dissolution kinetics study. *Geochim. Cosmochim. Acta* **64:** 2727-2735.

Scheidegger, A.M., M. Fendorf and D.L. Sparks. 1996a. Mechanisms of nickel sorption on pyrophyllite: Marcoscopic and microscopic approaches. *Soil Sci. Soc. Am. J.* **60:** 1763-1772.

Scheidegger, A.M., G.M. Lamble and D.L. Sparks. 1996b. Investigation of Ni sorption on pyrophyllite: An XAFS study. *Environ. Sci. Technol.* **30:** 548-554.

Scheidegger, A.M., G.M. Lamble and D.L. Sparks. 1996c. The kinetics of nickel sorption on pyrophyllite as monitored by x-ray absorption fine structure (XAFS) spectroscopy. *J. Phys. IV* **4:** 773-775.

Scheidegger, A.M., G.M. Lamble and D.L. Sparks. 1997. Spectroscopic evidence for the formation of mixed-cation hydroxide phases upon metal sorption on clays and aluminum oxides. *J. Colloid Interface Sci.* **186:** 118-128.

Scheidegger, A.M. and D.L. Sparks. 1996a. A critical assement of sorption-desorption mechanisms at the soil mineral/interface. *Soil Sci.* **161:** 813-831.

Scheidegger, A.M. and D.L. Sparks. 1996b. Kinetics of the formation and the dissolution of nickel surface precipitates on pyrophyllite. *Chem. Geol.* **132:** 157-164.

Scheidegger, A.M., D.G. Strawn, G.M. Lamble and D.L. Sparks. 1998. The kinetics of mixed Ni-Al hydroxide formation on clays and aluminum oxides: a time-resolved XAFS study. *Geochim. Cosmochim. Acta* **62:** 2233-2245.

Scheinost, A.C., R.G. Ford and D.L. Sparks. 1999. The role of Al in the formation of secondary Ni precipitates on pyrophyllite, gibbsite, talc, and amorphous silica: a DRS study. *Geochim. Cosmochim. Acta* **63:** 3193-3203.

Schlegel, M.L., A. Manceau and L. Charlet. 1997. EXAFS study of Zn and ZnEDTA sorption at the goethite (α-FeOOH)/water interface. *J. Phys. IV* **7:** 823-824.

Schulthess, C.P. and C.P. Huang. 1990. Adsorption of heavy metals by silicon and aluminum oxide surfaces on clay minerals. *Soil Sci. Soc. Am. J.* **54:** 679-688.

Sheppard, M.I. and D.H. Thibault. 1992. Desorption and extraction of selected heavy metals from soils. *Soil Sci. Soc. Am. J.* **56:** 415-423.

Spadini, L., A. Manceau, P.W. Schindler and L. Charlet. 1994. Structure and stability of Cd^{2+} surface complexes on ferric oxides. 1. Results from EXAFS spectroscopy. *J. Colloid Interface Sci.* **168:** 73-86.

Spark, K.M., J.D. Wells and B.B. Johnson. 1995. Characterizing trace metal adsorption on kaolinite. *Eur. J. Soil Sci.* **46:** 633-640.

Sparks, D.L. 1995a. Environmental Soil Chemistry. Academic Press, San Diego.

Sparks, D.L. 1995b. Kinetics of metal sorption reactions. *In* H.E. Allen, C.P. Huang, G.W. Bailey and A.R. Bowers (eds.) Metal Speciation and Contamination of Soil. Lewis Publishers, Boca Raton.

Sparks, D.L. and P.M. Jardine. 1984. Comparison of kinetic equations to describe potassium-calcium exchange in pure and in mixed systems. *Soil Sci.* **138:** 115-121.

Sparks, D.L., A.M. Scheidegger, D.G. Strawn and K.G. Scheckel. 1999. Kinetics and Mechanisms of Metal Sorption at the Mineral-Water Interface. pp. 108-135. *In* D.L. Sparks and T.J. Grundl (eds.) Mineral-Water Interfacial Reactions. Kinetics and Mechanisms. Am. Chem. Soc., Washington, D.C.

Sposito, G. 1989. The Chemistry of Soils. Oxford University Press, New York.

Strawn, D.G., A.M. Scheidegger and D.L. Sparks. 1998. Kinetics and mechanisms of Pb(II) sorption and desorption at the aluminum oxide-water interface. *Environ. Sci. Technol.* **32:** 2596-2601.

Stumm, W. 1992. Chemistry of the Solid-Water Interface. Wiley, New York.

Theis, T.L. and R.O. Richter. 1980. Adsorption reactions of nickel species at oxide surfaces. pp. 73-96. Particulates in Water. Characterixation, Fate, Effects, and Removal. Am. Chem. Soc., Washington D.C.

Thompson, H.A. 1998. Dynamic ion partioning among dissolved, adsorbed, and precipitated phases in aging cobalt(II)/kaolinite/water systems. Ph.D. Thesis. Stanford University.

Tiller, K.G., J. Gerth and G. Brummer. 1984a. The relative affinities of Cd, Ni and Zn for different soil clay fractions and goethite. *Geoderma* **34:** 17-35.

Tiller, K.G., J. Gerth and G. Brummer. 1984b. The sorption of Cd, Zn and Ni by soil clay fractions: procedures for partition of bound forms and their interpretation. *Geoderma* **34:** 1-16.

Towle, S.N., J.R. Bargar, G.E. Brown Jr. and G.E. Parks. 1997. Surface precipitation of Co(II)(aq) on Al_2O_3. *J. Colloid Interface Sci.* **187:** 62-82.

Traina, S.J. and H.E. Doner. 1985. Co, Cu, and Ca soprtion by a mixed suspension of smectite and hydrous manganese dioxide. *Clays Clay Miner.* **33:** 188-122.

Trainor, T.P., G.E. Brown Jr. and G.A. Parks. 2000. Adsorption and precipitation of aqueous Zn(II) on alumina powders. *J. Colloid Interface Sci.* **231:** 359-372.

Uren, N.C. 1992. Forms, reactions, and availabilty of nickel in soils. pp. 141-203. *In* D.L. Sparks (ed.) Advances in Agronomy. Academic Press, Inc., Boca Raton.

Webb, S.M., G.G. Leppard and J.-F. Gaillard. 2000. Zinc speciation in a contaminated aquatic environment: characterization of environmental particles by analytical electron microscopy. *Environ. Sci. Technol.* **34:** 1926-1933.

Wu, J., D.A. Laird and M.L. Thompson. 1999. Sorption and desorption of copper on soil clay components. *J. Environ. Qual.* **28.**

Xu, Y., F.W. Schwartz and S.J. Traina. 1994. Sorption of Zn^{2+} and Cd^{2+} on hydroxyapatite surfaces. *Environ. Sci. Technol.* **28:** 1472-1480.

Yin, Y., H.E. Allen, C.P. Huang, D.L. Sparks and P.F. Sanders. 1997. Kinetics of mercury(II) adsorption and desorption on soil. *Environ. Sci. and Technol.* **31:** 496-503.

Yin, Y., H.E. Allen, Y. Li, C.P. Huang and P.F. Sanders. 1996. Adsorption of mercury(II) by soil: effects of pH , chloride, and organic matter. *J. Environ. Qual.* **25:** 837-844.

Zachara, J.M., J.A. Kittrick, L.S. Dake and J.B. Harsh. 1989. Solubility and surface spectroscopy of zinc precipitates on calcite. *Geochim. Cosmochim. Acta* **53:** 9-19.

Zhang, M., A.K. Alva, C. Li and D.V. Calvert. 1997. Chemical association of Cu, Zn, Mn, and Pb in selected sandy citrus soils. *Soil Sci.* **162:** 181-188.

Chapter 2

AN XAFS STUDY OF THE KINETICS AND MECHANISMS OF MIXED NICKEL ALUMINUM HYDROXIDE FORMATION AND DISSOLUTION ON A SOIL CLAY MINERAL FRACTION

2.1 Abstract

The kinetics of nickel (Ni) sorption on the clay fraction of a soil was monitored using X-ray absorption fine structure (XAFS) spectroscopy. The initial Ni concentration was 3 mM and studies were performed at pH 6.0, 6.8, and 7.5 with a solid/solution ratio of 10 g L^{-1} in 0.1 M $NaNO_3$. Initial Ni sorption kinetics were rapid at all pH values, but differed at each pH for longer reaction times. The sorption kinetics at pH 7.5 were characterized by an extremely rapid initial step with nearly 75% of Ni sorbed within 20 hours, followed by a slower step with nearly 100% of the Ni removed from solution within 150 hours. XAFS data analysis of the pH 7.5 sorption samples indicated the formation of a mixed Ni-Al layered double hydroxide (LDH) within 15 minutes. At pH6.8 the sorption increased more gradually over time and XAFS analysis indicated the formation of a Ni-Al LDH within two hours. At pH 6.0 the sorption was much slower, reaching a plateau after 50 h, with 20% of the total Ni removed from

solution. XAFS analysis revealed no LDH formation at pH 6.0. XAFS analyses are presented for Ni sorption on a whole soil and indicate a similar mixed Ni-Al phase is forming at pH 7.5 after 24 hours of reaction. The amount of Ni removed from the soil clay was monitored as a function of reaction time and pH. Samples reacted from one day to one month at pH 7.5 showed a decrease in the amount of Ni released as reaction time increased. Clay samples reacted with Ni at pH 6.0, 6.8 and 7.5 for one month demonstrated a trend in less Ni being removed from the surface with increasing reaction pH. These findings indicate that mixed metal precipitate formation occurs in heterogeneous clay systems and whole soils, and therefore they should be considered when predicting and modeling the fate of metals in subsurface environments. Moreover, these phases have been shown to less likely to undergo dissolution as reaction pH and time are increased.

2.2 Introduction

Contamination of surface and subsurface environments by heavy metals has established the need to understand metal-soil interactions. Heavy metals may enter soil and aquatic environments via sewage sludge application, mine waste, industrial waste disposal, atmospheric deposition, and application of fertilizers and pesticides (Förstner, 1995). It is imperative to understand the sorption mechanisms by which metals such as As, Cd, Cr, Cu, Ni, or Pb partition to soil and soil components to aid in the development of remediation strategies and the formulation of models designed to predict the fate and mobility of contaminant metals.

Macroscopic studies have been performed to determine the effect of ionic strength (I), initial metal concentration, pH, solid/solution ratio, and competing ligands on the sorption of metals to soils, clay minerals, and metal oxides. (Bruemmer et al., 1988; Mattigod et al., 1979; Puls et al., 1991; Tiller et al., 1984; Ziper et al., 1988). While such macroscopic approaches are valuable in characterizing sorption behavior, they cannot elucidate molecular reactions (Sparks, 1995). In recent years, the application of advanced spectroscopic and microscopic tools has helped define the mechanisms controlling contaminant reactions in soils and aquatic environments (Bertsch and Hunter, 1998; Brown Jr. et al., 1995). X-ray absorption fine structure (XAFS) spectroscopy has been a valuable tool to characterize sorption mechanisms of metals sorbed to single-component metal oxides and reference clay minerals (Bargar et al., 1997a; Bargar et al., 1997b; Charlet and Manceau, 1992; Charlet and Manceau, 1994; Chisholm-Brause et al., 1990; O'Day et al., 1994; O'Day et al., 1996; Papelis and Hayes, 1996; Scheidegger et al., 1998; Spadini et al., 1994; Towle et al., 1997) and to determine the speciation of contaminants in soils (Manceau et al., 1996; Morris et al., 1996; O'Day et al., 1998; Pickering et al., 1995).

Recent XAFS studies have shown the formation of precipitates during metal sorption to mineral and oxide surfaces over rapid time scales, at pH levels undersaturated with respect to pure metal hydroxide solubility, and at metal surface coverages below a theoretical monolayer coverage (Charlet and Manceau, 1992; Chisholm-Brause et al., 1990; d'Espinose de la Callerie et al., 1995; Fendorf et al., 1994; O'Day et al., 1994a; O'Day et al., 1996; Scheidegger et al., 1996; Towle et al.,

1997; Weesner and Bleam, 1997; Xia et al., 1997). For example, Scheidegger et al. (1996) used XAFS to discern the local atomic structure of Ni sorbed on pyrophyllite (an Al-bearing 2:1 clay mineral). They observed the presence of a mixed Ni-Al hydroxide phase at low surface loading and at reaction conditions undersaturated with respect to the formation of $Ni(OH)_2(s)$. Towle et al. (1997) demonstrated that Co sorption on Al_2O_3 resulted in the formation of a layered double-hydroxide (LDH) phase containing both Co and substrate-derived Al ions from solutions undersaturated with respect to a pure Co hydroxide. Precipitate phases may also form in the presence of non-Al bearing minerals as demonstrated in a study by Scheinost et al. (1999). Using diffuse reflectance spectroscopy (DRS) they showed that α-$Ni(OH)_2$ formed upon Ni sorption to both talc and silica. The above studies demonstrate that the sorbent may determine the structure of the metal precipitate phase that forms upon metal sorption.

While the previously mentioned metal sorption studies have established that metal hydroxide precipitates may form on model clay minerals and synthesized oxides under specific reaction conditions, the results are difficult to apply to soil environments where multiple clay minerals are present and a range of pH values may occur. In addition, soil systems are rarely, if ever, at equilibrium making it important to study metal sorption reactions over a range of reaction times (Sparks, 1989). Characterizing metal sorption mechanisms on soils and sediments using XAFS spectroscopy has proven difficult since heterogeneous sorbents possess a broad array of sorption sites, each possessing a unique spectroscopic signature (O'Day et al., 1998). Isolating

specific fractions of whole soils for metal sorption studies may reduce these complications.

In order to determine the likelihood of metal precipitate formation in soils, the sorbent phase should be heterogeneous in order to simulate a soil environment while also being fully characterized to ease in the application of an analytical technique such as XAFS. Since in many soils the most reactive mineral sites for sorption are present in the < 2 μm size fraction, the clay fraction provides a good model for studying sorption in the mineral fraction of the whole soil while the removal of competing sorbents such as organic matter and amorphous metal oxides enables one to better identify specific metal-mineral interactions. The research approach was to make the progression from previous studies using model clay minerals to a soil clay mineral fraction and finally to a whole soil.

The objectives of this study were to (1) determine the conditions under which metal hydroxide precipitates form upon Ni sorption to a well-characterized soil clay fraction and the whole soil from which the clay was derived; and (2) determine the stability of these phases once they are formed as a function of reaction pH and time.

2.3 Materials and Methods

2.3.1 Materials

The soil used in this study was the Ap horizon of a Matapeake silt loam (Typic-Hapludult). For the whole soil experiments the <2mm fraction was isolated. For the clay fraction experiments a series of treatment steps were used to isolate the <2μm fraction.

Organic matter was removed by treatment with 4-6% NaOCl adjusted to pH 9.5 at a temperature of 70°C (Lavkulich and Wiens, 1970). Next, free Fe- and Al- oxides were extracted using the sodium dithionite-citrate-bicarbonate method (Mehra and Jackson, 1960). The <2μm size fraction was separated by centrifugation and decantation. The clay fraction was then Na-saturated by washing three times with 1.0 M NaCl followed by dialysis in deionized-distilled (DDI) water to remove excess salts. The clay fraction was then freeze dried prior to characterization. The purification procedures of the whole soil resulted in a relatively pure mixture of aluminosilicate clay minerals from the collected <2μm fraction.

The mineral suite of the soil was determined by powder X-ray diffraction using a Philips Norelco 1720 instrument equipped with Cu Kα radiation (40kV, 40mA). Data were collected between 3° and 70° 2θ with a 0.04° step and a counting time of 5 s per step. The mineralogy of the soil was as follows: Al-hydroxy interlayered vermiculite (HIV), ≥ kaolinite, >> mica. Minor amounts of gibbsite and quartz were also present. Thermal gravimetric analysis (TGA) and differential scanning calorimetry (DSC) indicated slightly more HIV than kaolinite (Karanthanasis and Harris, 1994). The total surface area of the <2mm fraction, as determined by the ethylene glycol monoethyl ether (EGME) method, was 15.5 $m^2 g^{-1}$ (Carter et al., 1986). The total surface area of the <2μm fraction, as determined by EGME, was 96.7 $m^2 g^{-1}$, and the external surface area as determined by BET-N_2 analysis was 41.1 $m^2 g^{-1}$ (Carter et al., 1986). The CEC of the clay as determined by Ca/Mg exchange at pH 6.5 was 60.5 $cmol_c kg^{-1}$ (Jackson, 1956).

2.3.2 Macroscopic Sorption Studies

Four separate reaction vessels were used to study the influence of pH on the rate of Ni sorption to the soil clay fraction. The pH values were determined by first constructing a pH adsorption edge on the clay fraction under the initial reaction conditions. A pH edge was constructed by reacting the soil clay with a solution containing an initial concentration of 3 mM Ni from a 0.1 M $Ni(NO_3)_2$ stock solution in a background of 0.1 M in $NaNO_3$ under an N_2-purged atmosphere. The Ni from the stock solution was gradually added (aliquot added every 3 minutes) in 100-μL portions using an automatic pipette. This gradual addition ensured that the solution was not locally oversaturated with respect to $Ni(OH)_2$. After all the Ni was added, ten-mL subsamples were removed from the stirring Ni-clay slurry and transferred into 15-mL tubes and the pH was adjusted down or up using either 0.1 M HNO_3 or 0.1 M NaOH, respectively. Various portions of acid or base were added in order to ensure a broad range pH values. After reacting for 24 hours on an end-over-end shaker the solids were separated from the solution via centrifugation (10,000 RPM for 10 minutes) and the samples analyzed for Ni using inductively coupled plasma (ICP) emission spectrometry.

Prior to initializing Ni sorption kinetics, the solids were hydrated for 24 hours by suspending approximately 5-g of soil clay or whole soil in 500-mL of 0.1 M $NaNO_3$ solution adjusted to pH 6.0, 6.8, or 7.5 using either 0.1 M HNO_3 or 0.1 M NaOH. For the whole soil study only pH 7.5 was selected to ensure sufficient metal loading and a strong XAFS signal as the heterogeneity of the soil results in a high level of spectral

noise. After hydration of the clay or soil, Ni from a 0.1 M $Ni(NO_3)_2$ stock solution was added in 100-μL aliquots to achieve initial conditions of $[Ni]_{initial}$ = 3 mM, I = 0.1 M, and a solid/solution ratio = 10 g L^{-1}. As for the sorption edge, Ni was added gradually to ensure local oversaturation of $Ni(OH)_2$ did not occur.

The initial Ni concentration of 3 mM was selected to directly compare this study to the work of Scheidegger et al. (1998). Mattigod et al. (1997) extensively studied the solubility of crystalline $Ni(OH)_2$ over a range of pH values and reaction times. Their results verify that under the reaction conditions similar to those found in this study (pH = 7.5, $[Ni]_o$ = 3mM), the solution was undersaturated with respect to $Ni(OH)_2$. Therefore it was concluded that the 3 mM $[Ni]_o$ was below the concentration required for the formation of $Ni(OH)_2$ in solution at all pH values used in this study and therefore the removal of Ni from solution was not due to the formation of $Ni(OH)_2$. Solubility data for mixed Ni-Al hydroxides is lacking in the literature and is therefore an area in need of investigation. Thompson et al. (1999) showed that cobalt hydrotalcites were the dominant stable phase at near-neutral pH values compared to Co hydroxide precipitates. Only above a certain threshold pH (> 7.5) was cobalt hydroxide a stable precipitate. They concluded that the availability of Al seemed to be a major factor in whether or not a Co hydrotalcite phase or a Co hydroxide phase formed. Similarly, one would expect a Ni-Al layer double hydroxide phase to be more stable than a $Ni(OH)_2$ precipitate under the reaction conditions studied here. To be certain of these assumptions, several samples were also prepared at an initial concentration of 1.5 mM Ni and yielded similar results.

During the first 48 h of sorption, the pH was held constant at 6.0, 6.8 or 7.5 by automatic titration with 0.1 M NaOH or 0.1 M HNO_3 using a pH-stat apparatus. The suspension was stirred at 350 rpm with a teflon stir bar, the temperature was maintained at 25°C using a water bath, and the vessels were purged with N_2 to eliminate CO_2. After 48 h, the vessels were placed on an orbital shaker operating at a speed of 150 orbits min^{-1} and the pH was adjusted daily with either 0.1 M NaOH or 0.1 M HNO_3. For reaction times up to 700 hours, 5-mL subsamples were transferred to centrifuge tubes and centrifuged at 12,000 RPM for 4 min. The supernatant was filtered through a 0.2 μm membrane filter and analyzed for dissolved Ni by ICP. The amount of sorbed Ni was calculated as the difference between the initial and final Ni concentration in solution. For XAFS analysis solids were isolated from 40-mL aliquots and were washed with 40-mL of DDI water to remove entrained solution. Insignificant quantities of sorbed Ni were removed from the soil clay by this washing procedure. Short-term samples (15 minutes – 2 hours) for XAFS analysis were prepared in a laboratory adjacent to the beamline (point of collection for XAFS spectra) in order to avoid possible storage effects.

2.3.3 Desorption Studies

Desorption studies were carried out on selected Ni-reacted clay samples to determine the reversibility of Ni sorption as a function of both time and reaction pH. To study the effect of time on Ni reversibility, samples reacted at pH 7.5 for a period of 1 hour, 1 day, 1 month and 6 months were used. For the pH study, samples reacted for

1 month at pH 6.0, 6.8 and 7.5 were selected. In both cases sample suspensions were removed from the reaction vessels, centrifuged, and supernatants decanted followed by washing the samples in DDI H_2O to remove any entrained solution. Na-saturated cation exchange resin beads were used for the desorption study. A 0.4 g portion of Na-saturated, dried (60° C) cation exchange resin beads (Dowex® HCR-W2; 16-40 micron bead size; CEC = 4.8 meq g^{-1}) were added to the moist pastes and suspended in a solution of 0.1 M $NaNO_3$ and 0.5 M HEPES buffer (to maintain pH to desired value), adjusted to the pH and solid:solution ratio of the original reaction vessel. The resin beads served as a sink for any Ni^{2+} ions removed from the clay surface and therefore eliminated any re-adsorption of Ni^{2+} to the clay. The samples were placed on a reciprocating shaker for a set amount of time (minutes – days) followed by separating the resin beads from the clay suspension using a wire mesh filter. Upon separation, the suspension pH was measured and it was found that the HEPES buffer maintained the pH to within ± 0.2 pH units. The Ni^{2+} adsorbed on the resin beads was removed by washing the beads with 10-mL of 7 M HCl. The amount of Ni^{2+} removed from the resin beads was taken to be the amount removed from the clay mineral fraction since no Ni^{2+} remained in the supernatant.

2.3.4 XAFS Analysis

XAFS spectra were collected for the Ni-reacted clay and soil samples at beamline X-11A at the National Synchrotron Light Source (NSLS) at Brookhaven National Laboratory, Upton, New York. The electron beam energy was 2.5 GeV with a

beam current between 120 and 240 mA. The monochromator consisted of two parallel Si (111) crystals with an entrance slit width of 0.5 mm. Higher order harmonics were removed by detuning I_o by 25% at the Ni K-edge (8333 eV). The samples were placed in Al holders and held in place with Kapton® tape. Samples were kept at 77 K with a cold finger to reduce dampening of the XAFS oscillation by thermal disorder (Scheidegger et al., 1996). Samples were also collected at room temperature in order to verify that there were no differences in structural information derived from collecting XAFS spectra at room temperature compared to collection at 77 K. Interference from the Cu cold finger was eliminated by covering the exposed portions with Pb foil. The data were collected in fluorescence mode using a Stern-Heald type detector filled with Ar gas and equipped with a 3 μm Co filter (Lytle et al., 1984).

The data analysis program MacXAFS was used for background subtraction and Fourier filtering of the XAFS data (Bouldin et al., 1995). Three scans were averaged for each sample and the energy position was normalized relative to E_o for Ni metal. The position of E_o within sample spectra was assigned to the maximum of the derivative. The χ-function was extracted from the raw data using a linear pre-edge background and a spline post-edge background. The data were then converted from energy to k-space. The χ-functions were weighted by k^3 in order to compensate for dampening of the XAFS amplitude with increasing k. The data were then Fourier transformed ($\Delta k = 3.2 - 14$ Å^{-1}) to yield a radial structure function (RSF).

The k^3-weighted spectra were fit in k-space using XFTools included in MacXAFS (Boyanov, 1997). Single-shell data and phase shifts for Ni-Ni, Ni-O, and

Ni-Al backscatterers were generated using FEFF 6.0 (Zabinsky et al., 1995). The input file was created with the program ATOMS using the β-$Ni(OH)_2$ structure with two of the Ni atoms at 3.117 Å replaced by Al atoms (Greaves and Thomas, 1986). The theoretical spectra were Fourier filtered over ranges identical to those used in the fits (Scheidegger et al., 1998). Multi-shell k-space fits were performed over a k-range of 3.2 – 14 Å and an R-range of 1.07 – 3.12 Å. For the Ni-reacted samples, the Debye-Waller factors for the Ni-Ni and Ni-Al shells were fixed at 0.005. This value has previously been used in XAFS studies to fit hydroxide precipitates containing both Ni-Al and Co-Al bonds (Scheidegger et al., 1998; Strawn et al., 1998; Towle et al., 1997). In addition, the Ni-Ni and Ni-Al bond distances were constrained to be equal during the fitting process. These constraints reduced the number of free parameters to 8. A single edge shift (ΔE_o) was minimized for all shells during the curve-fitting procedure.

The errors in the fitting were estimated based on the findings of other reseachers investigating systems with similar metal hydroxide formation (d'Espinose de la Callerie et al., 1995; O'Day et al., 1994b; Scheidegger et al., 1998). For example, Scheidegger et al. (1998) compared XAFS-derived structural parameters of a Ni-Al coprecipitate with parameters derived by XRD. They found R_{Ni-O} and R_{Ni-Ni} to be accurate to ±0.020 Å, the N_{Ni-O} and N_{Ni-Ni} values to be accurate to ±20%, the $N_{Ni-Al\ to}$ be accurate to ±60%, and R_{Ni-Al} to be accurate to ± 0.06 Å. These error estimates were applied to this research.

2.4 Results and Discussion

2.4.1 Macroscopic Ni Sorption

The sorption of Ni as a function of reaction pH is shown in Figure 2.1. Typical of transition metal sorption behavior on clay mineral surfaces, Ni sorption is minimal at low pH values (< 5.0) and increases with increasing pH with 100% of the initial Ni added being adsorbed above pH 8.0. The sorption edge position (point at which Ni sorption rises over a narrow pH range) is at a pH value of approximately 7.0. Based on the sorption edge results, three pH values were selected to perform sorption kinetic experiments combined with XAFS analysis: a low pH value where some Ni adsorption occurred (pH 6.0), a moderate pH value near the 'edge' of the pH edge (pH 6.8), and a high pH value where nearly all Ni was adsorbed within 24 hours (pH 7.5). The pH value of 7.5 also provided a direct comparison to previous studies.

The time-dependence of Ni sorption at pH 6.0, 6.8 and 7.5 on the soil clay fraction is shown in Figure 2.2. An initial rapid uptake occurred at all pH values. However, after several hours the rate of sorption at the various pH values differed. At any given time the Ni loading level on the soil clay surface increased with increasing pH. Figure 2.2a shows Ni sorption within 25 h at each pH value, while Figure 2.2b shows Ni sorption over the entire reaction period. At pH 6.0, 10% of the initial Ni was sorbed in less than one hour and this value increased to 20% within 500 hours. Although this is a large relative increase, the total amount removed is small compared to sorption at pH 6.8 and 7.5. At pH 6.8 the Ni sorption proceeded quite rapidly initially, with 40% of the initial Ni sorbed in 10 hours, followed by a more gradual

sorption period in which 80% of the initial Ni was sorbed within 800 hours. The kinetics at pH 7.5 were characterized by an extremely rapid initial step with nearly 75% of Ni sorbed after 12 hours, followed by a much slower sorption region where nearly 100% of the Ni was removed from solution within 200 hours.

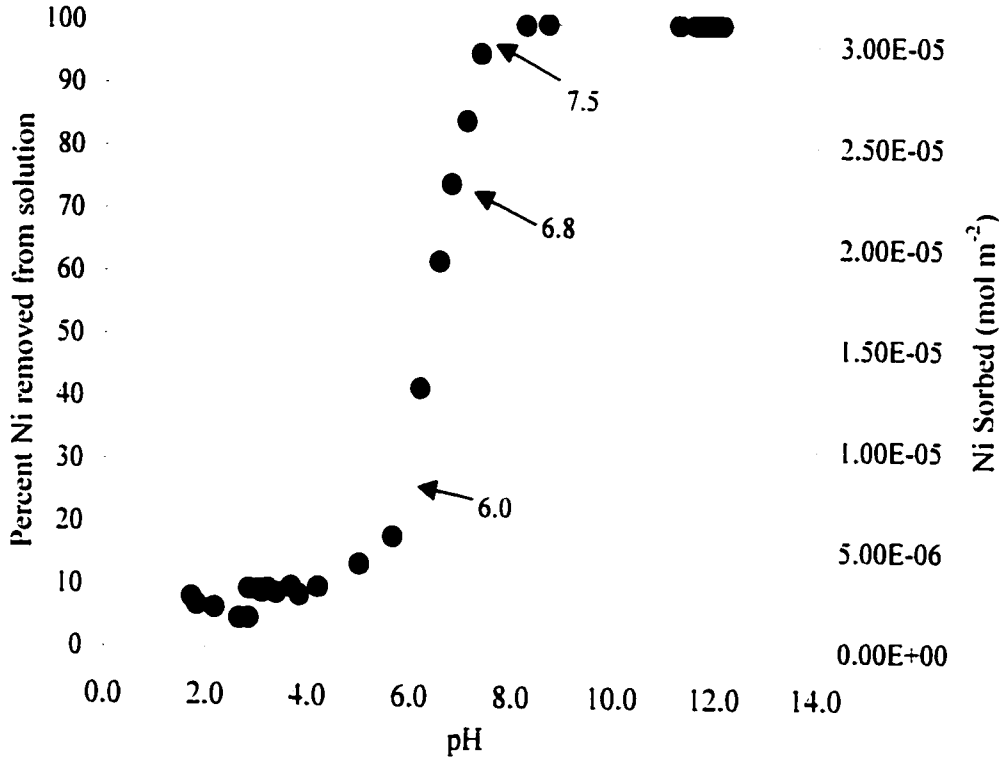

Figure 2.1 Nickel sorption edge on Matapeake soil clay fraction at an initial Ni(II) concentration of 3 mM. I = 0.1 M in $NaNO_3$, and 10 g L^{-1} solid/solution ratio. Arrows represent the pH values selected to perform the sorption kinetic and XAFS studies.

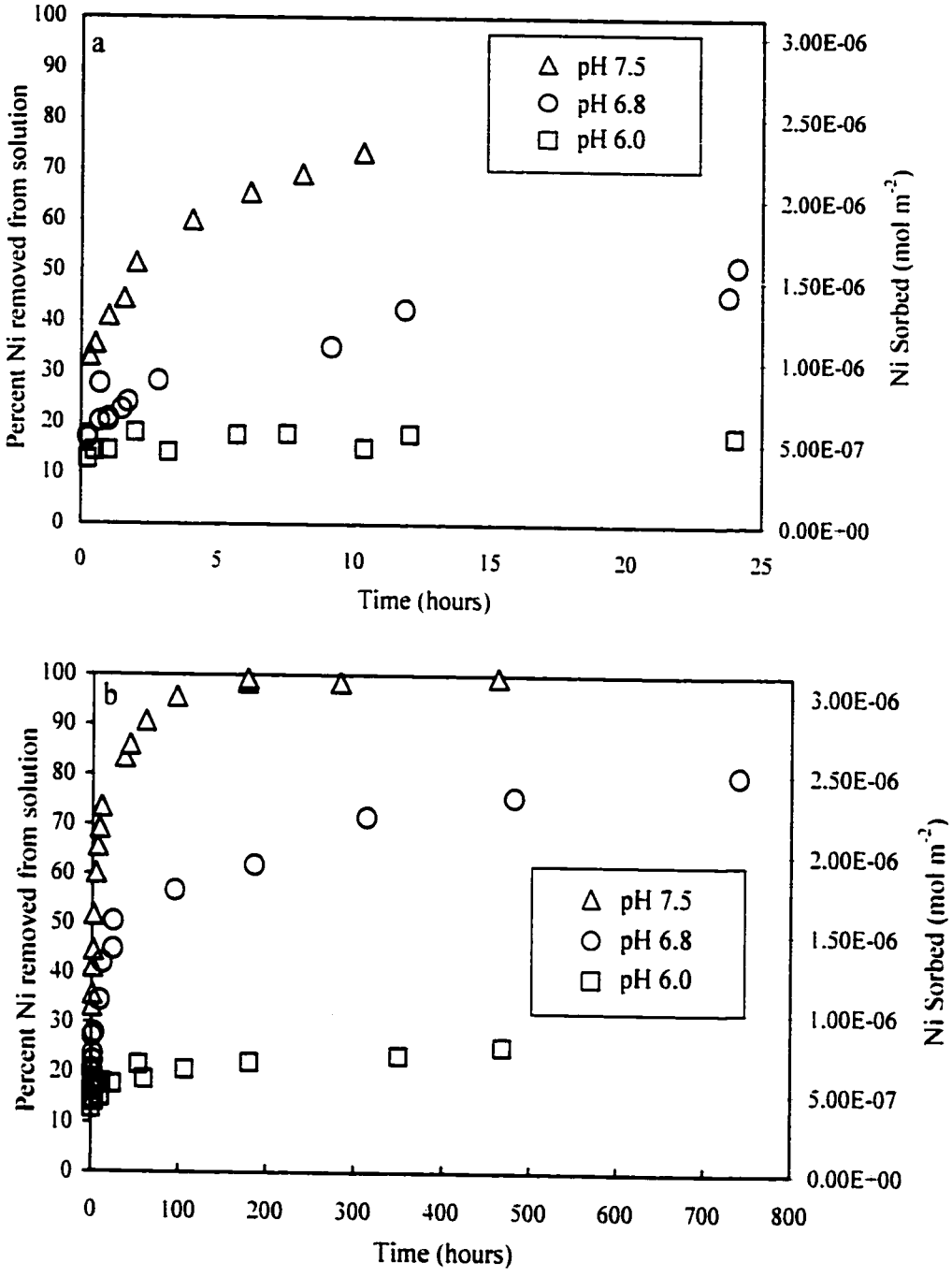

Figure 2.2 Ni sorption kinetics on soil clay fraction at pH = 6.0, 6.8 and 7.5. a) Ni sorption within 25 hours. b) Ni sorption over entire reaction period. I = 0.1 M in $NaNO_3$, $[Ni]_o$ = 3mM, solid/solution = 10g L^{-1}.

2.4.2 XAFS Analyses of Ni-reacted Clay at pH 7.5

The k^3-weighted, normalized, background-subtracted chi functions for Ni sorbed on the soil clay at pH 7.5 for different times are presented in Figure 2.3a. As reaction time increased from 10 minutes to 120 hours, the amount of Ni on the clay mineral surface increased leading to more pronounced oscillations in the XAFS signal at higher energies (> 8 $Å^{-1}$). At short reaction times (15 minutes – 90 minutes) spectral noise was more pronounced due to a lower Ni loading on the surface. The spectra were Fourier transformed to produce the radial structure functions shown in Figure 2.3b. These spectra are uncorrected for phase shift. The first peak at R ≅ 1.7 Å represents the first coordination shell of Ni and remains relatively constant in amplitude and position with increasing reaction time. A second peak at R ≅ 2.8 Å appears within 15 min and continuously increases in magnitude within 120 h. This peak is likely due to contributions from second nearest Ni neighbors around the central absorber, and indicates that some type of Ni precipitate is forming and continuing to grow over time.

Comparison of the k^3-weighted XAFS functions for the Fourier back-transformed spectra to the theoretical spectra derived by fitting theoretical Ni-O, Ni-Ni, and Ni-Al scattering paths to the raw data is shown in Figure 2.4. The comparison indicates that the theoretical paths provide a good representation of the experimental data. The structural parameters derived from the fits are presented in Table 2.1. Analysis shows that the first shell is consistent with Ni surrounded by ≅ 6 O atoms, indicating that Ni is in an octahedral coordination environment. The Ni-O bond

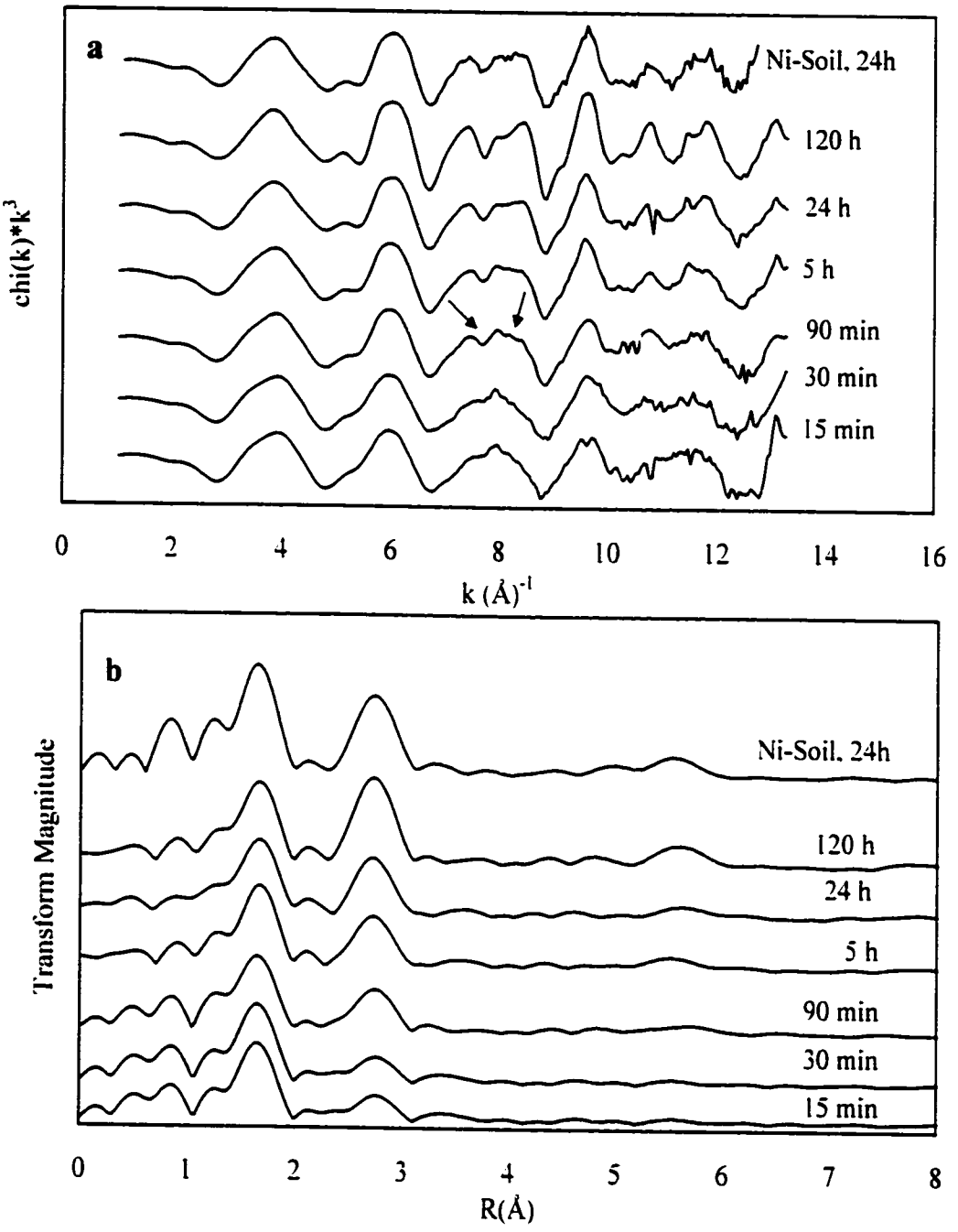

Figure 2.3 Results of XAFS experiments performed at pH 7.5. a) k^3-weighted, normalized, background-subtracted chi-functions for Ni sorbed on soil clay for different times and whole soil. b) Fourier transforms of chi-functions in Figure 2a, uncorrected for phase shift. The arrows in (a) show evidence of LDH formation.

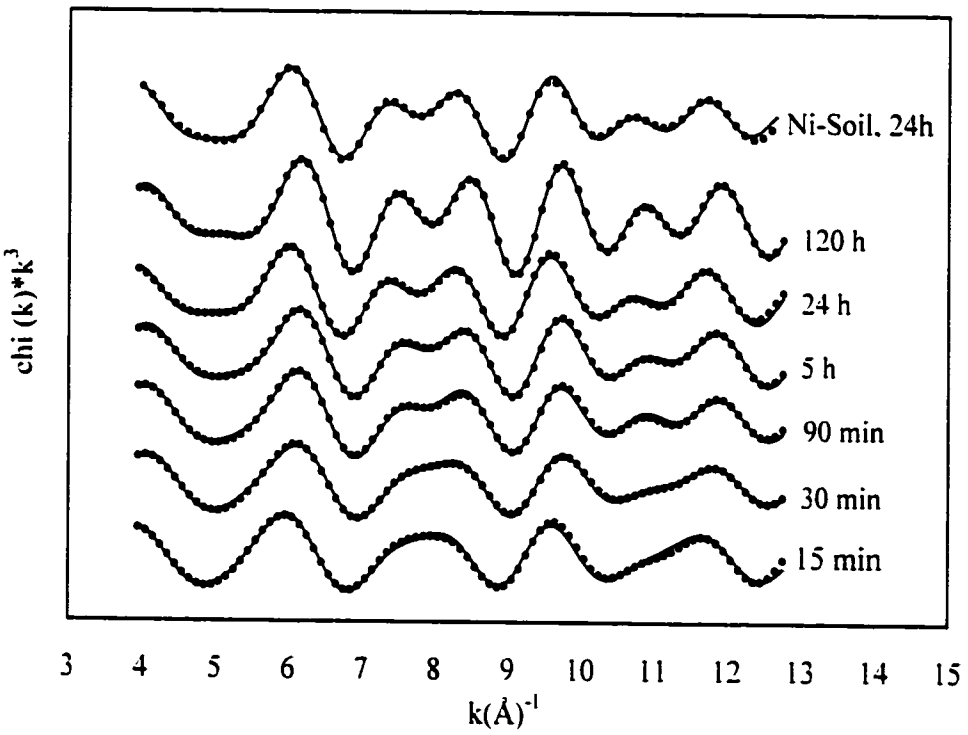

Figure 2.4 Experimental k^3-weighted XAFS data (solid line) of Fourier back-transformed spectra in comparison to theoretical spectra (dotted line) using multi-shell least-squares fitting for pH 7.5 samples.

distance (R_{Ni-O}) is approximately 2.05 Å in all samples and the coordination number (N) essentially remains constant with time. Analysis of the second shell indicates the presence of a second-neighbor Ni atom around the central absorber at a bond distance ≅ 3.05 Å. Al was included in fitting the second shell based on studies by Scheinost et al. (1999) investigating Ni sorption on Al-bearing and non Al-bearing metal oxides and reference clay mineral. Using DRS they showed that if Al was present in the sorbent structure (pyrophyllite, gibbsite) a Ni-Al layered double hydroxide (LDH) formed. In contrast, Ni sorption to non Al-bearing minerals (talc, silica) resulted in the formation of α-$Ni(OH)_2$ absent of any Al. Since the clay fraction contains potential sources of soluble Al (kaolinite, Al-HIV, gibbsite), it is safe to assume that Al was incorporated into the metal precipitates that formed. The fitting results supported this initial assumption. The N_{Ni-Ni} increased from 0.8 after 15 minutes to 5.6 after a reaction time of 120 hours. These results show that formation of a precipitate was occurring within 15 minutes at pH 7.5. The Ni-Ni bond distance in these samples resembles the Ni-Ni bond distance in a Ni-Al LDH phase (d'Espinose de la Callerie et al., 1995). For both Ni-Al LDH and the sorption samples, the Ni-Ni bond distance is shorter than the Ni-Ni bond in α-$Ni(OH)_2$ (R = 3.08 Å) (d'Espinose de la Callerie et al., 1995). This indicates that a mixed Ni-Al layered double hydroxide may be forming upon Ni sorption to the soil clay fraction.

Another line of evidence in proving the formation of a Ni-Al LDH rather than $Ni(OH)_2$ can be found in the unfiltered chi(k)*k^3 data (Figure 2.3a). According to Scheinost and Sparks (2000), an XAFS beat pattern at about 8 $Å^{-1}$ can be used as

Table 2.1 XAFS-derived structural parameters of Ni sorbed on soil clay at pH 6.0, 6.8, and 7.5 and for Ni-bearing minerals.

	First Shell			Second Shell					
	Ni-O			Ni-Ni			Ni-Al		
pH 7.5	R(Å)[a,d]	N[b,c]	$\Delta\sigma^2$ (Å^2)[c,e]	R(Å)[d,i]	N[c]	$\Delta\sigma^2$ (Å^2)[e,h]	R(Å)[f,i]	N[g]	$\Delta\sigma^2$ (Å^2)[e,h]
15 minutes	2.06	5.7	0.0027	3.05	0.8	0.005	3.05	0.9	0.0050
30 minutes	2.05	6.0	0.0040	3.05	1.7	0.005	3.05	1.2	0.0050
90 minutes	2.05	6.9	0.0054	3.06	2.5	0.005	3.06	0.8	0.0050
5 hours	2.05	5.4	0.0030	3.06	3.4	0.005	3.06	1.5	0.0050
24 hours	2.05	5.2	0.0028	3.06	4.0	0.005	3.06	1.1	0.0050
120 hours	2.05	5.8	0.0034	3.05	5.6	0.005	3.05	1.8	0.0050
pH 6.8									
15 minutes	2.05	5.9	0.0032						
2 hours	2.05	5.7	0.0033	3.05	1.6	0.0050	3.05	0.9	0.0050
72 hours	2.05	5.4	0.0028	3.04	3.3	0.0050	3.04	1.6	0.0050
pH 6.0									
2 hours	2.05	5.6	0.0052						
72 hours	2.06	5.7	0.0046						
References[j]									
α-Ni(OH)$_2$	2.03	5.1	0.0055	3.08	5.1	0.0079			
Ni-Al LDH	2.050	6.5	0.0073	3.06	4.8	0.0078	3.06	1.4	0.0078

[a] Interatomic distance; [b]Coordination number; [c]Debye-Waller factor

Fit quality estimated accuracy: [d]±0.02Å, [e]±20%, [f]±0.06Å, [g]±60%

[h] The Debye-Waller factors were fixed at 0.005Å

[i]Ni-Ni and Ni-Al distances constrained to be equal during fitting

[j]d'Espinose de la Caillerie et al., 1995

fingerprint to unequivocally distinguish LDH from α-type hydroxides. They attributed the beat pattern to multiple scattering at metal ion/Al ratios between 1 and 4. The beat pattern appears as a split in the oscillation of the peak, a feature absent in the case of α-$Ni(OH)_2$. In sorption samples, this feature can be seen after 90 minutes at pH 7.5, suggesting in the first 90 minutes of the reaction the amount of Al present in the precipitate is insufficient to yield the distinguishing spectroscopic feature.

The XAFS results obtained in this study closely resemble the findings of Scheidegger et. al. (1998) for Ni sorption on specimen clay minerals and aluminum hydroxide. The formation of precipitates was observed in the presence of pyrophyllite, kaolinite, gibbsite, and montmorillonite at pH 7.5. The precipitate was identified as a mixed Ni-Al LDH by XAFS spectroscopy. It was hypothesized that coprecipitated Al was derived from the sorbent structure. While the sorbent in these experiments was more heterogeneous and complex in nature than the sorbents used in the study by Scheidegger et al. (1998), the XAFS data indicate that a precipitate phase formed within 15 minutes. Other sorption processes may be occurring concurrently with precipitation as the soil clay has Al-OH and Si-OH sites as well as permanent-charge sites where Ni can potentially be sorbed as innersphere and outersphere complexes, respectively. The XAFS data indicated Ni was predominately present in a precipitated phase, however some Ni was most likely present in an adsorbed, inner-sphere complex. The adsorption of Ni is a precursor to the formation of a Ni-Al LDH phase and was therefore an important step in the first several minutes. The high ionic strength used most likely promoted inner-sphere complexation over outer-sphere complexation. The growth of

the Ni-Ni peak over time (Table 2.1) indicates that precipitate formation is an important mechanism in early reaction times and dominates Ni uptake at longer reaction times.

2.4.3 XAFS Analyses of Ni-reacted Clay at pH 6.8

The k^3-weighted, normalized, background-subtracted chi functions for Ni sorbed on the soil clay at pH 6.8 for different times are shown in Figure 2.5a. With increasing reaction time (15 min to 72 hours), a beat pattern developed within the XAFS spectra indicating multiple frequencies from second shell backscattering. The radial structure functions (uncorrected for phase shift) are shown in Figure 2.5b. Similar to the pH 7.5 system, the first peak at R ≅ 1.7 Å remains relatively constant in amplitude with increasing reaction time. The second peak at R ≅ 2.8 Å does not appear until after 2 hours of reaction time. Similar to the pH 7.5 system, this second shell peak increases in magnitude over time.

Comparison of the k^3-weighted XAFS functions for the Fourier back-transformed spectra to the theoretical spectra derived by fitting theoretical Ni-O, Ni-Ni, and Ni-Al scattering paths to the raw data is shown in Figure 2.6. The comparison indicates that the theoretical paths provide a good representation of the experimental data. The structural parameters derived from the fits are presented in Table 2.1. For the 15-minute sample a multishell fit was not reasonable since there was no higher RSF peak and it did not improve the fit quality. At this early time inner-sphere adsorption complexation is the primary mode of Ni removal from solution. Analysis shows the same results for the Ni-O shell as was found in the pH 7.5 system for all samples. For

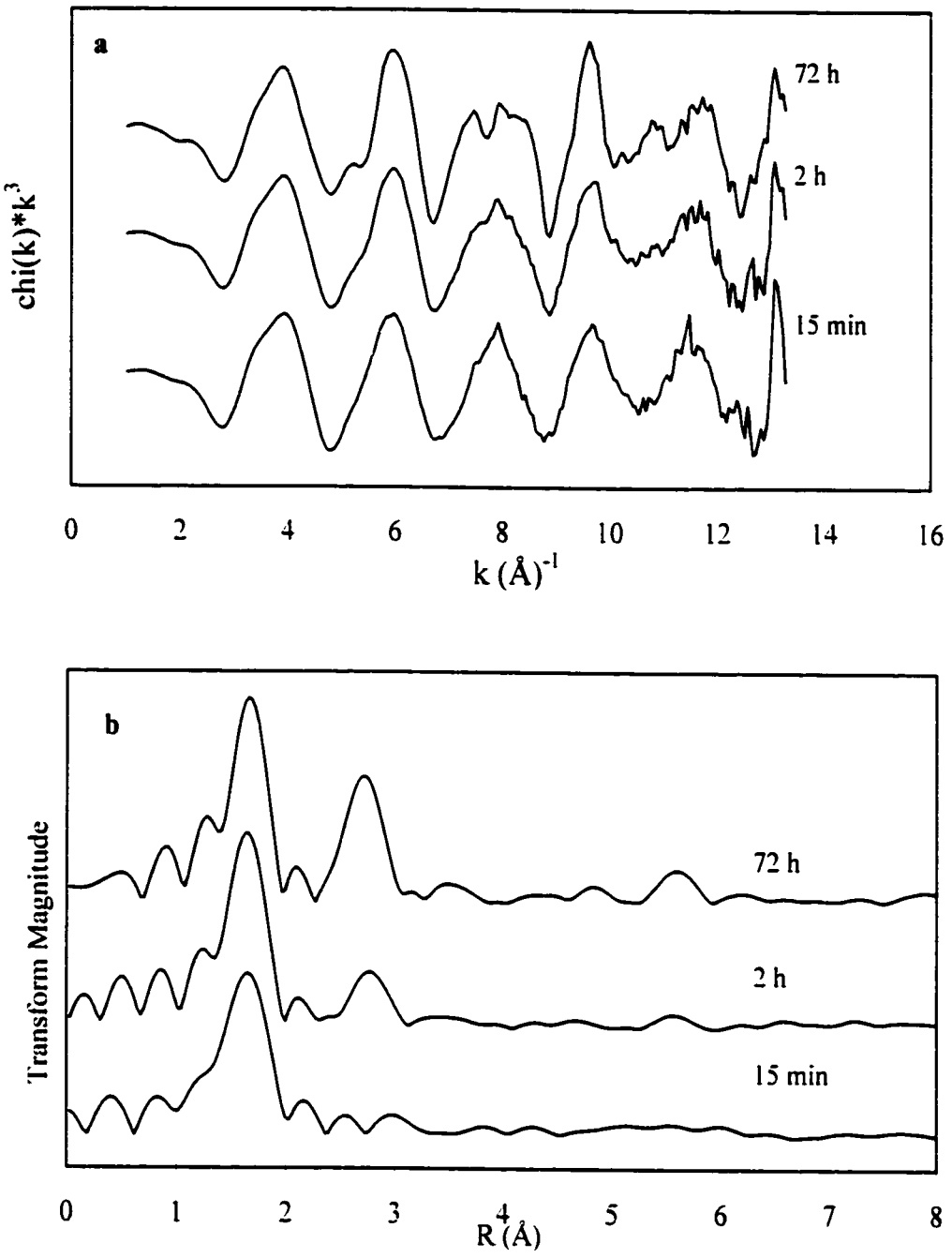

Figure 2.5 Results of XAFS experiments performed at pH 6.8. a) k^3-weighted, normalized, background-subtracted chi-functions for Ni sorbed on soil clay for different times. b) Fourier transforms of chi-functions in Figure 2.5a, uncorrected for phase shift.

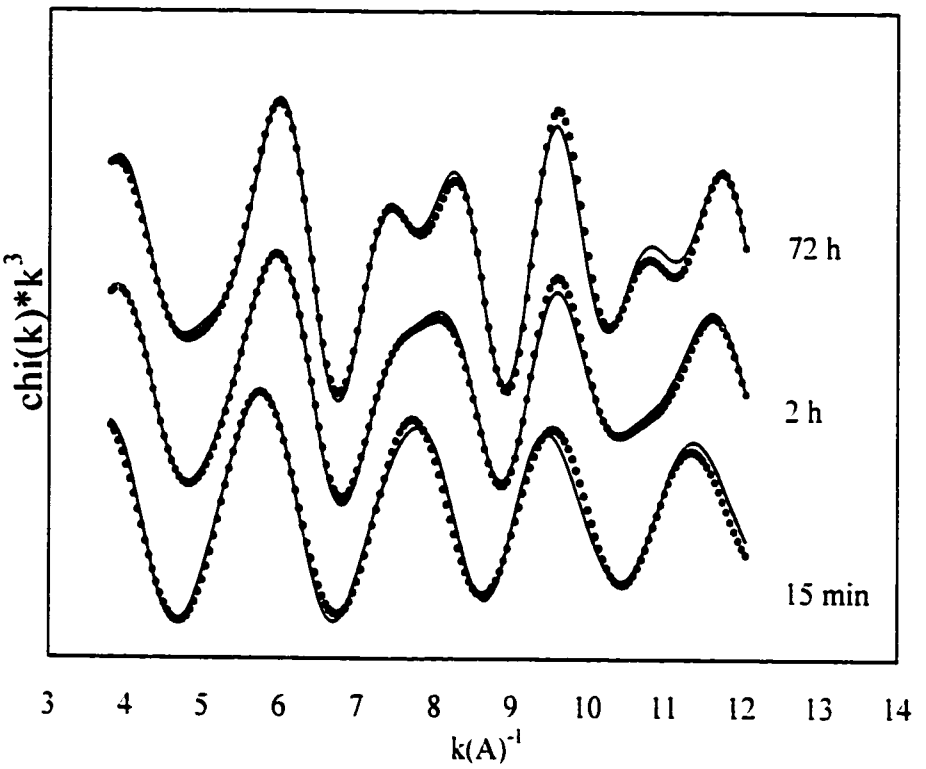

Figure 2.6 Experimental k^3-weighted XAFS data (solid line) of Fourier back-transformed spectra in comparison to theoretical spectra (dotted line) using multi-shell least-squares fitting for pH 6.8 samples.

the 2 and 72-hour samples the Ni-Ni and Ni-Al shell results were similar to the pH 7.5 system. The reduced Ni-Ni bond distance compared to α-$Ni(OH)_2$ suggests that the formation of a mixed Ni-Al LDH may be occurring within 2 hours at this pH. The distinguishing LDH feature in the chi data (Figure 2.5a) appears in the spectra after 72 hours, indicating that more than 2 hours are required to yield the split in the chi spectra oscillation due to the presence of Al in the precipitate structure.

2.4.4 XAFS Analyses of Ni-reacted Clay at pH 6.0

The k^3-weighted, normalized, background-subtracted chi functions for Ni sorbed on the soil clay at pH 6.0 for 2 hours and 72 hours are presented in Figure 2.7a. The simple single oscillation of the XAFS signal remains relatively constant over time, indicating no contribution from a heavy backscattering element. The RSFs are presented in Figure 2.7b and are uncorrected for phase shift. As was the case for the pH 7.5 and 6.8 systems, the Ni-O peak at $\cong$ 1.7 Å is observed and remains constant with increasing reaction time. In contrast to the pH 7.5 and 6.8 systems, no peak is present at R $\cong$ 2.8 Å in any of the spectra indicating that no second neighbor Ni atoms are present. This indicates that at this pH there is no formation of a precipitate within 72 hours. Since there is little additional sorption of Ni after 72 hours (Figure 2.2b), the formation of precipitates after longer times was not anticipated. For this reason the data were fit with only a Ni-O shell. The comparison of the k^3-weighted XAFS functions for the Fourier back-transformed spectra to the theoretical spectra derived with parameters from analysis of a single shell is presented in Figure 2.9. The comparison indicates

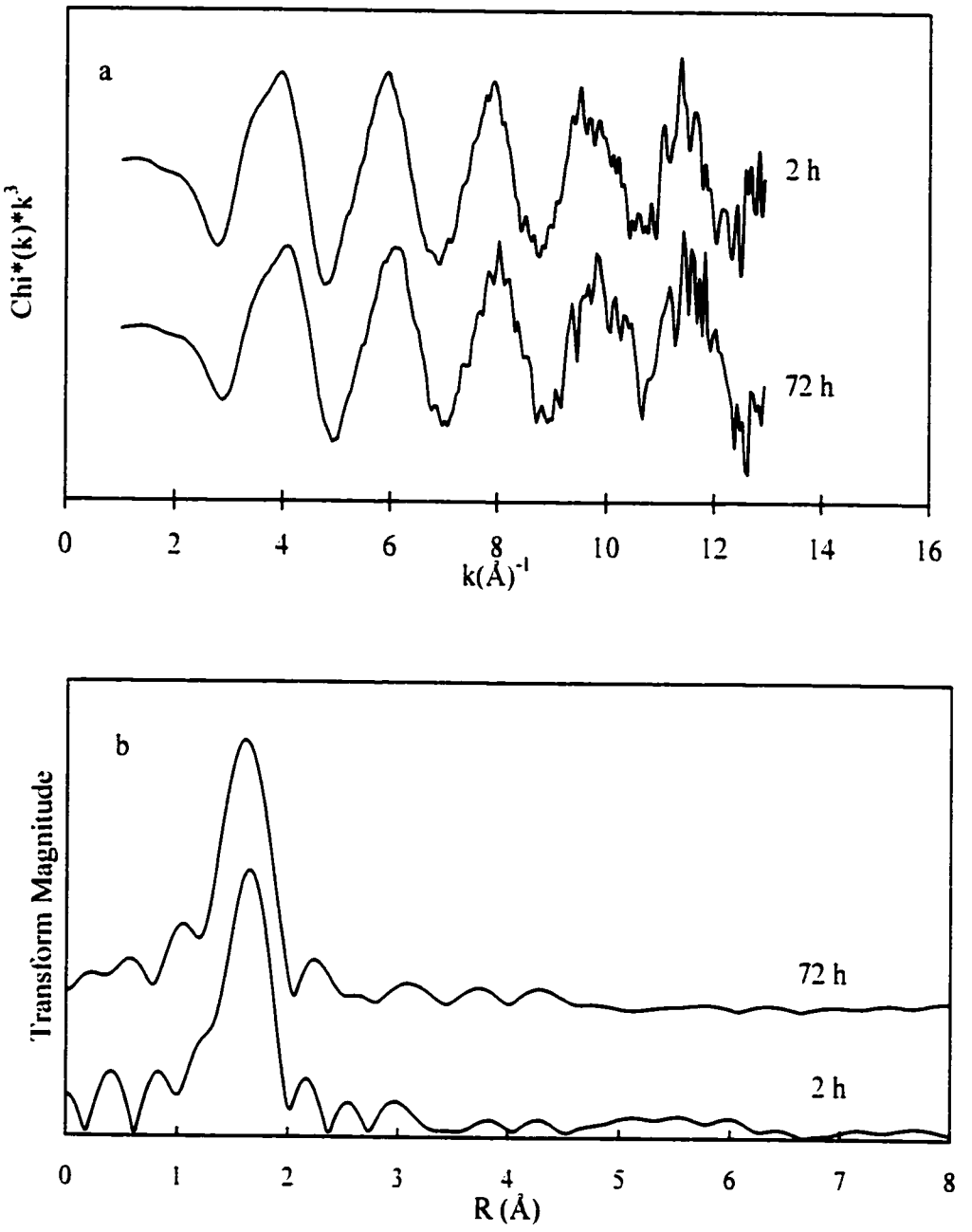

Figure 2.7 Results of XAFS experiments performed at pH 6.0. a) k^3-weighted, normalized, background-subtracted chi-functions for Ni sorbed on soil clay for different times. b) Fourier transforms of chi-functions in Figure 2.7a, uncorrected for phase shift.

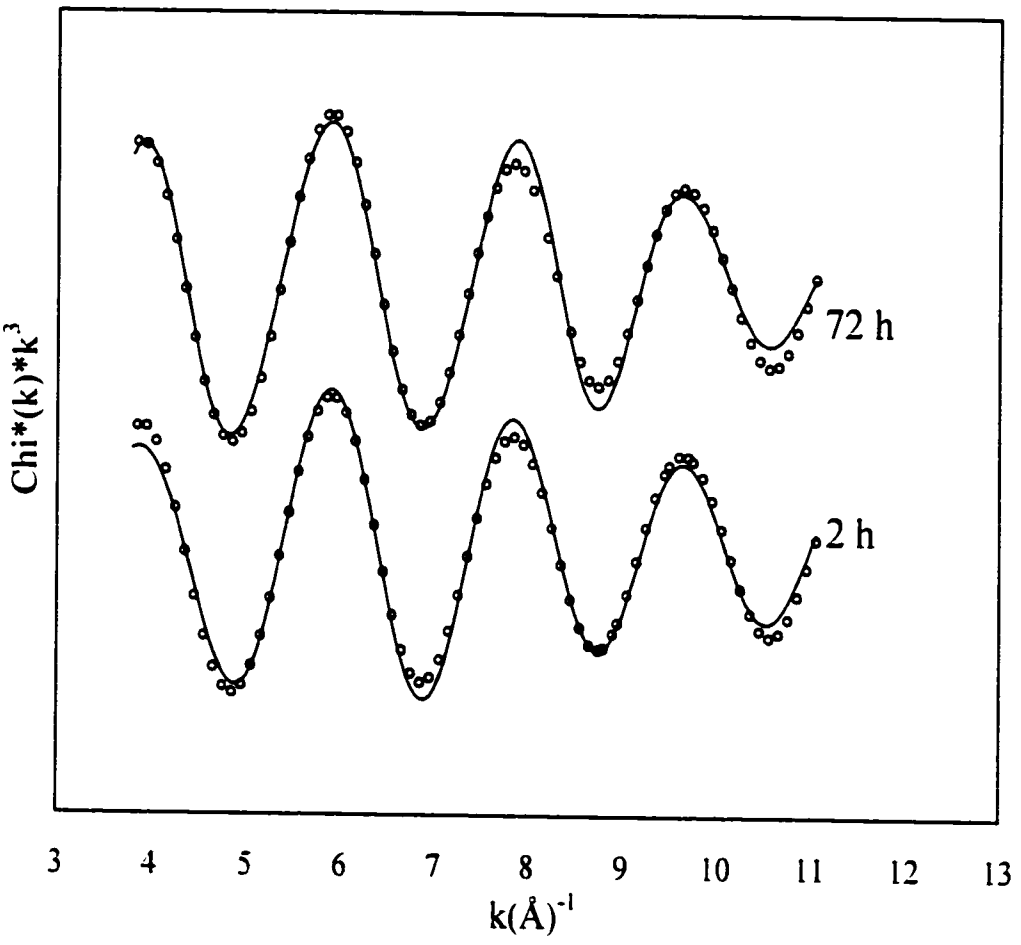

Figure 2.8 Experimental k^3-weighted XAFS data (solid line) of Fourier back-transformed spectra in comparison to theoretical spectra (dotted line) using multi-shell least-squares fitting for pH 6.0 samples.

good agreement between theoretical and experimental data. The structural parameters are presented in Table 2.1. XAFS data analysis indicated that Ni was in octahedral coordination with O with $N_{Ni\text{-}O} \cong 6$ and $R_{Ni\text{-}O} \cong 2.05$ Å (Table 2.1).

The results from the pH 6.0 system indicate that adsorption is the primary mode of Ni removal for reaction times up to 72 hours. Due to the heterogeneous nature of this soil clay, it is likely that both planar permanent-charge sites and edge surface-hydroxyl sites are competing for Ni sorption. The absence of precipitates at this low pH may be due to a pH effect and/or a surface-loading effect. Results from other studies investigating mixed-metal precipitate formation on clay minerals and oxides suggested that precipitate formation was dependent on the amount of metal ions sorbed to the surface at a given pH (O'Day et al., 1996; Scheidegger et al., 1996; Towle et al., 1997). At pH 6.0 not enough Ni was adsorbed to the soil clay so the necessary first step in precipitate formation was absent. Another explanation may be that a certain pH value must be attained prior to the formation of a metal precipitate phase, regardless of surface loading, in order to satisfy solubility requirements. The pH 6.0 system possibly needed more time to react with the soil clay prior to the formation of a precipitate. Figure 2.1b suggests, however, that even at longer times no precipitate will form since additional Ni-uptake after 72 hours is only minor.

2.4.5 XAFS Analyses of Ni-reacted Whole Soil at pH 7.5

The k^3-weighted, normalized, background-subtracted chi function for Ni sorbed on the whole soil at pH 7.5 for 24 h is presented in top of Figure 2.3a. Although

slightly noisier than the data collected for Ni sorbed on the soil clay at 7.5, similar features in the XAFS can be seen. The XAFS feature at ≈ 8 $Å^{-1}$ indicates the presence of an Al atom in addition to Ni as the second nearest neighboring atom. The spectrum was Fourier transformed to produce the radial structure function in the top of Figure 2.5b. These spectra are uncorrected for phase shift. The first peak at R ≅ 1.7 Å represents the first coordination shell of Ni. The second peak at R ≅ 2.8 Å is likely due to contributions from second nearest Ni neighbors around the central absorber, and indicates that some type of Ni precipitate is forming in the whole soil. The Fourier back-transformed spectrum compared to the theoretical spectrum derived by fitting theoretical Ni-O, Ni-Ni, and Ni-Al scattering paths to the raw data is shown in Figure 2.5c. The comparison indicates that the theoretical paths provide a good representation of the experimental data. The structural parameters derived from the fits are presented in Table 2.1. Analysis shows that the first shell is consistent with Ni surrounded by ≈ 6 O atoms, indicating that Ni is in an octahedral coordination environment. The Ni-O bond distance (R_{Ni-O}) is 2.05 Å the coordination number (N) is 5.82. Analysis of the second shell indicates the presence of a second-neighbor Ni atom around the central absorber at a bond distance ≅ 3.05 Å with a N_{Ni-Ni} of 3.0. Although sorption kinetic data are not presented for Ni sorbed on the whole soil, it can be noted that under the same reaction conditions (pH = 7.5, 24 h reaction time) the N_{Ni-Ni} for the Ni reacted whole soil (3.0) was significantly less than N_{Ni-Ni} for the Ni reacted soil clay fraction (4.0) indicating slightly slower kinetics of precipitation formation in the case of the whole soil. The results indicate the presence of organic matter and Fe oxides did not inhibit

the formation of mixed Ni-Al layer double hydroxides. Under the reaction conditions studied in this experiment, the formation of mixed metal precipitates in soil environments is a viable sorption mechanism.

2.4.6 Desorption of Ni from Soil Clay Fraction

To assess the stability of the Ni-Al precipitates formed at pH 7.5 with increasing aging time, the kinetics of Ni removal from the clay was measured using a batch technique coupled with a cation exchange resin. The percentages of Ni removed from the soil clay after an initial reaction of 1 hour, 1 day, 1 month and 6 months are presented in Figure 2.9. The sorption times indicate the amount of time the Ni reacted with the soil clay prior to initiation of the desorption step. In all cases the majority of Ni was removed within the first several hours, followed by a much slower rate of Ni desorption. The trend follows that as reaction time increased less Ni was likely to be removed from the clay, indicating an aging effect is occurring. After aging for a 6-month period a maximum of 5% of the Ni was removed from the surface while after a 1 hour aging time nearly 95% of Ni was removed.

Since the primary uptake mechanism of Ni under these reaction conditions has been shown to be Ni-Al LDH formation, it follows that this precipitate is undergoing a stabilization over time, accounting for the decrease in Ni release. The possible mechanisms responsible for this stability include (1) Ostwald ripening; (2) chemical modifications via incorporation of ions derived from the sorbent phase and (3) via physical isolation of the precipitate from the solution due to precipitation of secondary

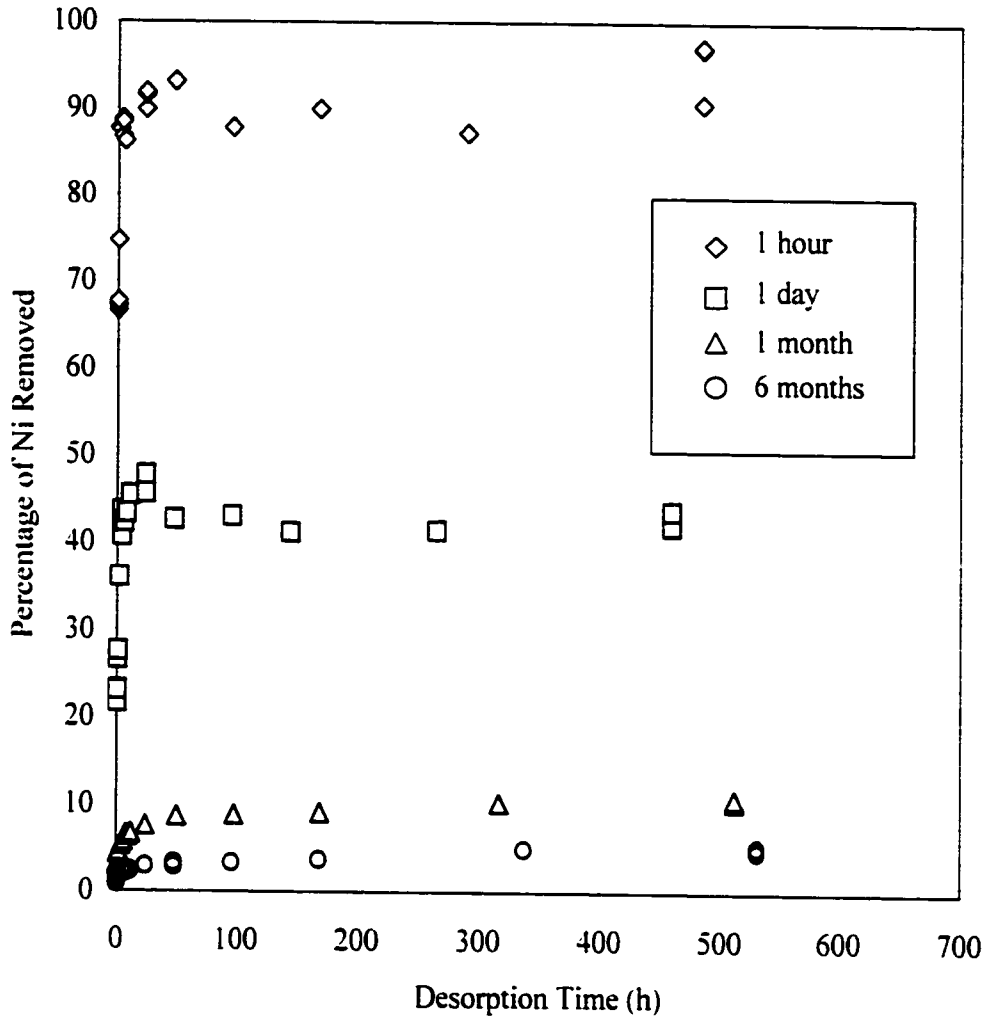

Figure 2.9 Nickel desorption kinetics from Matapeake soil clay fraction after an initial reaction time of 1 hour, 1 day, 1 month and 6 months at pH 7.5. The percentage removed is relative to the amount sorbed at the end of the specified reaction time.

Al- or Si- bearing phases during clay mineral weathering (Ford et al.. 1999). Studies by Scheckel et. al (2000) and Ford et al. (1999) investigated Ni desorption from aged Ni-pyrophyllite systems under similar reaction conditions and concluded that the Ni-Al LDH phases transformed into the precursor of a Ni-Al phyllosilicate-type phase and that this accounted for diminished Ni release with aging time. It is likely that a similar mechanism is responsible for the aging effect seen in this study. however the heterogeneity of the sorbent phases makes it difficult to implement many of the analytical techniques they employed to prove their hypothesis. Given the certainty that Al is incorporated into the structure of the neo-formed precipitate and there is a pronounced aging effect. it was concluded that a similar mechanism is occurring in this system.

The results from a comparison of aging the Ni-clay suspensions at pH 6.0. 6.8. and 7.5 are presented in Figure 2.10. The data are plotted as amount of Ni that is remaining on the surface relative to the total amount sorbed after a 1-month reaction period. More Ni remained on the surface at pH 7.5. with nearly 90% of the Ni remaining on the surface followed by the pH 6.8 system in which approximately 53% of the sorbed Ni remained on the clay. and finally the pH 6.0 system where only 5% of the Ni remained on the clay after 150 hours. The results can again be explained by the formation of the Ni-Al LDH phase. which occurred only above pH 6.8. At pH 6.0 a less-stable adsorption complex accounted for the more readily removable Ni from the clay. At pH 6.8 far less Ni was removed from the clay. but it appears that a high pH is

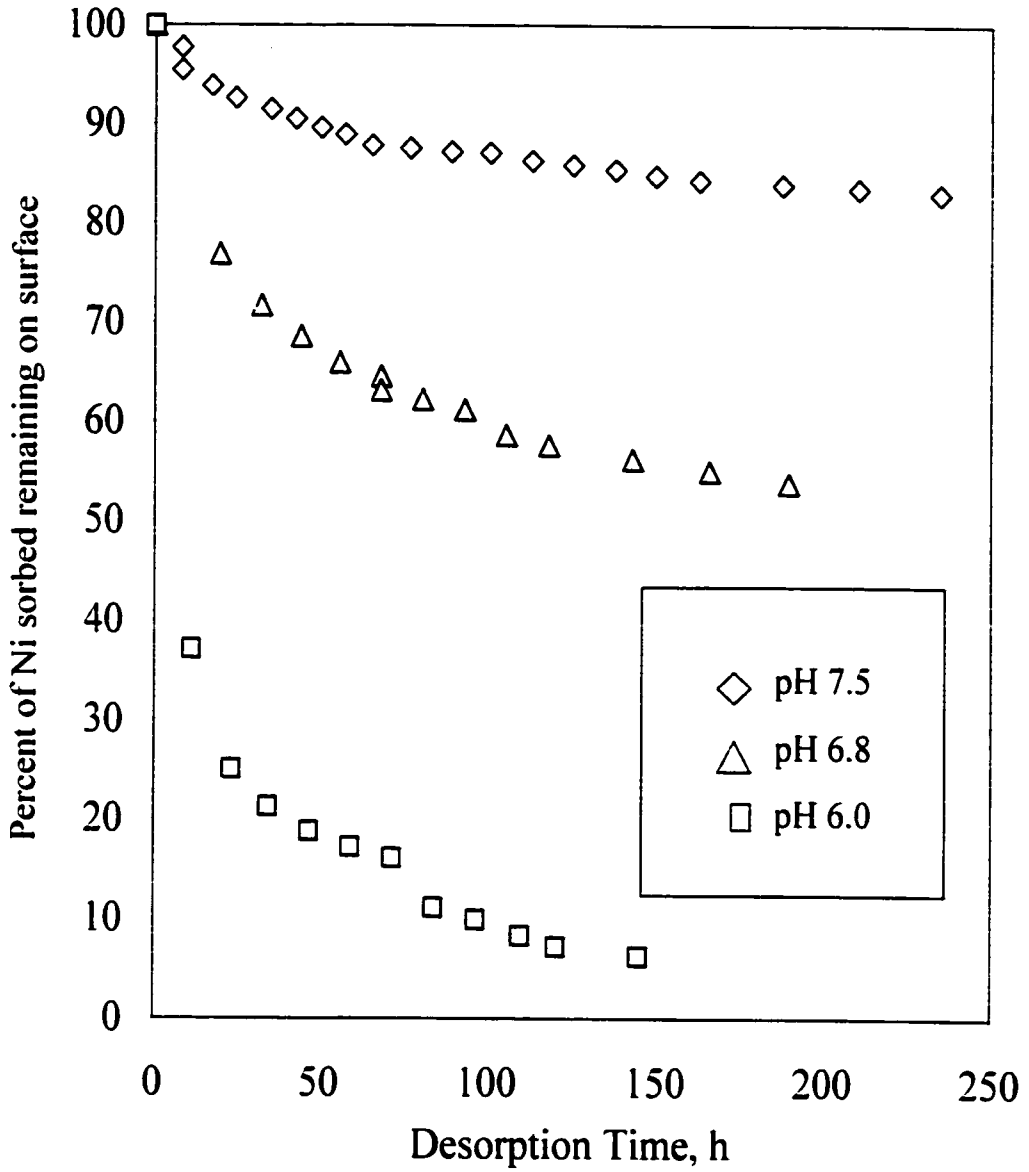

Figure 2.10 Nickel desorption kinetics from Matapeake soil clay fraction after an initial sorption time of 1 month at either pH 6.0. 6.8 or 7.5.

likely to make a more stable precipitate phase as more Ni remained on the clay in the pH 7.5 system.

The results from this study verify that Ni-Al LDH phases are likely to form in mixed-clay systems under the reaction conditions of this study. Moreover, the formation of these phases is likely in natural soil systems if the proper reaction conditions are met. The stabilization of these phases has been demonstrated to increase with both reaction time and pH. The identification of such phases and implications for their fate in soil environments was achievable by using a macroscopic kinetic approach coupled with spectroscopic techniques and desorption studies.

2.6 References

Bargar, J.R., G.E. Brown Jr. and G.A. Parks. 1997a. Surface complexation of Pb(II) at oxide-water interfaces: I. XAFS and bond-valence determination on mononuclear and polynuclear and polynuclear Pb(II) sorption products on aluminum oxides. *Geochim. Cosmochim. Acta* **61:** 2617-2637.

Bargar, J.R., G.E. Brown Jr. and G.A. Parks. 1997b. Surface complexation of Pb(II) at oxide-water interfaces: II. XAFS and bond-valence determination on mononuclear and polynuclear Pb(II) sorption products and surface functional groups on iron oxides. *Geochim. Cosmochim. Acta* **61:** 2639-2652.

Bertsch, P.M. and D.B. Hunter. 1998. Elucidating fundamental mechanisms in soil and environmental chemistry: The role of advanced analytical spectroscopic, and microscopic methods. pp. 103-122. *In* P.M. Huang, D.L. Sparks and S.A. Boyd (eds.) Future of Soil Chemistry. Soil Sci. Soc. Am., Madison, WI.

Bouldin, C., T. Elam and L. Furenlid. 1995. MacEXAFS - An EXAFS analysis package for Macintosh. *Physica B* **208/209:** 190-192.

Boyanov, B. 1997. XFTools Collection, unpublished. Source codes and executables are available at http:/ncstarg.physics.ncsu.edu/xftools, North Carolina State University.

Brown Jr., G.E., G.A. Parks and P.A. O'Day. 1995. Sorption at mineral-water interfaces: macroscopic and microscopic perspectives. pp. 129-183. *In* D.J. Vaughan and R.A.D. Pattrick (eds.) Mineral Surfaces. Chapman & Hall, London.

Carter, D.L., M.M. Mortland and W.D. Kemper. 1986. Specific surface. *In* A. Klute (ed.) Methods of Soil Analysis Part 1 - Physical and Mineralogical Methods. Soil Sci. Soc. Am., Madison, WI.

Charlet, L. and A. Manceau. 1992. X-ray absorption spectroscopic study of the sorption of Cr(III) at the oxide-water interface. II. Adsorption, coprecipitation, and surface precipitation on hydrous ferric oxide. *J. Colloid Interface Sci.* **148:** 443-458.

Charlet, L. and A. Manceau. 1994. Evidence of the neoformation of clays upon sorption of Co(II) and Ni(II) on silicates. *Geochim. Cosmochim. Acta* **58:** 2577-2582.

Chisholm-Brause, C.J., P.A. O'Day, G.E. Brown Jr. and G.A. Parks. 1990. Evidence for multinuclear metal-ion complexes at solid/water interfaces from X-ray absorption spectroscopy. *Nature* **348:** 528-531.

d'Espinose de la Callerie, J.-B., M. Kermarec and O. Clause. 1995. Impregnation of γ-alumina with Ni(II) or Co(II) ions at neutral pH: hydrotalcite-type coprecipitate formation and characterization. *J. Am. Chem. Soc.* **117:** 11471-11481.

Ford, R.G., A.C. Scheinost, K.G. Scheckel and D.L. Sparks. 1999. The link between clay mineral weathering and structural transformation in Ni surface precipitates. *Environ. Sci. Technol.* **33:** 3140-3144.

Förstner, U. 1995. Land contamination by metals - global scope and magnitude of problem. pp. 1-24. *In* H.E. Allen, C.P. Huang and G.W. Bailey (eds.) Metal Speciation and Contamination of Soil. CRC Press, Boca Raton, FL.

Greaves, C. and M.A. Thomas. 1986. Refinement of the structure of deuterated nickel hydroxide, $Ni(OD)_2$, by powder neutron diffraction and evidence for structural disorder in samples with high surface area. *Acta Cryst.* **B42:** 51-55.

Jackson, M.L. 1956. Soil chemical analysis - advanced course. *In.* Published by the author, Dept. of Soils, Univ. of Wis., Madison, Wis.

Karanthanasis, A.D. and W.G. Harris. 1994. Quantitative thermal analysis of soil materials. pp. 360-411. *In* J.E. Amonette and L.W. Zelazny (eds.) Quantitative Methods in Soil Mineralogy. Soil Sci. Soc. Am., Madison, WI.

Lavkulich, L.M. and J.H. Wiens. 1970. Comparison of organic matter destruction by hydrogen peroxide and sodium hypochlorite and its effects on selected mineral constituents. *Soil Sci. Soc. Amer. Proc.* **34:** 755-758.

Lytle, F.W. et al. 1984. *Nucl. Instrum. Methods Phys. Res.* 542-548.

Manceau, A. et al. 1996. Direct determination of lead speciation in contaminated soils by EXAFS spectroscopy. *Environ. Sci. Technol.* **30:** 1540-1552.

Mattigod, S.V., D. Rai, A.R. Felmy and L. Rao. 1997. Solubility and solubility product of crystalline $Ni(OH)_2$. *J. Solution Chem.* **26:** 391-403.

Mehra, O.P. and M.L. Jackson. 1960. Iron oxide removal from soils and clays by a dithionte-citrate-system buffered with sodium bicarbonate. *Clays Clay Miner.* **7:** 317-327.

Morris, D.E. et al. 1996. Speciation of uranium in Fernald soils by molecular spectroscopic methods: characterization of untreated soils. *Environ. Sci. Technol.* **30:** 2322-2331.

O'Day, P.A., G.E. Brown Jr. and G.A. Parks. 1994. X-ray absorption spectroscopy of cobalt (II) multinuclear surface complexes and surface precipitates on kaolinite. *J. Colloid Interface Sci.* **165:** 269-289.

O'Day, P.A., S.A. Carroll and G.A. Waychunas. 1998. Rock-water interactions controlling zinc, cadmium, and lead concentration in surface waters and sediments, U.S. tri-state mining district. 1. Molecular identification using x-ray absorption spectroscopy. *Environ. Sci. Technol.* **32:** 943-955.

O'Day, P.A., C.J. Chisholm-Brause, S.N. Towle, G.A. Parks and G.E. Brown Jr. 1996. X-ray absorption spectroscopy of Co(II) sorption complexes on quartz (α-SiO_2) and rutile (TiO_2). *Geochim. Cosmochim. Acta* **60:** 2515-2532.

Papelis, C. and K.F. Hayes. 1996. Distinguishing between interlayer and external sorption sites of clay minerals using X-ray absorption spectroscopy. *Colloids Surf., A* **107:** 89-96.

Pickering, I.J., G.E. Brown Jr. and T.K. Tokunaga. 1995. Quanitiative speciation of selenium in soils using X-ray absorption spectrosopy. *Environ. Sci. Technol.* **29:** 2457-2459.

Scheckel, K.G., A.C. Scheinost, R.G. Ford and D.L. Sparks. 2000. Stability of layered Ni hydroxide surface precipitates - a dissolution kinetics study. *Geochim. Cosmochim. Acta* **64:** 2727-2735.

Scheidegger, A.M., G.M. Lamble and D.L. Sparks. 1996. Investigation of Ni sorption on pyrophyllite: An XAFS study. *Environ. Sci. Technol.* **30:** 548-554.

Scheidegger, A.M., D.G. Strawn, G.M. Lamble and D.L. Sparks. 1998. The kinetics of mixed Ni-Al hydroxide formation on clays and aluminum oxides: a time-resolved XAFS study. *Geochim. Cosmochim. Acta* **62:** 2233-2245.

Scheinost, A.C., R.G. Ford and D.L. Sparks. 1999. The role of Al in the formation of secondary Ni precipitates on pyrophyllite, gibbsite, talc, and amorphous silica: a DRS study. *Geochim. Cosmochim. Acta* **63:** 3193-3203.

Scheinost, A.C. and D.L. Sparks. 2000. Formation of layered single- and double-metal hydroxide precipitates at the mineral/water interface: A multiple-scattering XAFS analysis. *J. Colloid Interface Sci.* **223:** 167-178.

Spadini, L., A. Manceau, P.W. Schindler and L. Charlet. 1994. Structure and stability of Cd^{2+} surface complexes on ferric oxides. 1. Results from EXAFS spectroscopy. *J. Colloid Interface Sci.* **168:** 73-86.

Sparks, D.L. 1989. Kinetics of Soil Chemical Processes. Academic Press, San Diego, CA.

Sparks, D.L. 1995. Environmental Soil Chemistry. Academic Press, San Diego.

Strawn, D.G., A.M. Scheidegger and D.L. Sparks. 1998. Kinetics and mechanisms of Pb(II) sorption and desorption at the aluminum oxide-water interface. *Environ. Sci. Technol.* **32:** 2596-2601.

Towle, S.N., J.R. Bargar, G.E. Brown Jr. and G.E. Parks. 1997. Surface precipitation of Co(II)(aq) on Al_2O_3. *J. Colloid Interface Sci.* **187:** 62-82.

Zabinsky, S.L., J.J. Rehr, A. Ankudinov, R.C. Albers and M.J. Eller. 1995. Multiple-scattering calculations of x-ray absorption spectra. *Phys. Rev. B: Condens. Matter* **52:** 2995-3006.

Chapter 3

DETERMINATION OF Zn(II) COMPLEXATION ON Al AND Si OXIDES USING XAFS SPECTROSCOPY

3.1 Abstract

Zn(II) sorption to Al and Si oxides was studied as a function of pH (5.0 – 7.5), sorption density, and $[Zn]_o$ in 0.1 M and 0.005 $NaNO_3$ background electrolyte. The chemistry of Zn(II) in soil and aquatic environments is intriguing in that Zn may occur in both octahedral (6-fold) and tetrahedral (4-fold) coordination in surface complexes and as precipitated phases. This study was carried out to determine the effects of reaction conditions on Zn complexation at oxide surfaces and to assess under what conditions surface precipitation occurs. In addition, the study was carried out to assess whether the coordination environment of the sorbent phases (4-fold for amorphous silica and 6-fold for gibbsite) determines the coordination environment of sorbed Zn. X-ray absorption fine structure (XAFS) spectroscopy was used to probe the Zn atomic environment at the metal oxide/aqueous interface. For both amorphous silica and high surface area gibbsite, Zn reaction kinetics were very rapid and reached completion within 24 hours. In contrast, Zn sorption on low surface area gibbsite was much slower, taking nearly

800 hours for complete Zn removal. The slow sorption was attributed to the formation of a Zn precipitate. XAFS results indicated that at low surface loadings Zn formed inner-sphere adsorption complexes on both amorphous silica and gibbsite. This agreed with the macroscopic observation that Zn sorption was independent of ionic strength. In the case of amorphous silica, Zn was in octahedral coordination up to a loading of approximately 0.4 μmol m^{-2} and switched to tetrahedral coordination as surface loading increased. In the case of gibbsite, Zn was in mixed tetrahedral and octahedral coordination over all loading levels. At the highest surface loadings Zn formed precipitates on both surfaces. On amorphous silica this phase resembled an amorphous zincite (ZnO) with XAFS fits improving when Si was included in the structure. For Zn on gibbsite at high surface loadings the precipitated phase was similar to a Zn-Al layered double hydroxide (LDH) phase. Aging sorption samples for over a year yielded no changes in the XAFS spectra in any of the systems studied.

3.2 Introduction

The migration of potentially toxic metal ions in soil and aquatic environments is often dictated by the complexation of these ions at the interfaces of solid surfaces. In these environments there exist numerous sorbent phases capable of adsorbing metal ions, namely clay minerals, metal oxides, organic materials and other solid constituents of soils. Along with reaction conditions (pH, metal concentration, ionic strength), the solid phase may play a significant role in the type of complex formed, and therefore in the potential of the metal ion to either become sequestered or mobilized. Some of the most reactive components in soils may be the coatings of metal oxides such as Fe

oxides (i.e., goethite), Mn oxides (i.e., birnessite), Al oxides (i.e., gibbsite), and Si oxides (i.e., allophane), which occur as the result of weathering of minerals bearing these elements and subsequent reprecipitation (Coston et al., 1995). An array of studies have established the importance of metal oxide surfaces in the retention of metals in adsorption experiments, generally relying on macroscopic observations in an effort to develop accurate complexation models (Baumgarten and Kirchhausen-Dusing, 1997; Kinniburgh and Jackson, 1981; Shuman, 1977; Spark et al., 1995). However, metal sorption mechanistic data can only be established using a direct molecular probe, such as X-ray absorption fine structure (XAFS) spectroscopy. Moreover, many surface complexation models have been carried out over a limited range of reaction conditions and few have considered precipitation of metal ions as a potential sorption mechanism (Fendorf et al., 1994).

A common element used in many of the previously mentioned studies is zinc (Zn). Zinc is a ubiquitous metal phase in soil and aquatic environments, at background levels posing no serious threat to biota and vegetation. In areas that have elevated levels of Zn as a result of smelting, land application of biosolids, or other industrial processes, Zn is often a detriment to the environment (Chaney, 1993). Zn has been shown to form a variety of complexes at the surfaces of clay minerals and oxides, often dependent on the reaction conditions under study, including pH, ionic strength (I), reaction time and surface loading. Recent observations on Zn(II) speciation in soils has verified Zn may form both octahedral and tetrahedral coordination complexes in soils (see chapter 4). In an extensive study, Huang and Rhoads (1989) investigated Zn sorption onto hydrous aluminosilicates over a range of pH, ionic strength and initial Zn

concentrations. They concluded that Zn adsorbed on aluminosilicates on constant charge sites and constant potential sites. At high pH values they speculated $ZnSiO_{3(s)}$ was forming on aluminosilicate surfaces but no direct evidence supported this hypothesis. Several other studies indicate that chemisoprtion to oxide and clay mineral surfaces is the primary Zn sorption mechanism (Ladonin. 1997; Metwally et al.. 1993; Vlasova and Davidenko. 1995). Others have suggested that Zn may form $Zn(OH)_2$ upon sorption on hydrous Al oxide at pH values above 8. again without providing direct evidence for solid phase formation (Shuman. 1977). Xu and Schwartz (1994) investigated the sorption of Zn on hydroxyapatite surfaces and observed an initial rapid sorption step followed by a much slower rate of Zn removal from solution. They conceded that their analytical techniques (XRD and SEM) were not sensitive enough to determine if precipitation was a major mechanism at high pH value (>7.0) using.

The application of XAFS to environmental systems has been a powerful tool into investigating metal sorption behavior at metal oxide and clay mineral surfaces (Elzinga and Sparks. 1999; Papelis and Hayes. 1996; Strawn et al.. 1998). Many of the studies have reported nucleation of metal hydroxides upon sorption of Pb. Co. Cr(III). Ni and Zn below pH and surface loadings one would predict such phases to be thermodynamically favorable (Scheidegger and Sparks. 1996). In some cases pure metal hydroxide phases were identified (Chisholm-Brause et al.. 1990; Fendorf et al.. 1994). Other studies established that ions from the sorbent phase were integrated into the neo-formed precipitate phase resulting in layered-hydroxide phases (Ford and Sparks. 2000; Scheinost et al.. 1999; Trainor et al.. 2000). Some have proposed the neo-formation of clays as a result of metal sorption to mineral and oxide phases (Charlet

and Manceau, 1994; Ford et al., 1999). In any case, the neo-formed precipitate may serve to stabilize the metal ion in soil environments.

Despite the numerous studies concerning metal sorption to geomedia and the direct observation of resulting surface complexes, there still remains a need to investigate sorption reactions with direct molecular tools. Moreover, there are few studies that compare macroscopic observation with molecular-scale investigations in an attempt to observe the continuum between different metal sorption mechanisms (outer-sphere complexation, inner-sphere complexation, precipitate formation). The interaction of Zn with gibbsite, the most common Al oxide mineral in soil environments and amorphous silica, an oxide identified in soil profiles as coatings on other minerals has yet to be studied with the above approach (Singh and Gilkes, 1993; Sparks, 1995a). Moreover, these metal oxides can be useful in determining if Zn coordination environment (4- vs. 6-fold) is controlled by the coordination environment of the metal oxide studied (4-fold for SiO_4 and 6-fold for $Al(OH)_3$). Therefore, the objectives of this study were to:

(1) Determine Zn complexation on Si and Al oxides as a function of pH, ionic strength, Zn concentration and aging time.

(2) Assess under what conditions Zn precipitation occurs on these surfaces using XAFS.

(3) Determine if the coordination environment of the metal in the metal oxide influences the coordination environment of adsorbed Zn.

3.3 Methods and Materials

3.3.1 Solid Materials

The silica used in this study was a Huber Zeofree® 5112 amorphous SiO_2 colloid. The PZC of amorphous silica was reported to be less than 2 (Huang and Rhoads, 1989) and therefore in this study it was de-protonated over all reaction conditions. The surface area as determined by the BET method was 90 $m^2 g^{-1}$ (Scheckel and Sparks, 2000). The gibbsite used in this study was synthesized following the procedure of Kyle et al. (1975) to achieve a phase with a high surface area. Briefly, 4 M NaOH was added dropwise to a 1 M $AlCl_3$ solution until a gelatinous precipitate appeared followed by dialysis for 30 days in DDI (distilled deionized) H_2O. X-ray diffraction (XRD) analysis identified the solid as $Al(OH)_6$ with all Al in octahedral coordination as determined by Al nuclear magnetic resonance (Al-NMR). The point of zero salt effect (PZSE) for the gibbsite was at pH 10.1 and its surface area was 96 $m^2 g^{-1}$ as determined by the BET-N_2 method. Additional sorption samples were prepared using γ-Al_2O_3 and a low surface area gibbsite containing 10% boehmite. For all solid phases the particle size was less than 2.0 μm. All solid phases were washed with background electrolyte and hydrated for at least 24 hours prior to the onset of Zn(II) sorption experiments.

In addition to sorption samples, XAFS data were collecting on Zn-bearing reference minerals to aid in data fitting and for comparison of spectra to sorption samples. These reference minerals included hydrozincite ($Zn_5(OH)_6(CO_3)_2$), a synthesized Zn-Al silicate and amorphous Zn silicate (Tiller and Pickering, 1974), smithsonite ($ZnCO_3$), willemite (Zn_2SiO_4), synthesized Zn-Al layered double hydroxide

(Crepaldi and Valim, 1998), and Zn hydroxide ($Zn(OH)_2$). The hydrozincite, smithsonite, and willemite were donated by the Smithsonian mineral reference library. Synthesized phases were prepared in a N_2-purged environment. Spectra were also collected for a 10 mM aqueous solution of $Zn(NO_3)_2$ at pH values 3.5 and 7.6. According to the speciation program MINEQL version 4.1 and the equilibrium constants of Baes and Mesmer (1976), Zn^{2+} was the dominant Zn phase in these solutions.

3.3.2 Adsorption Experiments

Batch Zn sorption experiments were conducted in a N_2-purged glovebox using boiled, DDI Milli-Q® water to prepare all solutions, ensuring complete removal of $CO_{2(g)}$ from the system. All reactions were carried out at 23 ± 1 °C. For pH edge experiments, a 10 g L^{-1} suspension of amorphous silica or gibbsite was equilibrated at pH 4 for 24 hours while constantly stirring followed by the addition of the necessary amount of Zn from an acidified 0.1 M $Zn(NO_3)_2$ stock solution to achieve an initial Zn concentration of 1 mM. The Zn was added in 100-μL increments over a period of several minutes (waiting at least a minute between adding the next aliquot) to ensure there was not a local oversaturation of any Zn solid phases. The I was adjusted to either 0.005 or 0.1 M using $NaNO_3$. The pH of the suspension was increased by drop-wise addition of 0.1 M NaOH. With each incremental increase in pH a certain a subsample of the suspension was removed from the main suspension vessel and transferred into a 40-mL centrifuge tube for equilibration on an end-over-end shaker for 24 hours at 30 rpm. After 24 hours the solids were separated from the suspensions by centrifugation at

12,000 rpm for 15 minutes. The supernatants were passed through 0.2 μm filters and analyzed for Zn using atomic absorption spectrometry (AAS).

Zn sorption kinetic experiments were carried using a pH-stat apparatus equipped with a deliver burette filled with CO_2-free 0.1 M NaOH. The kinetic experiments were performed outside the glovebox using boiled, DDI Milli-Q® water to prepare all solutions. N_2 was rapidly bubbled through the suspension to minimize the amount of $CO_{2(g)}$ in the system. The Nalgene® reaction vessel was covered with a plexiglass lid and Parafilm was used to seal any leaks which might have allowed $CO_{2(g)}$ penetration into the system. Sorption kinetics were carried out at pH 7.5 ± 0.05 with $[Zn]_o$ = 1 mM and I = 0.1 M in $NaNO_3$. All suspension densities were 10 g L^{-1} After pre-equilibrating the solid phases in the proper background electrolyte solution for at least 24 hours, Zn from a 0.1 M $Zn(NO_3)_2$ stock solution was added to the reaction vessels in 100-μL increments over a period of at least 10 minutes. This gradual addition of Zn ensured there was no local oversaturation with respect to Zn solid phases. The experimental parameters for Zn sorption kinetic measurements were selected on the basis that (a) complete Zn removal was expected based on pH edge experiments and (b) for comparison to numerous studies that have identified metal hydroxide formation at or near pH 7.5 for metal sorption to clay minerals and oxides (Ford and Sparks, 2000; Roberts et al., 1999; Scheidegger et al., 1996; Trainor et al., 2000). After the proper reaction time, samples were removed from the vessel and centrifuged at 12,000 rpm for 15 minutes followed by filtration and analysis for Zn using AAS. The amount of Zn sorbed was taken to be the difference between the amount remaining in solution and the initial Zn concentration.

3.3.3 XAFS Analysis and Interpretation

XAFS samples were prepared in the same manner as the sorption edges were, with a sample size large enough to yield at least 50 mg of solid for analysis. The solid suspension density and $[Zn]_o$ were varied to achieve a range of loading levels (Tables 3.1 and 3.2). For long-term samples, reaction tubes remained in the glovebox and pH values were checked and adjusted once a week. A range of reaction conditions and times were used in the Zn-amorphous silica and Zn-gibbsite sorption studies and the conditions for the representative samples for this study are presented in Tables 3.1 and 3.2, respectively. In some cases a significant amount of Zn remained in solution so some signal from aqueous Zn^{2+} could have produced a significant X-ray absorption signal. To minimize these signals, a complete separation of the solid paste from solution via vacuum filtration through a 0.2 μm filter was employed in lieu of centrifugation and decantation in which a small amount of solution tended to remained pooled atop the sample. This eliminated the need to wash the sample and potentially desorb any Zn from the sample. It was estimated that the aqueous Zn^{2+} did not significantly contribute to the overall XAFS signal (Elzinga and Sparks, 1999; O'Day et al., 1996).

XAFS spectra were recorded at Beamline X-11a at the National Synchrotron Light Source (NSLS), Brookhaven National Laboratory, Upton, NY. The beam current at NSLS varied from 100 to 300 mA at 2.5 GeV. The beamline monochromator consisted of two parallel Si(111) crystals adjusted to an entrance slit of 1 mm. Higher order harmonics were suppressed by reducing I_o (incoming energy) by 25% after

Table 3.1 Sample preparation conditions for Zn(II) sorption on amorphous silica. Electrolyte is $NaNO_3$ for all samples. Letters refer to spectra in Figure 3.5.

Sample	pH	Reaction time	$[Zn]_{initial}$	Solid/Solution Ratio	Ionic Strength, M	Γ, $\mu mol/m^2$
a	4.02		10 mM	$Zn(NO_3)_{2\ (aq)}$		
b	5.10	24 hours	1 mM	5 g/L	0.0048	0.11
c	6.12	24 hours	1 mM	5 g/L	0.049	0.23
d	6.56	24 hours	1 mM	5 g/L	0.11	0.79
e	7.45	24 hours	0.1 mM	3 g/L	0.10	0.37
f	7.35	24 hours	1 mM	10 g/L	0.12	1.08
g	7.35	18 months	1 mM	10 g/L	0.11	1.11
h	6.83	24 hours	2 mM	5 g/L	0.10	3.11
i	7.51	24 hours	1 mM	5 g/L	0.11	2.56

Table 3.2 Sample preparation conditions for Zn(II) sorption on Al oxides. Electrolyte is $NaNO_3$ for all samples. Samples a-f were performed on HSA gibbsite and sample g on LSA gibbsite. Letters refer to spectra in Figure 3.7.

Sample	pH	Reaction time	$[Zn]_{initial}$	Solid/Solution Ratio	Ionic Strength, M	Γ, $\mu mol/m^2$
a	6.03	24 hours	1 mM	5 g/L	0.005	0.3
b	6.56	24 hours	1 mM	10 g/L	0.10	1.03
c	7.50	24 hours	0.1 mM	3 g/L	0.11	0.33
d	7.50	24 hours	1 mM	10 g/L	0.10	1.07
e	7.52	18 months	1 mM	10 g/L	0.10	3.76
f	7.10	24 hours	2 mM	5 g/L	0.12	4.05
g	7.47	24 hours	1 mM	10 g/L	0.11	3.76
Zn γ-Al_2O_3 (fresh)	7.40	24 hours	1 mM	10 g/L	0.1	0.98
Zn γ-Al_2O_3 (aged)	7.41	24 hours	1 mM	10 g/L	0.1	0.96

optimization of the incoming beam. For sorption samples, moist pastes were mounted in aluminum sample holders and sealed with Kapton® tape. For reference samples, dry powders were diluted to 10% in a boron nitride powder to prevent the detector from being swamped. The beam energy was calibrated by assigning the first inflection to the absorption edge of metallic Zn foil to an energy value of 9659 eV. Samples were scanned in fluorescence mode at 25 °C using an Ar-filled Lytle detector equipped with a 3 μm Cu filter. At least three scans were collected per sample to increase the signal to noise ratio.

Numerical results were extracted from the EXAFS spectra using WinXAS version 1.3 (Ressler, 1997) combined with the FEFF 7.0 code (Zabinsky et al., 1995). The background was subtracted using a linear fit through the pre-edge region and a second order polynomial beyond the edge. The chi function was extracted from the background-subtracted raw data by fitting a linear function to the pre-edge region and a 6-knot spline function to the post-edge region. The data were converted to k space by applying the XAFS equation and subsequently weighted by k^3 to compensate for damping of oscillations at high k. The k^3 data were fit over similar k-ranges ($k \approx 3$ to 12 – 13) using a nonlinear least-squares approach with theoretical values for Zn-O, Zn-Si, Zn-Zn, and Zn-Al bonds from FEFF 7.0 using structural refinement data for Zn oxide, $ZnSi_2O_4$, and Zn-Al layered double hydroxide. Spectra were also Fourier-transformed (Bessel window) to produce radial structure functions (RSFs) that isolate frequency correlations between the central absorbing atom (Zn) and neighboring atoms as a function of bond distance (R). The amplitude reduction factor was set to 0.90, a value obtained by setting the coordination number (CN) for Zn in known octahedral

coordination ($Zn(NO_3)_2$) to 6 and using the obtained value. The same value has been used by researchers for similar systems (Ford and Sparks. 2000). During data fitting, the Debye-Waller factor (σ^2) was set to 0.01 $Å^2$ for the Zn-O shell. a value obtained by allowing this value to vary during fitting while constraining the CN and the amplitude reduction factor (Bargar et al.. 1997). In order to decrease the degrees of freedom. σ^2 values for 2^{nd}-neighbor atoms were also set to 0.01 $Å^2$. The errors in the first and second shell bond distances (R) were estimated to be accurate to R± 0.02 Å and CN were accurate to CN±30% based on a comparison of these values for hydrozincite and zinc oxide using XRD and XAFS and based on estimates in the literature (O'Day et al.. 1998: Scheidegger et al.. 1997).

3.4 Results and Discussion

3.4.1 Macroscopic Zn Sorption

The effects of ionic strength and pH on Zn adsorption on silica and gibbsite are shown in Figures 3.2 and 3.3. respectively. For both systems. a rapid jump from nearly zero Zn removal from solution to 100% Zn removal occurred over a very small pH range. otherwise known as a pH-edge. The pH edge for Zn on amorphous silica was shifted to the left relative to the Zn-gibbsite system. with approximately 50% of Zn removed at pH 6.8 for Zn-silica and at pH 7.25 for Zn-gibbsite (based on inflection points; data not shown). In both cases the adsorption was ionic strength-independent. suggesting an inner-sphere Zn complex to the surface of these solids as metal sorption via this mechanism can occur regardless of the solid surface charge (Sparks. 1995a). At pH 7.5 the silanol groups on the amorphous silica were most likely entirely

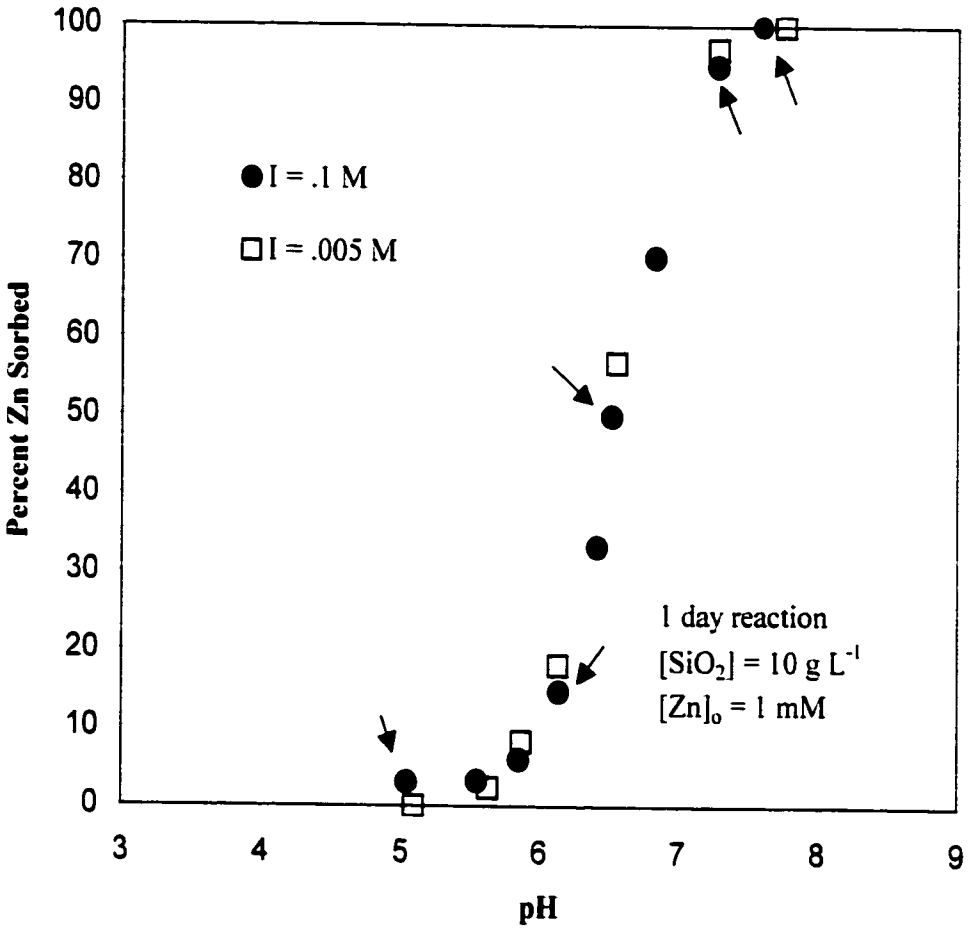

Figure 3.1 Zn sorption (pH) edges on amorphous silica at I = 0.1 M and I= 0.005 M $NaNO_3$. The arrows denote approximate reaction conditions under which XAFS samples were collected.

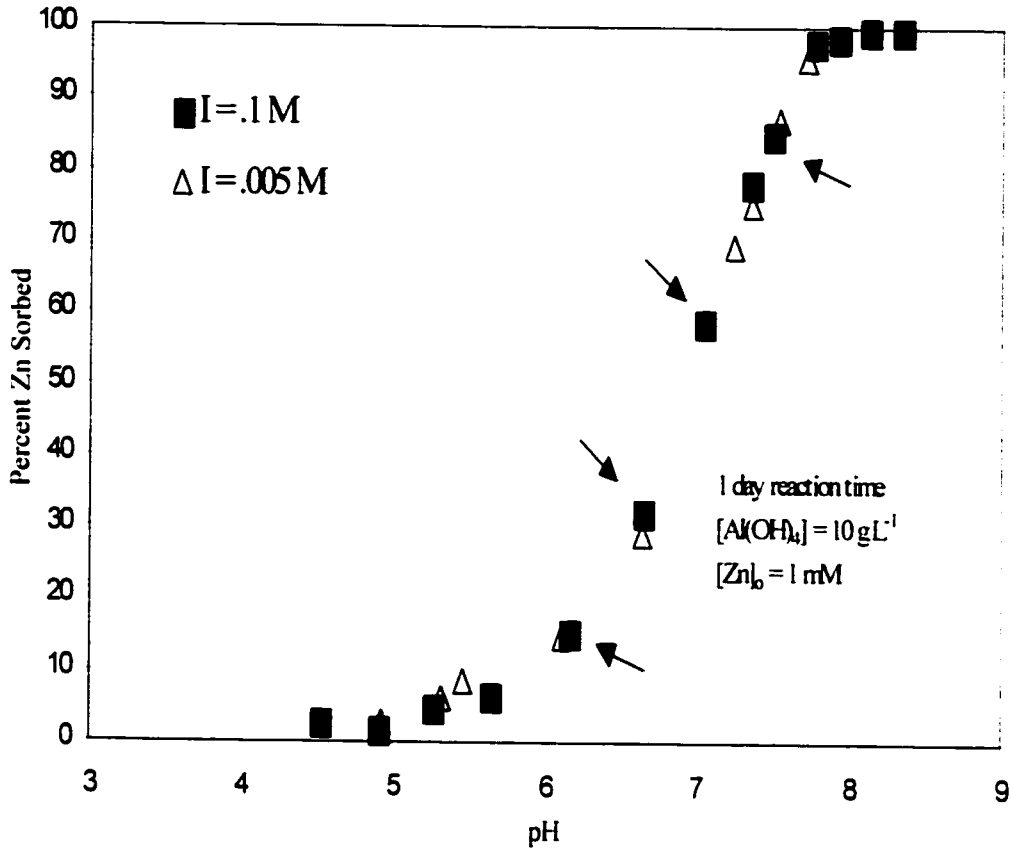

Figure 3.2 Zn sorption (pH) edges on HSA gibbsite at I = 0.1 M and I = 0.005 M $NaNO_3$. The arrows denote approximate reaction conditions under which XAFS samples were collected.

deprotonated (pKa < 2), while the aluminol groups on gibbsite may be partially deprotonated (pKa ≈ 10). Numerous studies with similar metal sorption pH edges have suggested this type of behavior is due to Zn adsorption at pH-dependent surface sites (Benjamin and Leckie, 1981; Huang and Rhoads, 1989). This type of sorption behavior would result in proton release from the solid as the metal binds to the surface, with the exact amount depending on the sorption complex formed (Spark et al., 1995). In all experiments constant base addition was required to maintain a nearly constant pH value thus implying Zn sorption at pH-dependent sites. Macroscopic observations of Zn sorption alone cannot determine exact modes of uptake as the adsorption of metals from solution is not necessarily a singular process and there may be a continuum between outer-sphere complexation, inner-sphere complexation and surface precipitation (Spark et al., 1995).

Figure 3.3 illustrates the kinetics of Zn sorption on amorphous silica while Figure 3.4 illustrates the kinetics of Zn sorption on low and high surface area gibbsite. Both systems had the same reaction conditions (1 mM $[Zn]_o$ and pH 7.5). For both Zn-silica and Zn-HSA gibbsite, Zn was removed from solution quite rapidly, with both systems eventually removing 100% of Zn from solution. For the Zn-silica system, Zn removal was extremely rapid with over 80% of added Zn removed from solution by the time the first sample was collected (15 minutes). Thereafter the sorption kinetics slowed slightly and 100% removal was achieved within 2 hours. For the Zn HSA-gibbsite system, slightly slower sorption kinetics was demonstrated relative to the Zn-

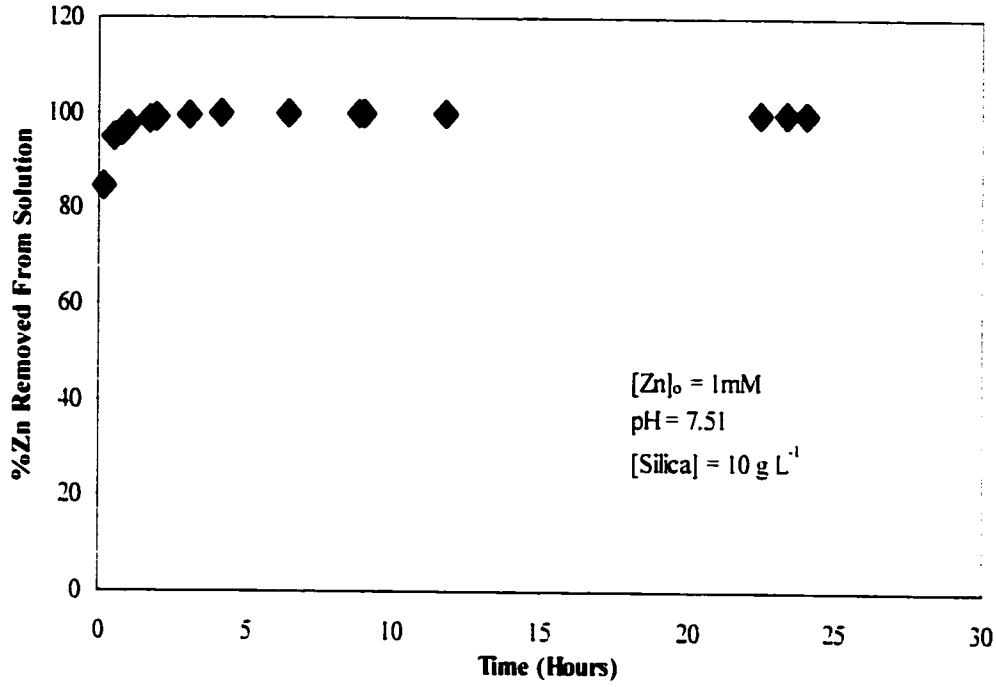

Figure 3.3 Zn sorption kinetics on amorphous silica.

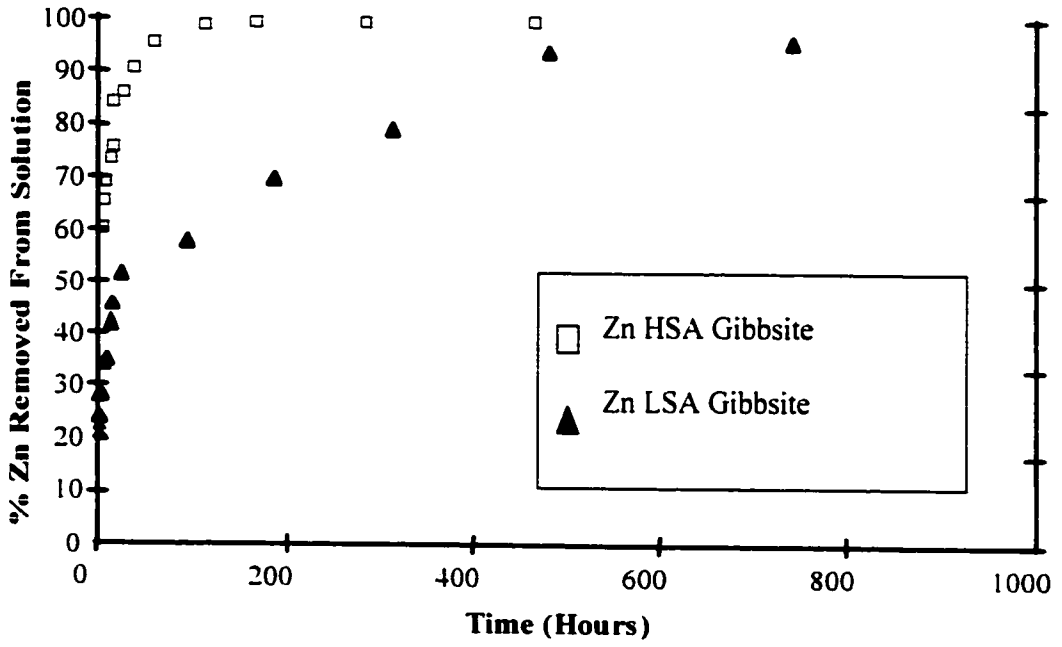

Figure 3.4 Zn sorption kinetics on LSA and HSA gibbsite.

silica system. For Zn on HSA gibbsite, 80% of Zn was removed from solution after 24 hours were required and a slightly slower second sorption step followed, with 100% Zn uptake within 200 hours. The slight contrast in Zn sorption kinetics between the two systems is intriguing in that both solids have similar surface areas (90 $m^2 g^{-1}$ for silica and 96 $m^2 g^{-1}$ for HSA gibbsite) with gibbsite having a slightly higher surface area. This suggests that total surface area was not a major factor in controlling Zn sorption kinetics, but rather the specific surface sites on the solids. As previously noted, the amorphous silica has more negatively charged sites under the reaction conditions studied. Moreover, the sites on amorphous silica may be more readily accessible or require less energy for adsorption to occur. In addition, the amorphous behavior of silica makes it more likely to have a greater site density. Strawn et al. (1998) observed an initial fast sorption step followed by a slower step for Pb(II) sorption on γ-Al_2O_3 (Al in octahedral coordination). They attributed the slower reaction step to either diffusion of Pb into the micropores of the alumina or as a result of heterogeneity of ligand sites on the γ-Al_2O_3 surface, a characteristic that could result in large activation energies.

Figure 3.4 demonstrates the effect of surface area on the kinetics of Zn sorption. Like the Zn-HSA gibbsite system, Zn sorption to low surface area (LSA) gibbsite demonstrated a rapid initial sorption step followed by a much slower sorption step. In contrast to the HSA system, only 50% of the Zn sorption was complete within the first 24 hours on the LSA system and the second, slower sorption step had a more linear shape. The same observation was made for Ni sorption kinetics on HSA gibbsite and LSA gibbsite by Yamaguchi et al. (2001). They attributed this difference to chemisorption playing the dominant role in Ni removal on HSA gibbsite, whereas

surface-induced precipitation of α-$Ni(OH)_{2(s)}$ controlled the kinetics of Ni removal in the LSA system. Other investigators have also identified slow metal sorption to gibbsite (Scheckel and Sparks, 2001; Scheidegger et al., 1998). To verify the mechanisms responsible for the differences between these two gibbsite systems and for identification of Zn surface complexes on amorphous silica and HSA gibbsite over a range of reaction conditions results from the XAFS spectroscopy studies were performed.

3.4.2 XAFS Analysis of Zn-reacted Amorphous Silica

The k^3-weighted Zn XAFS chi spectra and their corresponding fits from nonlinear least squares fitting for Zn on amorphous silica are presented in the left panel of Figure 3.5. The Fourier transforms of the chi spectra are presented in the right panel of Figure 3.5. Each of the chi spectra is characterized by a sin wave dominated by backscattering from first shell oxygen atoms around Zn with the signal amplitude decreasing as k increases. The radial structure functions magnify this characteristic Zn-O contribution indicated by large peaks at approximately 1.92 and 2.05 Å. The radial structure functions are uncorrected for phase shift so the value on the x axis does not necessarily indicate the true bond distance, R. The lack of significant structural features and diminishment of the signal at higher k values in the chi spectra indicate no heavy backscattering atoms are present around the local coordination environment of Zn in these samples. The chi spectra in Figure 3.6 demonstrate the effect of having heavy backscattering atoms in the Zn coordination environment. The Zn reference minerals in Figure 3.6 have second-neighbor Zn atoms present around the central Zn atom.

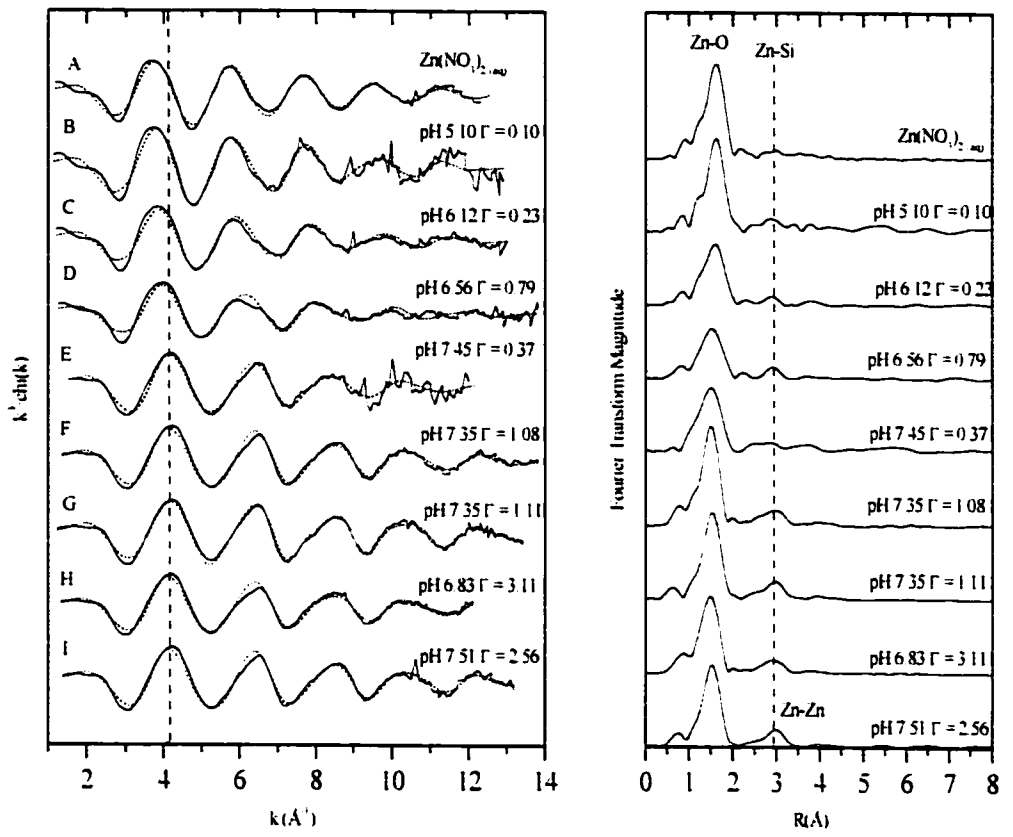

Figure 3.5 Zn-XAFS chi spectra weighted by k^3 (solid lines) and results from nonlinear least squares fitting (dotted lines) for Zn sorbed on amorphous silica (B-I). Corresponding Fourier transforms are in the right panel. The dotted line in the left panel serves to distinguish inner-sphere Zn spectra from outer-sphere Zn spectra.

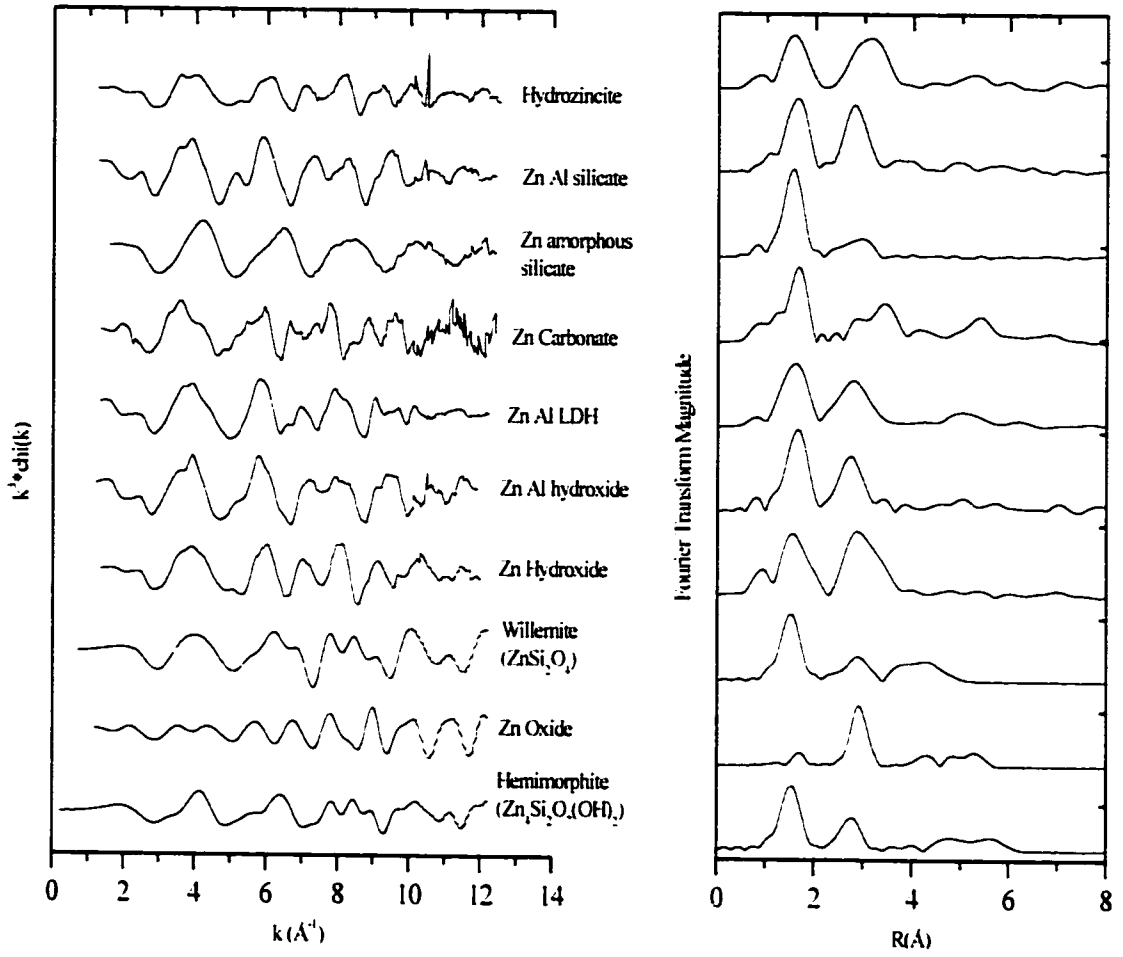

Figure 3.6 Zn-XAFS chi spectra weighted by k^3 (left) and corresponding Fourier transforms for Zn-bearing references compounds. The bottom three spectra are a result of simulations from FEFF 7.0.

resulting in the significant amount of structural features in the chi spectra (left panel). Upon Fourier transforming the data, one notes the presence of significant peaks beyond the first shell Zn-O peak. These are attributed to the presence of Zn, along with Si and Al in some instances. Figure 3.6 serves as a reference that demonstrates the kinds of features one would expect in XAFS data if neo-precipitated phases were forming in the sorption samples.

The top four chi spectra in the left panel of Figure 3.5 are shifted to slightly lower k values relative to the rest of the spectra (see dotted line as a reference) in the figure. This shift to lower k values is indicative of a higher Zn-O CN, namely octahedral coordination versus tetrahedral coordination. Zn has commonly been found in both four- and six-fold coordination environments with first-neighbor oxygen atoms in many aqueous compounds and solid phases (Trainor et al., 2000). The characteristic Zn-O distance in tetrahedral coordination has been reported to be between 1.92 and 1.99 Å while Zn in octahedral coordination has a Zn-O bond distance between 2.02 and 2.12 Å (Wilkinson, 1987). In some structures Zn can occur in both tetrahedral and octahedral coordination environments, i.e., in hydrozincite (O'Day et al., 1998). The nonlinear, least-squares fit results for Zn sorbed on silica are presented in Table 3.3. Results indicated that Zn is in octahedral coordination with O atoms in $Zn(NO_3)_{2\,(aq)}$ at both low and high (data not shown) pH values indicated by a $R_{Zn\text{-}O}$ of 2.07 Å and $CN_{Zn\text{-}O}$ of approximately 6. For the lowest Zn loading levels of $\Gamma = 0.10$ and 0.23 μmol m^{-2} at pH 5.12 and 6.0, respectively, the $CN_{Zn\text{-}O}$ and $R_{Zn\text{-}O}$ values are indicative of Zn in octahedral coordination. These results suggest that either (a) outer-sphere Zn complexes dominate the Zn speciation at the solution-silica interface or (b) the signal

Table 3.3 Results from XAFS analysis of Zn sorbed to amorphous silica.

	Zn-O			Zn-Si			Zn-Zn		
Sample	R (Å)[a]	CN[b]	σ^{2} [c]	R (Å)	CN	σ^{2}	R (Å)	CN	σ^{2}
(B) pH 5.10; Γ = 0.10	2.05	6.9	0.01						
(C) pH 6.12; Γ = 0.23	2.02	5.3	0.01	3.06	0.8	0.01			
(D) pH 6.56; Γ = 0.79	1.98	4.4	0.01	3.08	1.0	0.01			
(E) pH 7.45; Γ = 0.37	1.93	4.9	0.01	3.10	1.0	0.01			
(F) pH 7.35; Γ = 1.08	1.92	5.2	0.01	3.11	1.2	0.01			
(G)pH 7.35; Γ = 1.11	1.92	5.3	0.01	3.11	1.4	0.01			
(H) pH 7.35; Γ = 1.11	1.92	4.2	0.01	3.11	1.4	0.01			
(I) pH 6.83; Γ = 3.11	1.92	4.5	0.01	3.10	1.1	0.01			
(J) pH 7.51; Γ = 2.56	1.92	5.3	0.00	3.13	1.3	0.01	3.29	1.5	0.01
References									
(A) $Zn(NO_3)_{2\,(aq)}$	2.07	6.1	0.01						
Zincite (ZnO)	1.970	4.3	0.01				3.23	6.8	0.01

[a] Interatomic distance; [b]Coordination number;[c]Debye-Waller factor

from entrained Zn(II) in solution is dominating the XAFS spectra, resulting in spectra that strongly resemble $Zn(NO_3)_{2(aq)}$. On the one hand, the lack of an ionic strength dependence in the sorption edge (Figure 3.1) and minimal amount of Zn sorbed at these low pH values would suggest entrained Zn(II) is being measured. On the other hand, the extremely rapid uptake of Zn on silica (Figure 3.3) would suggest outer-sphere complexation is the primary Zn sorption mechanism since these types of complexes form on micro second time scales (Sparks, 1995b). Given the slight reduction of $R_{Zn\text{-}O}$ for these two samples relative to $R_{Zn\text{-}O}$ for $Zn(NO_3)_{2(aq)}$, it follows that an outer-sphere adsorption mechanism occurred but was indistinguishable from an inner-sphere mechanism from macroscopic observations alone.

As pH, and therefore Zn loading on the surface, increased the values for $R_{Zn\text{-}O}$ and $CN_{Zn\text{-}O}$ decreased, indicating the transition from octahedral Zn to tetrahedral Zn. This is visually observed in the chi spectra (Figure 3.5) as a shift in the entire spectrum from low k to high k. Excluding the $\Gamma = 0.79$ sample at pH 6.56, the average $R_{Zn\text{-}O} =$ 1.92 Å and average $CN_{ZN\text{-}O} \approx 4.8$. Although the $\Gamma = 0.79$ pH 6.56 sample has a higher surface loading value compared to the $\Gamma = 0.37$ pH 7.45 sample it has a longer $R_{Zn\text{-}O}$ distance, suggesting pH and changes in the silica surface plays a more significant role than surface loading alone. In addition to a transition from octahedral Zn to tetrahedral Zn, including a Zn-Si contribution in the least square fitting improved the data fit (decreased the residual value). This is evidence that Zn forms a direct bond to Si tetrahedra in the amorphous silica.

For spectra e-h the average $R_{Zn\text{-}Si} = 3.11$ Å and $CN_{Zn\text{-}Si} = 1.2$. The measured bond distances are indicative of bonding between Zn tetrahedra and Si tetrahedra in a

monodentate manner, based on average O-O edge distances ranging from 2.58 to 2.67 Å in SiO_4 tetrahedra (Cheah et al., 1998; Trainor et al., 2000). The only sample that a Zn-Zn shell was able to fit was spectrum I (Figure 3.5), reacted at pH 7.51 with a $\Gamma = 2.56$ μmol m^{-2}. The $R_{Zn\text{-}Zn}$ value for this sample was 3.29 Å and $N_{Zn\text{-}Zn}$ was 1.5. Although this sample has a lower surface loading relative to sample h, the pH value of the reaction was 0.7 units greater, suggesting a minimum pH value needed to be reached prior to the onset of precipitation. The $R_{Zn\text{-}Zn}$ of 3.29 Å is not indicative of a particular phase, although it was nearest the value of 3.23 Å for $R_{Zn\text{-}Zn}$ in zincite (ZnO). Of particular interest is the fact that zincite was the predicted Zn solid phase most likely to form by calculations using MINEQL. In fact, in all cases zincite was predicited to form and in only one case did this actually happen. This demonstrates the importance of the sorbent phase in predicting the speciation of a metal ion in an aqueous environment.

The difference between $R_{Zn\text{-}Zn}$ in sample I and the $R_{Zn\text{-}Zn}$ in zincite could be a result of Si incorporation into the solid, although more studies on coprecipitated of this variety would need to be performed to confirm this. Aging the sample for 18 months at pH 7.2 had no effect on the overall Zn speciation, with Zn remaining as a monodentate complex to silica tetrahedra.

3.4.3 XAFS Analysis of Zn-reacted Gibbsite

The k^3-weighted Zn XAFS spectra (chi) and their results from nonlinear, least-sqaures fitting for Zn gibbsite are presented in the left panel of Figure 3.7. The corresponding Fourier transforms of the chi spectra are presented in the right panel of Figure 3.7. Much like the XAFS spectra for the Zn-silica samples (Figure 3.5), each of

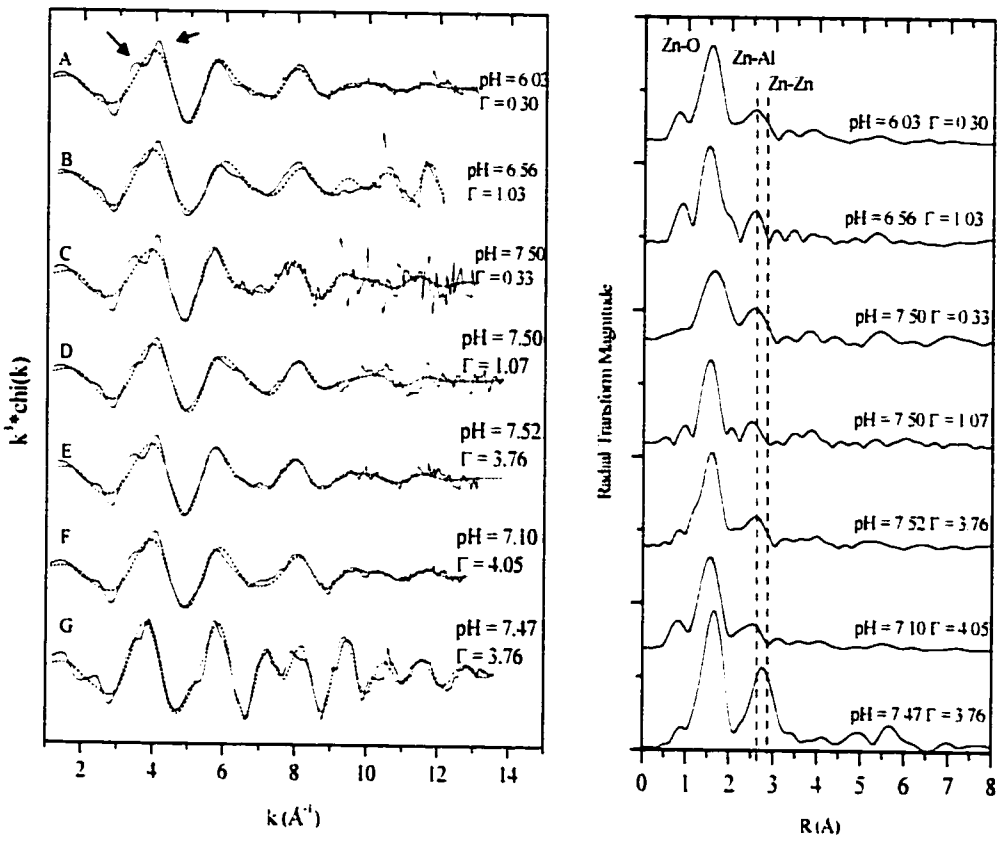

Figure 3.7 Zn-XAFS chi spectra weighted by k^3 (solid lines) and results from nonlinear least squares fitting (dotted lines) for Zn sorbed on HSA gibbsite (A-F) and LSA gibbsite (G). Corresponding Fourier transforms are in the right panel. The arrows on the left panel point out the splitting in the oscillations.

the chi spectra is characterized by a sin wave dominated by backscattering from first shell oxygen atoms around Zn with the signal amplitude decreasing as k increased. In contrast to the Zn-silica samples, the chi spectra have more features relative to the spectra for $Zn(NO_3)_{2(aq)}$, pointed out with guide arrows in the left panel of Figure 3.7. The most striking difference between the Zn-silica and Zn-gibbsite samples is the split in the first oscillation of the chi spectra at $k \approx 4$ Å^{-1} for the Zn-gibbsite samples. While the exact reason for this feature is not totally evident, it appears to be correlated to Zn being in either a distorted octahedron or present as tetrahedral and octahedral Zn.

The fit results in Table 3.4 indicate the average $R_{Zn\text{-}O} = 2.0$ Å for samples E-F, a value close to the average distance of Zn in octahedral coordination and tetrahedral coordination. Our fitting approach did not allow was to distinguish between two separate Zn-O shell distances, but the average $R_{Zn\text{-}O}$ does suggest that Zn may be in octahedral and tetrahedral coordination at the gibbsite surface. Another, and perhaps more likely, explanation is that Zn is present in a distorted octahedron at the gibbsite surface. This is more likely since in performing XAFS fitting only one Zn-O distance was determined in the Zn-gibbsite samples. Given the difference in bond distances between tetrahedral and octahedral Zn (approximately 0.1 Å), it is possible to resolve two distinct bond distances using nonlinear, least-squares analysis.

Evaluation of the second nearest Zn shell via Fourier transforming the XAFS data into radial structure functions (Figure 3.7, right panel) should help glean the mechanism for Zn adsorption in these samples. The average $R_{Zn\text{-}Al} = 3.02$ Å and average $CN_{Zn\text{-}Al} = 2.5$, with samples c and g having discrepancies relative to the average values. In samples A-F the inclusion of a Zn atom in the fitting procedure did not

Table 3.4 Results from XAFS analysis of Zn sorbed to Al oxides.

	Zn-O			Zn-Al			Zn-Zn		
Sample	R (Å)[a]	CN[b]	σ^2 c	R (Å)	CN	σ^2	R (Å)	CN	σ^2
(A) pH 6.03; Γ = 0.30	1.99	4.5	0.01	3.01	2.5	0.01			
(B) pH 6.56; Γ = 1.03	1.97	4.2	0.01	3.00	1.9	0.01			
(C) pH 7.50; Γ = 0.33	2.05	4.9	0.01	3.05	3.3	0.01			
(D) pH 7.50; Γ = 1.07	1.98	4.3	0.01	3.02	1.6	0.01			
(E) pH 7.52; Γ = 3.76	2.01	4.6	0.01	3.01	2.6	0.01			
(F) pH 7.10; Γ = 4.05	2.00	4.5	0.01	3.03	2.9	0.01			
(G) pH 7.47; Γ = 3.76	2.07	6.9	0.01	3.13	4.1	0.01	3.09	4	0.01
ZnGamma-Al (fresh)	1.97	4.6	0.01	3	1.04	0.01			
ZnGamma-Al (aged)	1.97	4.5	0.01	3.03	0.93	0.01			

[a] Interatomic distance; [b]Coordination number; [c]Debye-Waller factor

improve fit quality indicating the lack of neo-precipitate formation in these samples. Assuming R_{Al-O} = 1.85 – 1.97 Å and R_{O-O} = 2.52 – 2.86 Å for the gibbsite structure (Saalfeld and Wedde, 1974), and the average R_{Zn-O} of 3.02 Å from the sorption samples, it follows that an edge-sharing bidentate adsorption geometry (inner-sphere complex) is the main mechanism for Zn uptake on the gibbsite surface. Geometric considerations would allow Zn to be in either a tetrahedral or octahedral coordination in this arrangement (Bargar et al., 1997). The R_{Zn-Al} distance of 2.05 Å for sample C nearly falls in the range of values whereby an edge- sharing bidentate complex could form. The poor spectra quality as a result of low Zn concentrations makes the exact determination of Zn complexes difficult for this sample.

Zn XAFS were also measured on LSA gibbsite and γ-Al_2O_3 to determine the identity of the sorbent phase on Zn complexation. The purpose of using γ-Al_2O_3 was that Al is found as both AlO_6 octahedra and AlO_4 tetrahedra in this solid phase so the role of Al in both octahedral and tetrahedral on Zn complexation could be determined. Evidence suggest that within a few days all AlO_4 tetrahedra convert to AlO_6 octahedra upon contact with water (Bargar et al., 1997). Therefore, a sample was prepared where the γ-Al_2O_3 had less than one day of equilibration in background solution (fresh) as well as one in γ-Al_2O_3 that was aged in 0.1 M $NaNO_3$ for a month (aged). The reaction was carried out in a glovebox with $[Zn]_o$ = 1 mM and pH = 7.4. The fit results (data not shown) are presented in Table 3.4. There was no apparent difference in the mode of Zn sorption compared between the fresh and aged samples nor between Zn sorbed on gibbsite and Zn sorbed on γ-Al_2O_3.

In contrast, a major difference occurred between Zn sorbed on HSA gibbsite and LSA gibbsite (pH = 7.5; $[Zn]_o$ = 1 mM; I = 0.1 M) as can be observed in comparing spectra G to the rest of the samples in Figure 3.7. Significant structural features are evident in the LSA gibbsite sample, most notably a split in the third oscillation of the chi spectrum at $k \approx 8$ Å^{-1} (Figure 3.7). In addition, the radial structure function shows a large second peak at $R \approx 2.8$ Å. Fit results indicated the Zn formed a Zn Al layered double hydroxide (LDH) phase upon sorption to the LSA gibbsite. This conclusion was reached based on the values $R_{Zn\text{-}O} = 2.07$, $R_{Zn\text{-}Al} = 3.13$ Å and $R_{Zn\text{-}Zn} = 3.09$ Å, nearly identical to the bond distances for Zn found in synthesized Zn Al LDH (Ford et al., 1999). Similar findings have been reported for Zn adsorbed on α-Al_2O_3 and pyrophyllite at $\Gamma > 1.7$ μmol m^{-2} and 0.8 μmol m^{-2} Zn coverage, respectively. Results from this study indicated the slow sorption of Zn on LSA gibbsite was a result of Zn Al LDH formation, whereas the more rapid kinetics of Zn sorption on HSA gibbsite were a result of inner-sphere, monodentate Zn complex formation. Moreover, aging the sample for 18 months in the presence of HSA gibbsite did not result in identifiable changes in Zn speciation.

3.5 Concluding Points

Zn sorption on amorphous silica and HSA gibbsite was characterized by rapid sorption with no dependence on ionic strength. Under the studied reaction conditions, XAFS confirmed Zn complexation via mononuclear bidentate surface complex formation as the major mechanism of adsorption. With high pH values and loading levels, Zn precipitate formation became a viable sorption mechanism in these systems.

It should be noted that sorption mechanisms are often in continuum and multiple mechanisms may be in operation at any given point in an experiment and all should be considered in applying a model to a set of sorption studies. Our hypothesis that Zn coordination would follow the coordination environment of the metal oxide it is adsorbed to held true for Zn sorption to amorphous silica (SiO_4 tetrahedron), whereas for the HSA gibbsite, a distorted Zn octahedron was evident.

3.6 References

Baes, C.F. and B.E. Mesmer. 1976. The hydrolysis of cations. Wiley and Sons, New York.

Bargar, J.R., G.E. Brown Jr. and G.A. Parks. 1997. Surface complexation of Pb(II) at oxide-water interfaces: I. XAFS and bond-valence determination on mononuclear and polynuclear and polynuclear Pb(II) sorption products on aluminum oxides. *Geochim. Cosmochim. Acta* **61:** 2617-2637.

Baumgarten, E. and Kirchhausen-Dusing. 1997. Sorption of metal ions on alumina. *J. Colloid Interface Sci.* **194:** 1-9.

Benjamin, M.M. and J.O. Leckie. 1981. Multi-site adsorption of Cd, Co, Zn, and Pb on amorphous iron oxyhydroxide. *J. Colloid Interface Sci.* **79:** 1999-2010.

Chaney, R.L. 1993. Zinc phytoxicity. pp. 135-144. *In* A.D. Robson (ed.) Zinc in Soils and Plants. Kluwer Academic Publishers, The Netherlands.

Charlet, L. and A. Manceau. 1994. Evidence of the neoformation of clays upon sorption of Co(II) and Ni(II) on silicates. *Geochim. Cosmochim. Acta* **58:** 2577-2582.

Cheah, S., G.E.J. Brown and G.A. Parks. 1998. XAFS spectroscopy study of Cu(II) sorption on amorphous SiO_2 and γ-Al_2O_3: effect of substrate and time on sorption complexes. *J. Colloid Interface Sci.* **208:** 110-128.

Chisholm-Brause, C.J., P.A. O'Day, G.E. Brown Jr. and G.A. Parks. 1990. Evidence for multinuclear metal-ion complexes at solid/water interfaces from X-ray absorption spectroscopy. *Nature* **348:** 528-531.

Coston, J.A., C.C. Fuller and J.A. Davis. 1995. Pb^{2+} and Zn^{2+} adsorption by a natural aluminum- and iron-bearing surface coating on an aqufier sand. *Geochim. Cosmochim. Acta* **59:** 3535-3547.

Crepaldi, E. and J. Valim. 1998. Layered double hydroxides: structure, synthesis, properties and applications. *Quim. Nova* **21:** 300-311.

Elzinga, E.J. and D.L. Sparks. 1999. Nickel sorption mechanisms in a pyrophyllite-montmorillonite mixture. *J. Colloid Interface Sci.* **213:** 506-512.

Fendorf, S.E., G.M. Lamble, M.G. Stapleton, M.J. Kelley and D.L. Sparks. 1994. Mechanisms of chromium (III) sorption on silica: 1. Cr(III) surface structure derived by extended x-ray absorption fine structure spectroscopy. *Environ. Sci. Technol.* **28:** 284-289.

Ford, R.G., A.C. Scheinost, K.G. Scheckel and D.L. Sparks. 1999. The link between clay mineral weathering and structural transformation in Ni surface precipitates. *Environ. Sci. Technol.* **33:** 3140-3144.

Ford, R.G. and D.L. Sparks. 2000. The nature of Zn precipitates formed in the presence of pyrophyllite. *Environ. Sci. Technol.* **34:** 2479-2483.

Huang, C.P. and A. Rhoads. 1989. Adsorption of Zn(II) onto hydrous aluminosilicates. *J. Colloid Interface Sci.* **131:** 289-306.

Kinniburgh, D.G. and M.L. Jackson. 1981. Cation adsorption by hydrous metal oxides and clay. pp. 91-160. *In* M.A. Anderson and A.J. Rubin (eds.) Adsorption of Inorganics at Solid-Liquid Interfaces. Ann Arbor Sci., Ann Arbor, MI.

Kyle, J.H., A.M. Posner and J.P. Quirk. 1975. Kinetics of isotopic exchange of phosphate adsorbed on gibbsite. *J. Soil Sci.* **26.**

Ladonin, D.V. 1997. Specific adsorption of copper and zinc by some soil minerals. *Eurasian Soil Sci.* **30:** 1478-1485.

Metwally, A.I., A.S. Mashhady, A.M. Falatah and M. Reda. 1993. Effect of pH on zinc adsorption and solubility in suspensions of different clays and soils. *Z. Pflanzenernähr. Bodenk.* **156:** 131-135.

O'Day, P.A., S.A. Carroll and G.A. Waychunas. 1998. Rock-water interactions controlling zinc, cadmium, and lead concentration in surface waters and sediments, U.S. tri-state mining district. 1. Molecular identification using x-ray absorption spectroscopy. *Environ. Sci. Technol.* **32:** 943-955.

O'Day, P.A., C.J. Chisholm-Brause, S.N. Towle, G.A. Parks and G.E. Brown Jr. 1996. X-ray absorption spectroscopy of Co(II) sorption complexes on quartz (α-SiO_2) and rutile (TiO_2). *Geochim. Cosmochim. Acta* **60:** 2515-2532.

Papelis, C. and K.F. Hayes. 1996. Distinguishing between interlayer and external sorption sites of clay minerals using X-ray absorption spectroscopy. *Colloids Surf., A* **107:** 89-96.

Ressler, T. 1997. WinXAS: A new software package not only for the analysis of energy-dispersive XAS data. *J. Phys. IV* **7:** 269-270.

Roberts, D.R., A.M. Scheidegger and D.L. Sparks. 1999. Kinetics of mixed Ni-Al precipitate formation on a soil clay fraction. *Environ. Sci. Technol.* **33:** 3749-3754.

Saalfeld, H. and M. Wedde. 1974. Refinement of crystal-structure of gibbsite $Al(OH)_3$. *Z. Kristallogr.* **139:** 129-135.

Scheckel, K.G. and D.L. Sparks. 2000. Kinetics of the formation and dissolution of Ni precipitates in a gibbsite/amorphous silica mixture. *J. Colloid Interface Sci.* **229:** 222-229.

Scheckel, K.G. and D.L. Sparks. 2001. Temperature effects on nickel sorption at the mineral-water interface. *Soil Sci. Soc. Am. J.* **65:** 719-728.

Scheidegger, A.M., G.M. Lamble and D.L. Sparks. 1996. The kinetics of nickel sorption on pyrophyllite as monitored by x-ray absorption fine structure (XAFS) spectroscopy. *J. Phys. IV* **4:** 773-775.

Scheidegger, A.M., G.M. Lamble and D.L. Sparks. 1997. Spectroscopic evidence for the formation of mixed-cation hydroxide phases upon metal sorption on clays and aluminum oxides. *J. Colloid Interface Sci.* **186:** 118-128.

Scheidegger, A.M. and D.L. Sparks. 1996. A critical assement of sorption-desorption mechanisms at the soil mineral/interface. *Soil Sci.* **161:** 813-831.

Scheidegger, A.M., D.G. Strawn, G.M. Lamble and D.L. Sparks. 1998. The kinetics of mixed Ni-Al hydroxide formation on clays and aluminum oxides: a time-resolved XAFS study. *Geochim. Cosmochim. Acta* **62:** 2233-2245.

Scheinost, A.C., R.G. Ford and D.L. Sparks. 1999. The role of Al in the formation of secondary Ni precipitates on pyrophyllite, gibbsite, talc, and amorphous silica: a DRS study. *Geochim. Cosmochim. Acta* **63:** 3193-3203.

Shuman, L.M. 1977. Adsorption of Zn by Fe and Al hydrous oxides as influenced by aging and pH. *Soil Sci. Soc. Am. J.* **41:** 703-706.

Singh, B. and R.J. Gilkes. 1993. The recognition of amoprhous silica in indurated soil profiles. *Clay Miner.* **28:** 461-474.

Spark, K.M., B.B. Johnson and J.D. Wells. 1995. Characterizing heavy-metal adsorption on oxides and oxyhydroxides. *Eur. J. Soil Sci.* **46:** 621-631.

Sparks, D.L. 1995a. Environmental Soil Chemistry. Academic Press, San Diego.

Sparks, D.L. 1995b. Kinetics of metal sorption reactions. *In* H.E. Allen, C.P. Huang, G.W. Bailey and A.R. Bowers (eds.) Metal Speciation and Contamination of Soil. Lewis Publishers, Boca Raton.

Strawn, D.G., A.M. Scheidegger and D.L. Sparks. 1998. Kinetics and mechanisms of Pb(II) sorption and desorption at the aluminum oxide-water interface. *Environ. Sci. Technol.* **32:** 2596-2601.

Tiller, K.G. and J.G. Pickering. 1974. The synthesisof zinc silicates at 20°C and atmospheric pressure. *Clays Clay Miner.* **22:** 409-416.

Trainor, T.P., G.E. Brown Jr. and G.A. Parks. 2000. Adsorption and precipitation of aqueous Zn(II) on alumina powders. *J. Colloid Interface Sci.* **231:** 359-372.

Vlasova, N.N. and N.K. Davidenko. 1995. The adsorption of dipyridyl and its complex with zinc(II) on silica surfaces. *Colloids Surf., A* **104:** 53-56.

Wilkinson, G. 1987. Comprehensive coordination chemistry. Pergamon. Oxford.

Xu, Y., F.W. Schwartz and S.J. Traina. 1994. Sorption of Zn^{2+} and Cd^{2+} on hydroxyapatite surfaces. *Environ. Sci. Technol.* **28:** 1472-1480.

Yamaguchi, N., A.C. Scheinost and D.L. Sparks. 2001. Surface-induced nickel hydroxide precipitation in the presence of citrate and salicylate. *Soil Sci. Soc. Am. J.* **65:** 729-736.

Zabinsky, S.L., J.J. Rehr, A. Ankudinov, R.C. Albers and M.J. Eller. 1995. Multiple-Scattering Calculations Of X-ray-Absorption Spectra. *J. Phys. Rev., B.* **52:** 2995-3009.

Chapter 4

ZINC SPECIATION IN CONTAMINATED SOILS IN THE VICINITY OF THE PALMERTON, PA SMELTER USING BULK AND MICRO-XAFS SPECTROSCOPIES

4.1 Abstract

Soils contaminated as a result of Zn smelting operations from the historic Palmerton, PA smelting facility were characterized using X-ray absorption fine structure (XAFS) spectroscopy coupled with electron microprobe (EM), X-ray diffraction (XRD), and micro-focused synchrotron-based spectroscopies. Surface (0-5 cm) and subsurface (5-10 cm) soil samples were collected from a non-vegetated region on Blue Mountain, the pH was measured and total metal concentrations were determined using an acid extraction technique. The surface soil had a Zn concentration of 6196 ppm with a pH of 3.19 while the subsurface soil had a Zn concentration of 900 ppm and a pH of 3.86. XRD analysis indicated the main Zn mineral phase in the surface soil was franklinite ($ZnFe_2O_4$), while Zn-containing phases of the subsurface soil were not detected using XRD. Both bulk and micro-focused XAFS analyses were performed on both soils and on a variety of Zn-bearing mineral phases and synthesized Zn sorption samples to aid in identifying Zn species. XAFS revealed the Zn distribution

in the surface soil consisted of approximately 66% franklinite and 34% sphalerite (ZnS), material aerially deposited from the smelter. Bulk XAFS revealed that Zn in the subsurface soil was dominated by sorption complexes to Al-bearing minerals and to a lesser extent to Fe oxides. More labile outer-sphere complexes were also present in this sample. Micro-focused XAFS revealed information about the heterogeneity of Zn in the soil over small areas and helped verify the findings achieved using bulk XAFS. Stirred-flow desorption studies revealed Zn was more stable in the surface soil relative to the subsurface soil. These results show the utility of micro-focused, synchrotron-based methods in speciating metal-contaminated soils beyond what other techniques alone can achieve.

4.2 Introduction

The impact of smelting and processing of metal ores on environmental quality has been a major issue in industrialized countries for several decades. Often ore processing results in atmospheric emissions of acid and metals, resulting in increased trace metal concentrations and acidic pH values in topsoils in the vicinity of smelter facilities. One significant metal contaminant in soils near smelters is zinc, as it is mined in 50 countries and smelted in 21 countries (Dudka and Adriano, 1997). In addition to releasing Zn to the environment, Zn ore processing may also introduce Cd and Pb to soils as Zn ores often contain trace amounts of these elements. Under acidic, oxidizing conditions Zn is one of the most soluble and mobile of the trace metal cations (McBride, 1994) and in strongly acid soil Zn phytoxicity is the most extensive microelement phytotoxicity after Al and Mn (Chaney, 1993). Consequently, soils near

Zn smelters have a decline in the number of soil microorganisms, reduced soil fertility, damaged vegetation, and increased soil erosion. Moreover, human exposure to Zn exists due to inhalation of soils containing Zn-bearing particles. The environmental and human risk associated with Zn-impacted soils underscores the need to elucidate the fate of Zn introduced into soil environments.

Once Zn^{2+} is released from metal-bearing phases i.e., from ZnS (sphalerite), it may mobilize in the soil profile and potentially become immobile as a result of: 1) secondary precipitate (bulk or surface) formation; 2) adsorption to soil minerals; 3) partitioning to organic matter; or 4) coprecipitation in other minerals (McBride, 1994). The pathway Zn^{2+} follows is dependent on the environmental conditions (pH, soil mineralogy, organic matter content), and there is often a continuum between these mechanisms in a system. The degree of Zn mobility, and therefore bioavailability, is strongly dependent on the form it takes in soil, making speciation of Zn of paramount importance prior to making risk assessments and implementing remediation strategies.

Research investigating Zn sorption in 'simplified' oxide and clay minerals systems and in soils displays its variable reactivity and speciation, with the identified Zn species being dependent on the experimental conditions (pH, metal concentration, reaction time). Macroscopic sorption studies has shown Zn can effectively form adsorption complexes to Mn oxides (Murray, 1975; Stahl and James, 1991; Zasoski and Burau, 1988), Fe (hydr)oxides, Al (hydr)oxides (Kinniburgh et al., 1976; Melis et al., 1987), and aluminosilicates (Huang and Rhoads, 1989; Ladonin, 1997; Spark et al., 1995), with the degree of adsorption increasing with pH. At alkaline pH values with high Zn concentrations, the precipitation of $Zn(OH)_2$, $Zn(CO)_3$, and $ZnFe_2O_4$ may

control Zn speciation in these systems (Metwally et al., 1993; Sadiq, 1991). Researchers have also concluded that diffusion of Zn into the micropores of Fe oxides may effectively immobilize Zn in soils (Bruemmer et al., 1988; Gerth et al., 1992; Manceau et al., 2000b). While these studies have improved our understanding of Zn in soil environments, more direct approaches are necessary to provide precise speciation.

Direct spectroscopic and microscopic investigations have demonstrated the variable reactivity and speciation of Zn. Using X-ray absorption fine structure (XAFS) spectroscopy to monitor zinc sorption to oxides under neutral to basic pH values, researchers have demonstrated that Zn can form both inner-sphere surface complexes and Zn hydrotalcite-like phases upon sorption to Al-bearing minerals (Ford and Sparks, 2000; Trainor et al., 2000); inner-sphere surface complexes upon sorption to goethite (Schlegel et al., 1997); and both inner-sphere and multinuclear hydroxo-complexes upon Zn sorption to manganite (Bochatay and Persson, 2000). By applying XAFS and electron microscopy to Zn-contaminated soils and sediments, Zn has been demonstrated to occur as ZnS in reduced environments, often followed by repartitioning into Zn hydroxide and/or ZnFe hydroxide phases upon oxidation (Hesterberg et al., 1997; O'Day et al., 1998; Webb et al., 2000). Manceau et al. (2000a) used a variety of techniques, including XAFS and micro-focused XAFS to demonstrate that upon weathering of Zn-mineral phases, Zn was taken up by the formation of Zn-containing phyllosilicates and, to a lesser extent, by adsorption to Fe and Mn (oxyhydr)oxides. These studies demonstrate that in any given system, Zn may be present in one of several forms making direct identification of each species difficult using traditional approaches.

Although total content of metals can give insight into the degree of pollution, it gives no information regarding bioavailability or chemical behavior (de Groot, 1995). Slightly better at assessing metal speciation in soils are sequential extraction techniques, which are favorable in terms of standard routine capable of expediting the characterization process, but they may transform chemical forms and overlook minor phases (Webb et al., 2000). To alleviate such shortcomings, analytical techniques providing more direct identification of species [i.e., X-ray diffraction (XRD), thermal gravimetric analysis (TGA), x-ray photoelectron spectroscopy (XPS)] have been adopted to characterize metals in contaminated soils. Despite their clear advantage in giving more accurate descriptions of metal speciation relative to extraction approaches, these techniques may introduce artifacts from sample alterations and detection limits are often far above background concentrations of the target metal.

The application of synchrotron-based spectroscopic techniques to study environmental samples has enabled researchers to estimate the chemical environment of contaminants without relying solely on indirect sequential extraction methods and less sensitive, ex-situ analytical techniques. XAFS spectroscopy is a technique that can provide detailed chemical and structural information about a specific absorbing element, be it a major component of a solid phase (crystalline or amorphous), a trace component of the bulk phase, or a surface-associated component (Bertsch and Hunter, 1998). Several research studies have demonstrated the utility of XAFS to elucidate sorption mechanisms of metal ions on single-component metal oxides and clay mineral systems (Bargar et al., 1997; Charlet and Manceau, 1992; Fendorf et al., 1994; Manceau et al., 1996; Scheidegger et al., 1998; Schlegel et al., 1999; Strawn et al., 1998; Towle et

al., 1997). Subsequently, XAFS studies have been performed using mixtures of oxides and clay minerals to better simulate metal sorption behavior in natural systems (Elzinga and Sparks, 1999; Scheckel and Sparks, 2000). These studies have enabled researchers to take this technique one step further, enabling researchers to use XAFS to characterize metal-contaminated environmental samples with a relatively high degree of success (Hesterberg et al., 1997; Manceau et al., 1996; Morin et al., 1999; Morris et al., 1996; O'Day et al., 1998; Ostergren et al., 1999). While these studies have been critical in improving the understanding of metal sorption mechanisms in geomedia, one must realize that standard (bulk) XAFS probes an area of several millimeters in a sample, providing only an average speciation of the metal of interest in a sample. This may pose a problem when one is analyzing XAFS data collected on heterogeneous samples since the spectra may represent several species and without the proper database of reference samples the data are difficult to decipher (Hunter and Bertsch, 1998). Moreover, in samples where the metal may be in present in numerous phases, the detection limit for minor species is indefinite and all species may not be represented upon spectral analyses since high Z elements are preferentially represented over low Z elements (Manceau et al., 2000a).

To overcome the lack of spatial sensitivity of bulk XAFS there are other techniques capable of probing an element in an environmental sample at a scale more indicative of the most reactive sites in soils (micron level). Using electron microscopy coupled with energy-dispersive X-ray fluorescence spectroscopy (EDXS) one can attain both quantitative (elemental composition) and qualitative (contaminant distribution) with good spatial resolution (< 1 μm) (Webb et al., 2000). However, the information

gleaned from X-ray EDS only provides elemental concentrations, making it difficult to distinguish between sulfur and sulfate, for example. This technique also requires elements be present in nearly crystalline phases in concentrations greater than 1%, limiting its application to many contaminated systems.

One of the most promising techniques to examine heterogeneous soil and environmental samples is spatially resolved micro(μ)-XAFS (μ-X-ray absorption near edge (μ–XANES) and μ-EXAFS) combined with micro-synchrotron-X-ray fluorescence spectroscopy (μ-SXRF), whereby discrete regions within a complex mixture can be interrogated on a micron scale (Bertsch and Hunter, 1998; Manceau et al., 2000a). The high flux of third generation light sources combined with the ability to focus the X-ray beam down to only a few microns can enable one to probe domains representing distinct chemical environments present in heterogeneous samples at a micro-scale (Hunter and Bertsch, 1998). The advantage of using synchrotron-based radiation relative to standard electron microprobe techniques is the increased sensitivity to metal concentrations. Moreover, synchrotron-based techniques such as μ-XANES, μ-XAFS and μ-SXRF are useful in assessing the validity of bulk-XAFS analysis in that one can determine if the small-scale speciation is well represented by bulk-scale speciation. Despite its clear advantages in characterizing contaminated environmental samples, only few studies utilized this technique (Bertsch and Hunter, 1998; Duff et al., 1999; Hunter and Bertsch, 1998; Manceau et al., 2000a).

The objective of this study was to characterize Zn in the topsoil of smelter-impacted soils by directly identifying Zn-bearing mineral phases and any secondary

complexes or precipitates that form in the soil as a result of their weathering. We have combined a variety of analytical techniques to meet this objective, including XRD, electron microprobe, bulk-XAFS, μ-XANES, μ-XAFS and μ-SXRF analysis. In addition, the stability of Zn in these soils was assessed using a stirred-flow desorption approach and correlations between speciation and metal bioavailability are subsequently made.

4.3 Methods and Materials

4.3.1 Site Description and Sampling

Over 2,000 acres of land on the north-facing slope of Blue Mountain have been contaminated from the emissions of the nearby Palmerton Zn smelting plant. The zinc smelting facilities (Smelters I and II) are located in east-central Pennsylvania near the confluence of Aquashicola Creek and the Lehigh River in the town of Palmerton (Storm et al., 1993). The first of two smelting plants was opened in 1898 by the New Jersey Zinc Company in order to process zinc sulfide (sphalerite) from ore brought in from New Jersey. In 1980 the plants stopped zinc smelting and in 1982 the U.S EPA placed the area on its National Priorities List as a Superfund Site as a result of years of environmental degradation. The sphalerite ores contained approximately 55% zinc, 31% sulfur, 0.15% cadmium, 0.30% lead, and 0.40 % copper (Buchauer, 1973). Over the 82 years the smelters produced approximately 47 tons/year of Cd, 95 tons Pb/year, and 3,575 tons/year of Zn and that daily metal emissions since 1960 have ranged from 6,000 to 9,000 kg of Zn and 70-90 kg of Cd (Buchauer, 1973; Lalo, 1988). In addition to metals, smelting processes produce sulfuric acid that can then be deposited into

surrounding areas and contribute to acidic pH values of the soil. At one time Blue Mountain was densely vegetated but extremely high phytotoxic metal concentrations and low pH values resulted in the loss of most vegetation and subsequent soil erosion. Several attempts have been made to revegetate the site but thus far an effective remediation strategy has yet to be adopted (Ketterer et al., 2001).

Soil samples were collected along the Appalachian Trail, which follows the crest of the Blue Mountain SE of Palmerton. The most heavily contaminated soil collected from a profile directly above Smelter II was selected for more detailed experiments. Due to the complete devegetation of the area, the original soil has been almost completely eroded at this location, and the bedrock is exposed. The soil was collected in a shallow pit, where a shallow soil profile < 15 cm in depth persisted. The topsoil consisted of a 3-6 cm thick layer of dark, dry organic debris consisting of partially decomposed plant residue, twigs, and loess material. The consolidated subsoil is most likely the remainder of the original Dekalb and Laidig series stony loams derived from shale, sandstone, and conglomerate (Storm et al., 1993).

4.3.2 Methods

Samples were air dried and first dry sieved to collect the <2 mm size fraction and wet sieved to collect the <250 μm fraction. The soil pH was determined in 0.01 M $CaCl_2$. Total metal concentration was measured using a HNO_3/HCl/HF extraction followed by boric acid extraction (Lin and Herbert Jr., 1997). The solutions were then analyzed for metal concentration using inductively coupled plasma mass spectrometry (ICP-MS) (Rose and Ghazi, 1998).

The bulk mineralogy of the <250 μm fraction of the soils was determined by powder X-ray diffraction using a Philips Norelco 1720 instrument equipped with Cu Kα radiation (40kV, 40mA). Data were collected between 3° and 70° 2θ with a 0.04° step and a counting time of 5 s per step. Electron microprobe analysis was performed on resin-embedded soil thin sections (30 – 100 μm thick) mounted on pure quartz slides using a JEOL JXA-8600 microprobe equipped with wavelength dispersive spectrometers (WDS). Compositions of small grains in the samples were determined and elemental maps collected on several elements (Si, Al, S, P, K, Ca, Zn, Mn, Fe, Pb) throughout the samples.

4.3.3 X-ray Absorption Fine Structure (XAFS)

Zn K-edge (9659 eV) XAFS data were collected on the soils, Zn reference compounds, and Zn-sorption samples at beamline X-11A at the National Synchrotron Light Source (NSLS), Upton, NY. The electron beam energy was 2.5 GeV beam current varied from 300 mA to 100 mA. The beamline monochromator consisted of two parallel Si(111) crystals adjusted to an entrance slit of 1 mm. The monochromator was detuned by reducing I_o by 25% after optimizing the incoming beam. All samples were run under ambient conditions (24°C) using an unfocussed beam. For the surface soil, the air-dried soil was sieved to collect the < 2mm size fraction and subsequently mounted into Teflon sample holders and sealed with Kapton® tape with no further alteration. For the subsurface soil, three samples were used: 1) the < 2mm fraction, 2) the <250 μm fraction collected by sedimentation in water and subsequent freeze drying,

and 3) dark 'nodules' (0.5 – 2 mm in diameter) distinct from the bulk of the light colored soil which were hand collected and ground in a mortar and pestle. All three samples were mounted in sample holders in the same manner as the surface soil. The Zn reference minerals were ground in a mortar and pestle and diluted to ten weight percent in boron nitride and thoroughly mixed prior to being loaded in the sample holders. Data were collected in florescence mode using a Stern-Heald-type (Lytle) detector filled with Kr gas and equipped with a 3-μm Cu filter (Lytle et al., 1984). In the case of high Fe-containing samples, two to four sheets of Al foil were placed in front of the Cu filter to dampen the Fe fluorescence signal. Multiple scans were collected on each sample, depending on metal concentration and Fe content, to improve the signal to noise ratio.

To provide an extensive reference library of Zn XAFS spectra for the purpose of linear combination fitting, Zn reference minerals and sorption samples were used in the study. Several Zn-bearing mineral phases were supplied by the Smithsonian Institute mineral collection for use as reference materials. They include $ZnFe_2O_4$ (franklinite), $(Mn,Zn,Fe)_{0.2}MnO_2$ (chalcophanite), $Zn_5(OH)_6(CO_3)_2$ (hydrozincite), $ZnCO_3$ (smithsonite). Other standards include ZnS (sphalerite, Aldrich, 99.9+% purity) and $Zn(NO_3)_2$ (Zn nitrate, Aldrich, 99.9+% purity). A Zn-Al layered double hydroxide phase was synthesized in the laboratory following the method of Ford et al. (2000). In addition to the mineral phases, synthetic sorption samples were prepared in our laboratory and include Zn reacted with ferrihydrite (2-line, freshly precipitated) (Schwertmann and Cornell, 1991), high-surface area gibbsite (synthesized and aged 30 days, 90 $m^2 g^{-1}$), birnessite (45 $m^2 g^{-1}$) (McKenzie, 1971), kaolinite (University of Missouri Source Clays Repository, Kga-1, cleaned, 10$m^2 g^{-1}$), vermiculite and hydroxy-

Al interlayered vermiculite (University of Missouri Source Clays Repository, Sanford vermiculite, cleaned, $90 m^2 g^{-1}$), and fulvic acid (Aldrich, 99% purity). All sorption samples were prepared in an N_2 atmosphere in a glovebox using ACS reagent grade chemicals and CO_2-free DDI H_2O. Solid suspensions of 10 g L^{-1} were adjusted to pH 6.0 ± 0.3 using 0.1 M HNO_3 and the ionic strength was 0.1 M in $NaNO_3$. Zn from a 0.1 M $ZnNO_3$ stock solution was added to achieve a coverage of approximately 1.5 $\mu mol/m^2$ after 100% Zn was removed from solution (with the exception of the ferrihydrite and high-loading birnessite samples). Reactions were carried out for 24 hours in an end-over-end shaker and the pH was adjusted to 6.0 ± 0.3 every 6 hours. Solids were separated by centrifuging at 10,000 RPM for 10 minutes followed by passing the supernatant through a 0.2-μm filter. Solutions were then analyzed for Zn concentration using ICP optical emission spectroscopy. Moist pastes were mounted into Teflon sample holders and sealed with Kapton® tape for XAFS analysis.

All XAFS data were fit using non-linear least-squares fitting of individual coordination shells. Using the program WinXAS97 ver. 1.3 (Ressler, 1997), k^3-weighted chi data were extracted from the raw data and subsequently Fourier transformed over the range of 1.5 – 12 $Å^{-1}$. Zn-O, Zn-S, Zn-Fe, Zn-Al and Zn-Zn scattering paths were generated by FEFF7 (Zabinsky et al., 1995) from theoretical paths generated using the program ATOMS based on structural refinement data of Zn-bearing minerals. To reduce the number of adjustable parameters, the amplitude reduction factor, S_o^2, was fixed at 0.85 during fitting. The errors in the first and second shell bond distances (R) were estimated to be accurate to R± 0.02 Å and coordination numbers (N) were accurate to N±30% based on a comparison of these values for franklinite and

sphalerite using XRD and XAFS (XRD data not shown) and based on estimates in the literature (O'Day et al., 1998; Scheidegger et al., 1997). In addition to the shell fitting approach, the soil samples were analyzed using direct least squares fitting of the k^3 chi(k) data using linear combination of known Zn references. This approach was used since conventional shell-by-shell fitting in multi-component systems can lead to impractically large values for the fitting parameters (Manceau et al., 2000a; Morin et al., 1999). Fitting was performed using the program WinXAS97 1.3 and fits were optimized by minimizing the fit residual, defined as the normalized root square difference between the data and the fit (Ostergren et al., 1999). The accuracy of the fitting is dependent on the data quality, range of fitting, and how well the standards represent the unknown sample (Ostergren et al., 1999). It has been reported that using this approach, estimates are accurate to within plus or minus 25% of the actual atomic fractions present and it is capable of identifying contributions on the order of 10% (Manceau et al., 2000a; Morin et al., 1999).

4.3.4 Micro-XAFS and Micro-SXRF

Spatially resolved μ-XANES and μ-SXRF for the surface and subsurface samples were measured on beamline 10.3.2 at the Advanced Light Source (ALS), Lawrence Berkeley National Lab, Berkeley, CA. Spatially resolved μ-XAFS and μ-SXRF were measured on subsurface and surface soil at the GSECARS beamline 13-ID-C at the Advanced Photon Source (APS), Argonne National Lab, Chicago, IL. Both facilities have similar capabilities, with the APS having a greater overall flux and therefore capability to collect extended XAFS data on samples with lower

concentrations. Soil samples were embedded in acrylic resin (LR-White), cut, and polished into 50 μm-thick thin sections. Both beamlines were equipped with a pair of Si(111) channel-cut monochromator crystals in the path of the beam. The beams were focused down to approximately 2-5 μm using a set of grazing incidence platinum-coated elliptically bent Kirkpatrick-Baez (K-B) focusing mirrors (MacDowell et al., 1998). Samples were placed on a digital x-y-z stage and set at an angle of 45° to the incident beam. Fluorescence X-rays were detected with either a Si solid-state detector (10.3.2) or a Ge 9-element detector (13-ID-C) positioned approximately 1-2 cm from the sample, depending on the Zn concentration in the sample. At the ALS, SXRF maps were collected over 800 × 800 μm^2 areas with a 5 μm step size and 500 msec count time. The beam energy was set to 11 keV during mapping so elements with absorption energies below this value could be measured.

The μ-XANES spectra were collected on selected regions in the samples based on elemental associations obtained from μ-SRXF mapping. XANES were collected from 100 eV below to 300 eV above the Zn K edge in varying step increments from 0.05 to 10 eV with a count time of 10 s. Zn foil was used to calibrate to the Zn K edge, with few calibrations necessary given the stability of the X-ray source. At the APS, μ-SXRF maps were collected over 300 × 300 μm^2 areas with a 5 μm step size and 500 msec count time. The μ-XAFS were collected using the same settings as the bulk-XAFS collected at NSLS. For the μ-XANES data, linear combination fitting of reference XANES spectra was used to identify the Zn species present in the samples. All μ-XAFS

data were fit in the same manor as the bulk XAFS data (non-linear least-squares fitting and linear combination fitting).

4.3.5 Desorption Experiments

The experimental setup for the Zn desorption studies from the contaminated surface and subsurface soils was similar to that used by Strawn et al. (1998) for Pb desorption from soils. Briefly, a stirred-flow reaction chamber connected to an HPLC pump at one end and fraction collector at the other end was employed (Figure 4.1). The chamber was approximately 30 cm in diameter and 40 cm high with a total volume of 9-mL. A 0.2 M $CaCl_2$ solution adjusted to the pH of the soil was pumped through the chamber at a flow rate of 0.5 mL min^{-1} and the fraction collector was set up to collect 5-mL per tube. The chamber was equipped with a 25 mm filter membrane with a 0.2 μm pore size to separate the solid from the solution. Enough soil was added to the chamber to make a 28 g L^{-1} suspension upon addition of background solution. Stirring was held constant at 400 rpm for the duration of the experiments via a magnetic stir bar and stir plate. The collected samples were analyzed for Zn using atomic absorption spectrometry (AAS).

4.4 Results and Discussion

4.4.1 Bulk Phase Analysis

Zn concentration in the surface litter material is 6.196 mg/kg and decreased to 892 mg/kg in the subsurface soil. The pH of the surface material was 3.19 and increased to 3.86 with depth. The other soils collected (data not shown) show the

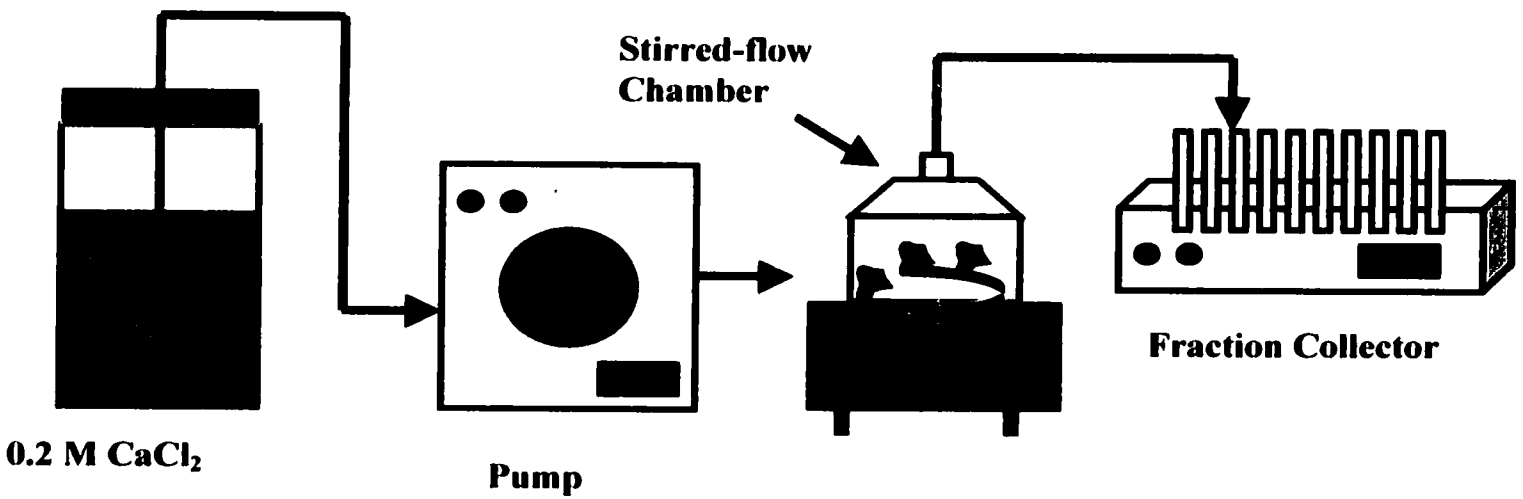

Figure 4.1 Schematic illustrating the experimental design of the stirred-flow setup.

trend and samples collected farther away from the smelting plant have relatively lower metal concentrations, suggesting introduction of metals via smelter emissions. The XRD data revealed quartz was an abundant mineral in the both surface and subsurface samples. Diffractograms from the surface sample indicate that the second most abundant mineral was franklinite ($ZnFe_2O_4$), a Zn-bearing mineral with a normal spinel-type structure that often contains manganese in addition to zinc and iron. XRD analyses revealed little on the mineralogy of Zn-bearing mineral phases in the subsurface soil, suggesting their concentrations were below the detection limit of the instrument or Zn-bearing solid phases are not present. Traces of goethite, kaolinite, and an aluminum oxide phase were detected in the fine fraction of the subsurface soil. Electron microprobe (EM) analysis revealed similar mineral phases in the surface soil. An EM back-scattered electron (BSE) image and corresponding elemental maps typical of those collected on the surface material is presented in Figure 4.2. The main spherical entity in the image is an organic cluster with moieties of metal bearing phases distributed throughout, indicated by the bright white spots in the BSE. In general, the greatest amount of Zn was in spots measuring 1-4 μm in diameter and were associated with Fe and S. No quantitative information was revealed from this analysis, but based on elemental ratios from the EDX, it can be estimated that the Zn-Fe grains are franklinite. The Zn-S associations may be sphalerite (ZnS) or Zn sulfate, with no way to differntiate between the two with this technique alone. Spots of Si and K are also present, most likely representing quartz and K-feldspars, respectively. The BSE and elemental maps

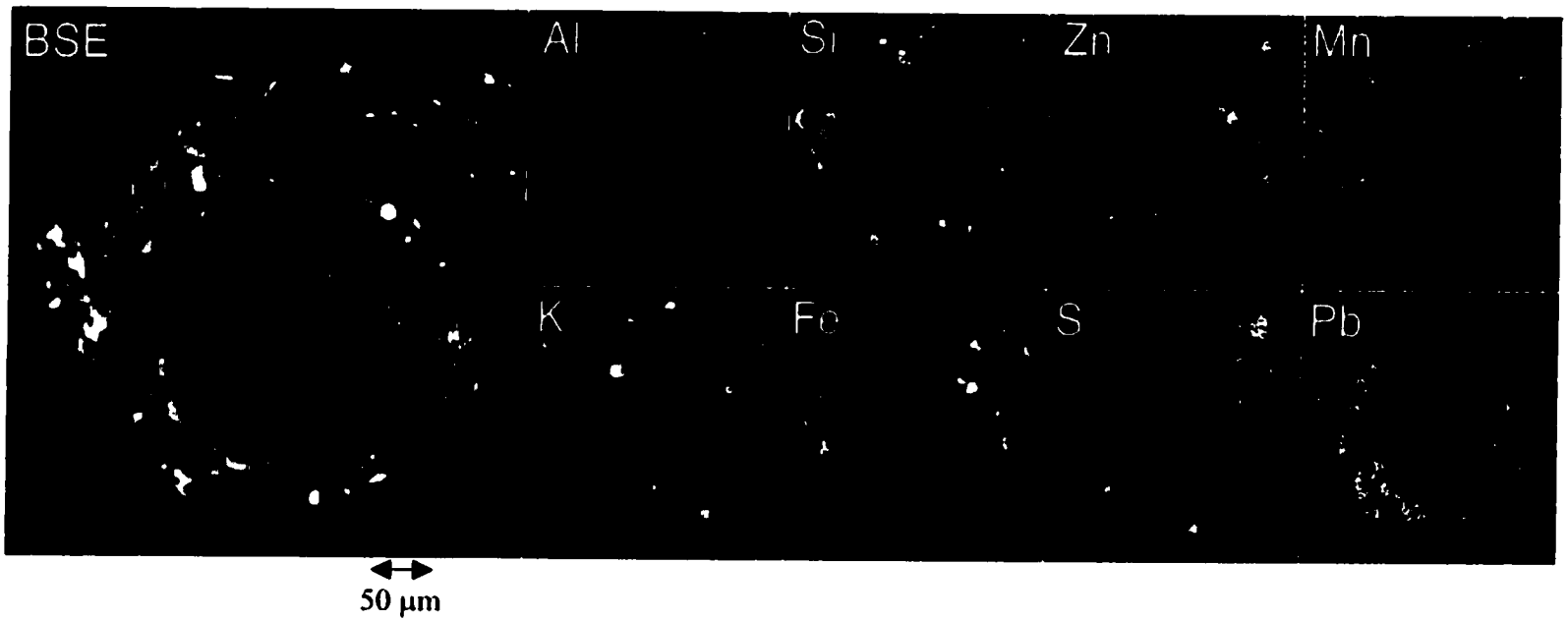

Figure 4.2 Representative backscattered electron (BSE) image and X-ray elemental dot maps for Al, Si, Zn, Mn, K, Fe, S, and Pb in the surface soil. Data collected on polished, thin sections using electron microprobe.

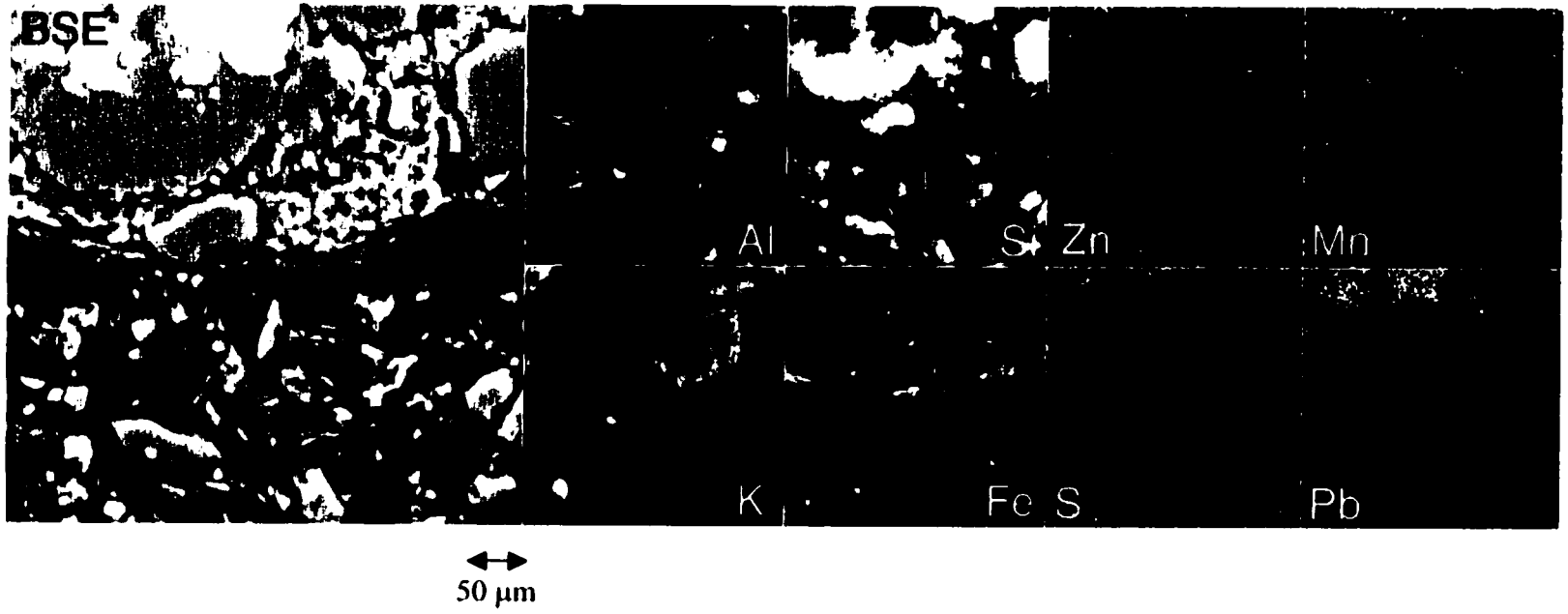

Figure 4.3 Representative backscattered electron (BSE) image and X-ray elemental dot maps for Al, Si, Zn, Mn, K, Fe, S, and Pb in the subsurface soil. Data collected on polished, thin sections using electron microprobe.

shown in Figure 4.3 were collected on the subsurface soil. EM analysis of the subsurface soil revealed that Zn was at or below the detection limit of the instrument, revealing little on its potential phase distribution. Sulfur was also below detection limits or not present at all in this sample. Appreciable amounts of Al, Si, K and Fe were detected, indicating minerals bearing these elements were present, but no further quantitative analysis was performed to determine the exact mineralogy.

4.4.2 Bulk XAFS Analysis

The raw chi(k) x k^3 XAFS data for the reference mineral and sorption samples are presented in Figure 4.4. In general, the mineral samples had more strong oscillations and structural features compared to the sorption samples. This aided in our initial identification of Zn species in our samples, as did certain features specific to each spectra. Fit results using non-linear least-squares fitting of individual coordination shells are presented in Table 4.1 for the reference samples. The bulk chi(k) x k^3 XAFS data and corresponding radial structure functions (RSFs) for the surface and subsurface samples are presented in the Figure 4.5. The fit results from linear combination fitting are represented by dashed lines in the left panel and the corresponding fit results are presented in Table 4.3. Fit results using non-linear least-squares fitting of individual coordination shells are represented by dashed lines in the right hand panel and fitting parameters are presented in Table 4.2. For the surface litter material, linear combination fitting revealed the best fit (lowest residual value) was attained using 66% franklinite and 34% sphalerite. Despite the large amount of organic material in this sample, adding the Zn-fulvic acid spectra did not reduce the fit residual. This does not

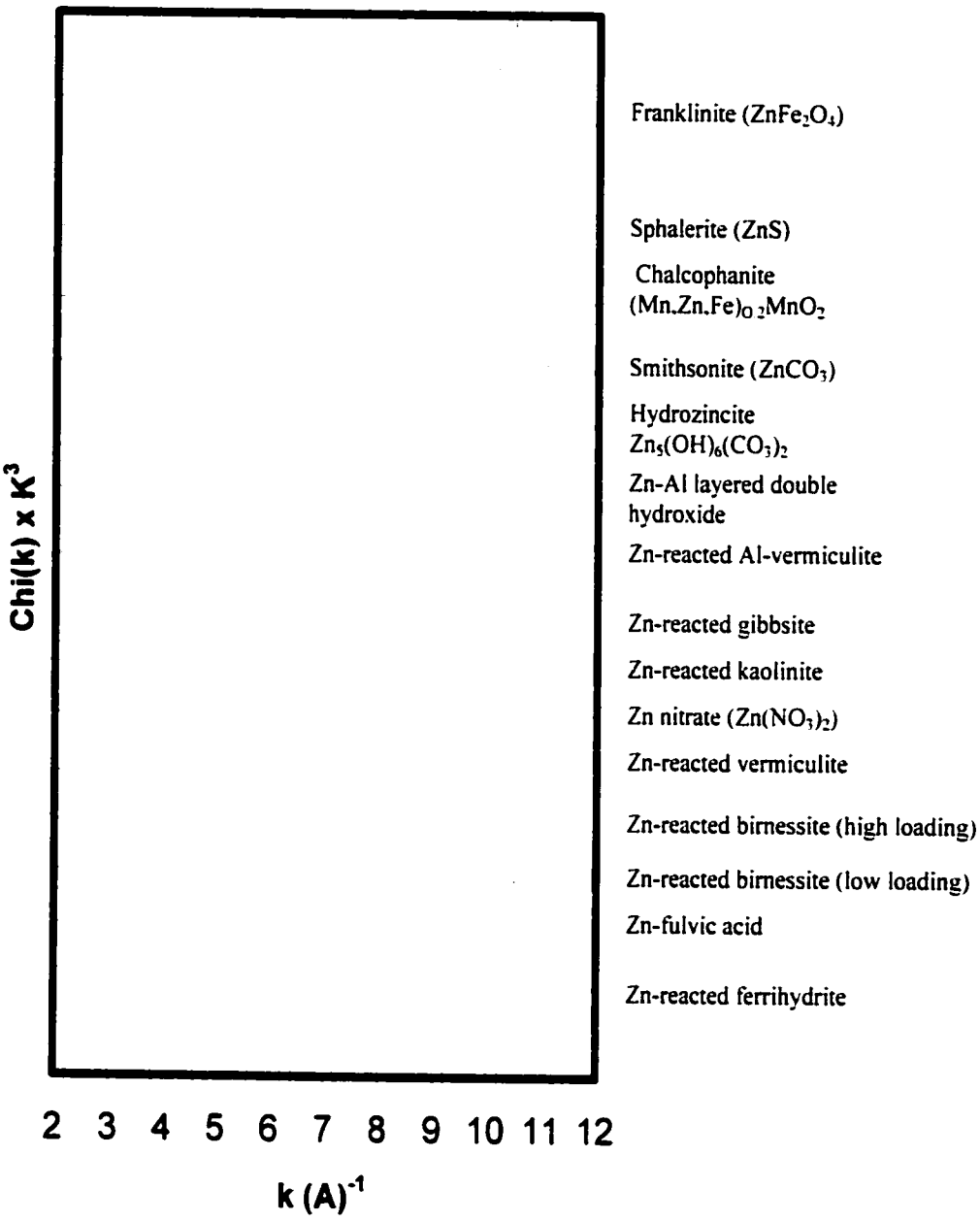

Figure 4.4 Normalized Zn-XAFS chi spectra weighted by k^3 of reference Zn-bearing minerals and sorption phases.

Table 4.1 XAFS Parameters for Reference Mineral and Sorption Samples

	First Shell			Second Shell								
	Zn-O Zn-S			Zn-Al			Zn-Fe Zn-Zn			Zn-Mn Zn-Zn		
Sample	R(Å)[a]	N[b]	σ^2(Å^2)[c]	R(Å)	N	σ^2(Å^2)	R(Å)	N	σ^2(Å^2)	R(Å)	N	σ^2(Å^2)
Franklinite ($ZnFe_2O_4$)	1.97	3.65	0.003				3.50	11	0.0085			
Sphalerite (ZnS)	2.34	4[d]	0.0037				3.87	12	0.008			
Zn Al LDH	2.07	6	0.009	3.06	2.4	0.01	3.08	4.3	0.01			
Zn-reacted birnessite (high loading)	2.07	5.6	0.007							3.5	8	0.008
Zn-reacted birnessite (low loading)	2.02	5.1	0.01									
Zn-reacted ferrihydrite	1.94	4[d]	0.005				3.34	2	0.017			
Zn-reacted fulvic acid	2.06	7	0.01									
Zn-reacted gibbsite	2.01	5	0.01	2.94	2.0	0.008						
Zn-reacted kaolinite	2.01	5.2	0.007	3.02	1.8	0.004						
Zn-reacted vermiculite	2.06	6	0.009	3.07	2.7	0.005	3.10	2.7	0.009			
Zn-reacted Al-vermiculite	1.97	6	0.009	3.05	2.5	0.005						
Zn Nitrate	2.06	6	0.007									
Zn Fulvic acid	2.06	7	0.01									

[a] Bond distance. [b] Coordination number. [c] Debye - Waller factor. [d] Parameter fixed during least square fits.

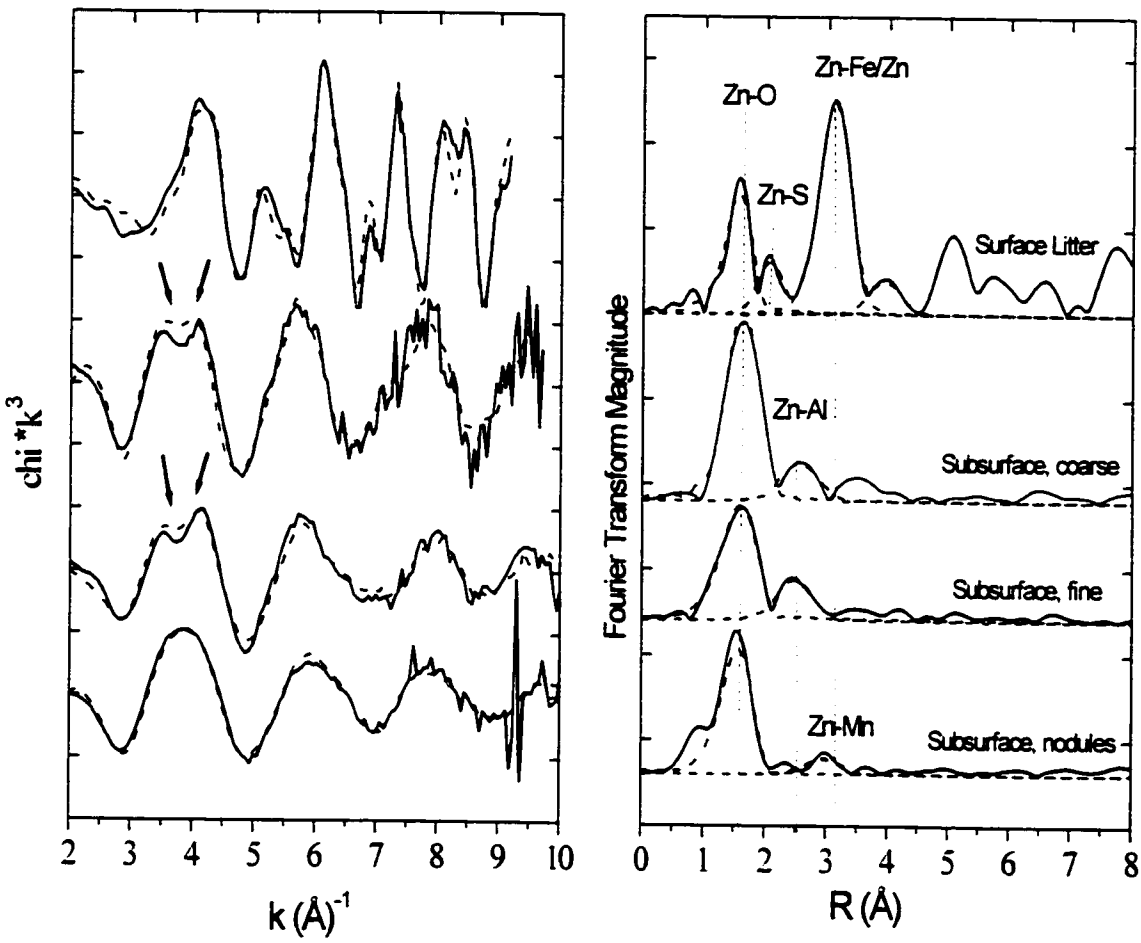

Figure 4.5 Normalized Zn-XAFS chi spectra weighted by k^3 (left panel) and corresponding Fourier transforms (right panel) of surface and subsurface samples using bulk-XAFS. In the left panel, the solid lines are the raw data and the dotted lines are fit results from linear combinations of chi data. In the right panel, solid lines represent experimental data and dashed lines represent results from non-linear, least squares fitting of individual shells.

Table 4.2 XAFS Fit Results for Soil Samples

	First Shell			Second Shell								
	Zn-O Zn-S			Zn-Al			Zn-Fe Zn-Zn			Zn-Mn		
Sample	R (Å)[a]	N[b]	σ^2(Å^2)[c]	R (Å)	N	σ^2(Å^2)	R (Å)	N	σ^2(Å^2)	R (Å)	N	σ^2(Å^2)
Bulk XAFS												
Surface (<2mm)	1.98	3.7	0.007				3.49	11.5	0.009			
	2.35	3.8	0.008				4.03	1.5	.005[d]			
Sub (<2mm)	2.08	5.7	0.004	3.04	1.2	0.003						
Sub (<50 μm)	2.03	6.2	0.01	2.99	2.01	0.005						
Sub (Nodules)	2.02	5.5	0.007							3.36	2.4	0.01
Micro XAFS												
Surface - spot 1	1.97	4.03	0.008				3.52	13	0.01			
Surface - spot 2	1.98	4.1	0.007				3.51	8	0.01			
Subsurface -spot 1	2.04	5.6	0.005[d]	3.01	1.6	.005[d]						
Subsurface -spot 2	1.99	2.9	.005[d]	3.12	1.6	.005[d]						
Subsurface -spot 3	1.98	3.4	.005[d]							3.42	1.4	.005[d]

[a] Bond distance. [b] Coordination number. [c] Debye - Waller factor. [d] Parameter fixed during least-squares fits.

ecessarily mean that Zn is not associated with organic material but, as pointed out by Manceau et al. (2000a), organic compounds generally yield a weak XAFS signal, which can be masked by the more intense signal from inorganic compounds. Fit results using non-linear least-squares fitting of individual coordination shells are presented in Table 4.2. Zn was found to be coordinated to both O and S in the first shell, both in tetrahedral coordination. The bond distances for Zn-O and Zn-S were 1.98 Å and 2.35 Å, respectively. These first shell R and N values for Zn are indicative of Zn in franklinite and sphalerite phases. The second shell had Zn-Fe(Zn) and Zn-Zn bonds at 3.49 Å and 4.03 Å, respectively. The bond at 3.49 Å matches the 3.50 Å Zn-Fe, Zn-Zn bonds found in franklinite (Table 4.1). The similar distance between Zn-Zn and Zn-Fe bonds makes it difficult to distinguish between these two bonds in a single phase. The Zn bond at 4.03 Å may be from backscattering from Zn in sphalerite, though it is a slightly larger distance than is reported in the literature (Effenberger et al., 1981). The peaks in the RSF from the range of 4.5 Å to 6 Å are most likely a result of back scattering from another set of O or S and no attempts were made to fit these contributions.

The presence of franklinite and sphalerite as determined by XRD and XAFS can be explained by history of the smelting facility. The main Zn ore used in the smelting process at Palmerton was sphalerite. During smelting, sphalerite is exothermally converted at 900°C to zinc oxide, a more soluble Zn mineral phase (Elgersma et al., 1995). Due to the presence of significant amounts of iron in the sphalerite ores, zinc ferrite ($ZnFe_2O_4$, franklinite) is formed during the roasting process, and given smelting inefficiencies, portions of this material are released as atmospheric emissions along with

non-smelted sphalerite. Given the oxidizing environment in this surface litter one would expect ZnS to oxidize and release Zn and SO_4^{2-} and therefore not be present after several decades. However, biological activity in this surface material is probably minimal and limited microbial oxidation of sphalerite may explain its persistence in this non-reducing environment even after many decades. Also, Pb and Cd present in the sphalerite may decrease its solubility. A study by Venditti et al. (2000) on soils contaminated as a result of metallurgical activities also revealed the persistence of sphalerite and franklinite in contaminated agricultural soils.

In the subsurface soil samples, the chi spectrum has far fewer structural oscillations, suggesting the Zn is not present as mineral phases as it is in the surface soil. Considering the acidic pH of the soil (3.86) and relatively low Zn concentration (900 mg/kg), we expect the conditions are well below the solubility limit of any secondary Zn precipitates in the subsurface soil. Our inability to fit a second-neighbor Zn atom in any of the subsurface samples confirmed this initial hypothesis. Therefore, adsorption to mineral surfaces and/or substitution of Zn for other ions in mineral structures are the suspected uptake mechanisms for Zn in the subsurface soil. The chi spectra for the coarse (<2 mm) and fine (< 50 μm) fractions of the soil have similar structural features, with a splitting of the first major oscillation at approximately 3.8 $Å^{-1}$ being the major distinction to the chi spectrum of the nodule sample. A similar observation was made by Manceau et al. (2000b) in a study investigating Zn coordination in metal oxides. Using XAFS they saw a characteristic split of the first oscillation maximum with a minimum at 3.8 $Å^{-1}$, which they attributed to presence of 'light' Al atoms in the coordination shell of Zn instead of 'heavy' Fe and Mn atoms. In

addition, research presented in Chapter 3 of this dissertation demonstrated a similar structural feature upon Zn sorption to gibbsite. The reason for the spectral split at 3.8 $Å^{-1}$ was attributed to Zn present in a distorted octahedron at the gibbsite surface. Reference chi samples of Zn bound to Al minerals (regardless of a specific sorption mechanism) demonstrates this first-oscillation splitting feature, which is absent when Zn is adsorbed on minerals absent of Al (Figure 4.4). We used this spectral feature as a diagnostic tool to indicate whether or not Zn is bound to Al in our samples or to Mn and/or Fe (either as an adsorption complex or bound in a mineral structure).

The first shell of the subsurface soil coarse and fine fractions has $R_{Zn\text{-}O}$ values of 2.08 and 2.06 Å with $N_{Zn\text{-}O}$ values of 5.7 and 4.9, respectively. According to crystallographic studies, the $R_{Zn\text{-}O}$ for Zn in tetrahedral coordination is approximately 1.96 Å, increasing to 2.08 Å for Zn in octahedral coordination (Trainor et al., 2000). The values for the subsurface coarse and fine fractions suggest Zn is in octahedral coordination. In contrast, the $R_{Zn\text{-}O}$ for the Zn-nodule sample is 2.03 Å with a $N_{Zn\text{-}O}$ of 4.3, suggesting tetrahedral coordination, or a mixture of octahedral and tetrahedral coordination, or a distorted Zn octahedron. Since Zn has no crystal field stabilization energy, Zn(II) will accept either tetrahedral coordination or octahedral coordination (Barak and Helmke, 1993). The second shell of the coarse and fine samples was best fit with an Al atom, with $R_{Zn\text{-}Al}$ = 3.04 Å and 3.03 Å, respectively. This confirmed the split in the first oscillation of the chi spectra was in fact due to the presence of Al bound to Zn.

The uncertainty associated with the second shell bond distance and the heterogeneous nature of soils (i.e., Al may be present in tetrahedral and octahedral

coordination) makes it difficult to assign a specific sorption complex based on these bond distances. However, the values do fall in the range of innersphere sorption of Zn to an AlO_6 octahedron (Ford and Sparks, 2000, Table 4.1) and are shorter than Zn found in Zn-Al precipitates (Ford and Sparks, 2000; Trainor et al., 2000). The nodule sample had a second shell bond at 3.36 Å, which was fit equally well by both Fe and Mn, indicating the nodule was a mixture of Fe and Mn oxides. Using linear-combinations fitting, both the coarse and fine spectra were best represented by Zn reacted with gibbsite and Zn nitrate in solution, while the nodule spectrum was best fit with Zn sorbed to birnessite (low loading), ferrihydrite and Zn nitrate in solution (Table 4.3). These results suggest that Zn is bound as two complexes: directly bound as an innersphere complex to Al and Fe/Mn oxides and as electrostatic outersphere complexes, as indicated by similarities to the $Zn(NO_3)_2$ reference spectra. Our results thus far imply that Zn^{2+} has been released from the Zn-bearing phases in the surface litter and transported to the underlying soil where it was partially readsorbed to both Al and Fe/Mn oxides. To better understand the speciation of Zn in these soil samples, we now turn to micro-focused analysis, a useful approach for speciating metals in heterogeneous materials.

4.4.3 Micro-Spectroscopic Analysis

The μ-SXRF maps collected on the surface and subsurface samples are presented in Figures 4.6 and 4.7, respectively. The relative concentrations of the elements are represented by the scale at the right of each panel. The surface soil indicates a strong correlation between Zn and Fe in concentrated spots throughout the

Figure 4.6 Micro-SXRF elemental maps for Mn, Zn, and Fe in the Palmerton surface sample. The numbered arrows indicate points where μ-XANES spectra were collected (Figure 4.8). The color bar to the right indicates relative metal concentration (arbitrary units).

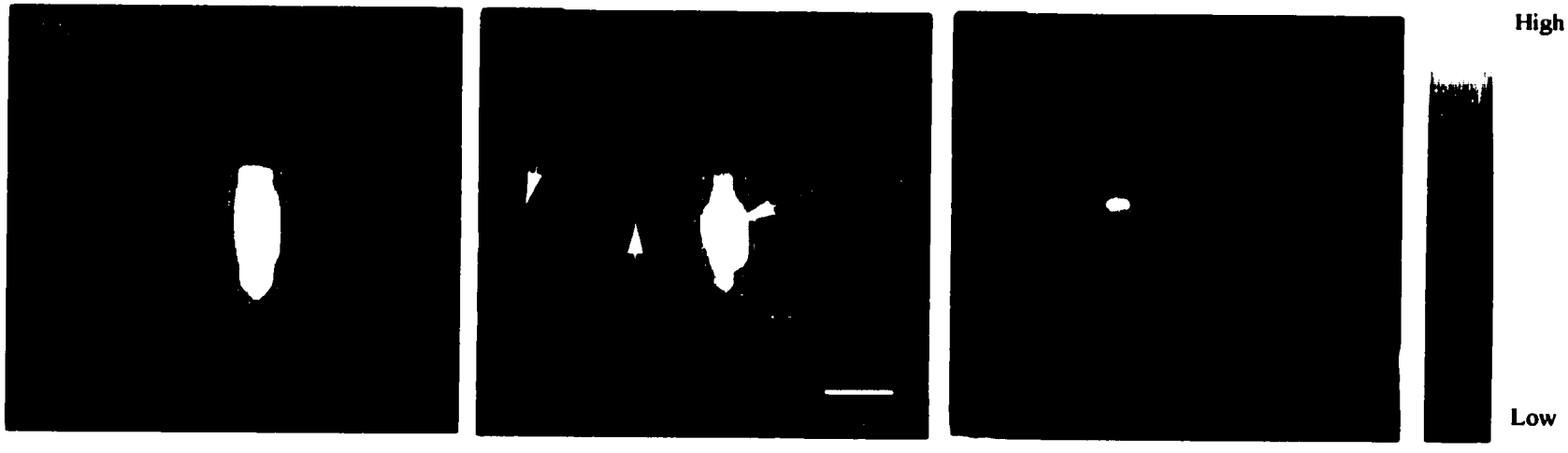

Figure 4.7 Micro-SXRF elemental maps for Mn, Zn, and Fe in the Palmerton subsurface sample. The numbered arrows indicate points where μ-XAFS spectra were collected (Figure 4.9). The color bar to the right indicates relative metal concentration (arbitrary units).

sample, similar to the EM results. The three numbered arrows in the middle map (Zn) of Figure 4.6 represent spots where Zn μ-XANES spectra were collected in the surface sample (Figure 4.8). Spot 3 was best fit using 100% franklinite; spot 2 consisted of 80% sphalerite, 5% franklinite, and 15% Zn sorbed to ferrihydrite; and spot 1 was a mix of 88% franklinite, 7% Zn-ferrihydrite and 5% Zn sorbed to birnessite (Table 4.3). Micro-XAFS were collected on the surface sample in two spots (without the reliance on a μ-SXRF map) and the spectra are located in Figure 4.5. These two spectra are best represented by Zn present in franklinite (Tables 4.2 and 4.3). Out of the five spots (3 μ-XANES, 2 μ-XAFS) taken on the surface soil, four out of five were dominated by franklinite and only one by sphalerite suggesting that franklinite is the most abundant phase in the sample, in agreement with results from bulk XAFS analysis.

In the subsurface sample, Zn is strongly correlated to Mn in the center of the sample, with Fe in other portions of the sample, and with neither Mn or Fe in some portions of the sample (Figure 4.7). This micro-scale heterogeneity in elemental associations suggests Zn may be present in different phases over a small sample area, a finding that one would be unable achieve relying on most analytical techniques considering the low concentration of Zn in the sample. The strong correlation between Zn and Mn in the sample does not necessarily indicate that Zn is bound to a Mn-oxide phase as Zn^{2+} and Mn^{2+} may simply be complexed in the sample at the same spot. Under such acidic conditions one would not expect Mn oxides to be present in any abundance, as confirmed by EM of this sample.

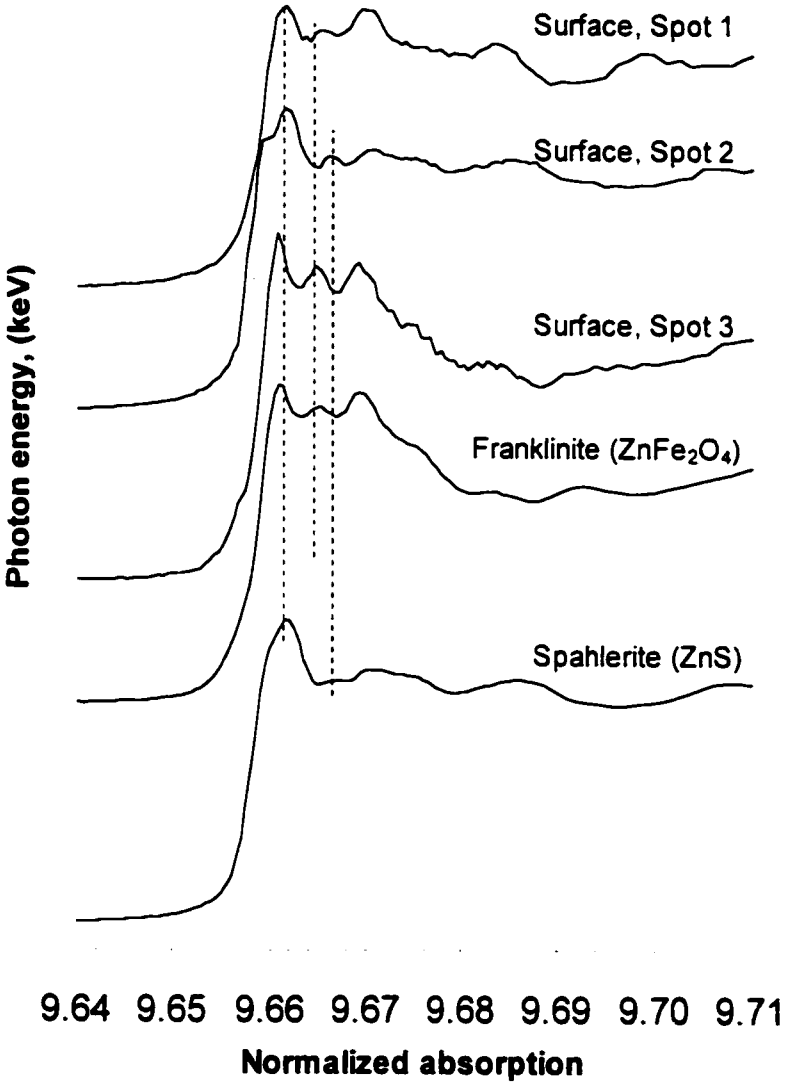

Figure 4.8 Micro-XANES spectra for three Zn spots in the surface soil (Figure 4.6) compared to reference sphalerite and franklinite minerals.

Table 4.3 Linear combinations of fit results.

	$ZnFe_2O_4$	ZnS	Zn-Ferrihydrite	Zn-Birnessite	Zn-Gibbsite	Zn-Nitrate
Bulk XAFS			(%)			
Surface	66	34	0	0	0	0
Subsurface (<2mm)	0	0	13	10	40	37
Subsurface (<50μm)	0	0	15	0	63	22
Subsurface Nodules	0	0	40	20	0	40
Micro-XAFS						
Surface, spot 1	100	0	0	0	0	0
Surface, spot 2	85	0	15	0	0	0
Suburface, spot 1	0	0	15	0	50	35
Subsurface, spot 2	0	0	40	0	15	45
Subsurface, spot 3	0	0	45	0	15	40
Micro-XANES						
Surface, spot 1	88	0	7	5	0	0
Surface, spot 2	5	80	15	0	0	0
Surface, spot 3	100	0	0	0	0	0

Micro-focused XAFS were collected on three regions in this sample (labeled 1,2 and 3 on Zn map) and are presented in Figure 4.5. Much like the bulk XAFS spectra collected on the subsurface soil samples, the μ-XAFS show chi data with less oscillations relative to the samples from the surface litter material. The μ-XAFS revealed Zn was present both in octahedral and tetrahedral coordination, depending on the location within the sample. The spectra from the first spot (spot 1), has a split in the first oscillation at 3.8 $Å^{-1}$, much like the spectra from the bulk analysis. Incidentally, this spot is where neither Fe nor Mn is present from elemental mapping, suggesting Al may be the associated element. Unfortunately, μ-SXRF could not collect data for Al in this sample to verify this hypothesis. The fit results from multi-shell fitting (Table 4.2) indicate that Zn is octahedrally coordinated (R_{Zn-O} = 2.04) and bound to an Al-bearing phase in this spot (R_{Zn-Al} = 3.01 Å), similar to the results from bulk XAFS on the fine and coarse fractions. For spots 2 and 3, Zn is intetrahedral coordination (R_{Zn-O} = 1.99), with broad second shell peaks that were difficult to assign to an individual atomic contribution. Spot two had a R_{Zn-Al} = 3.12 Å while spot three had a $R_{Zn-Fe/Mn}$ = 3.42 Å. Linear combination fit results indicate subsurface spot 1 was best fit with Zn-reacted gibbsite with contributions from $Zn(NO_3)_2$ and Zn-ferrihydrite (Table 4.3). Spots 2 and 3 were best fit with major contributions from Zn-ferrihydrite and minor contributions from $Zn(NO_3)_2$ and Zn gibbsite. These results aid in confirming the results from bulk XAFS and indicate mixed Zn speciation, even on a micron size scale. Given that Zn is in octahedral coordination in $Zn(NO_3)_2$, it follows that spot 1 was dominated by Zn in octahedral coordination and had more significant contributions from $Zn(NO_3)_2$ compared to spectra for spots 2 and 3.

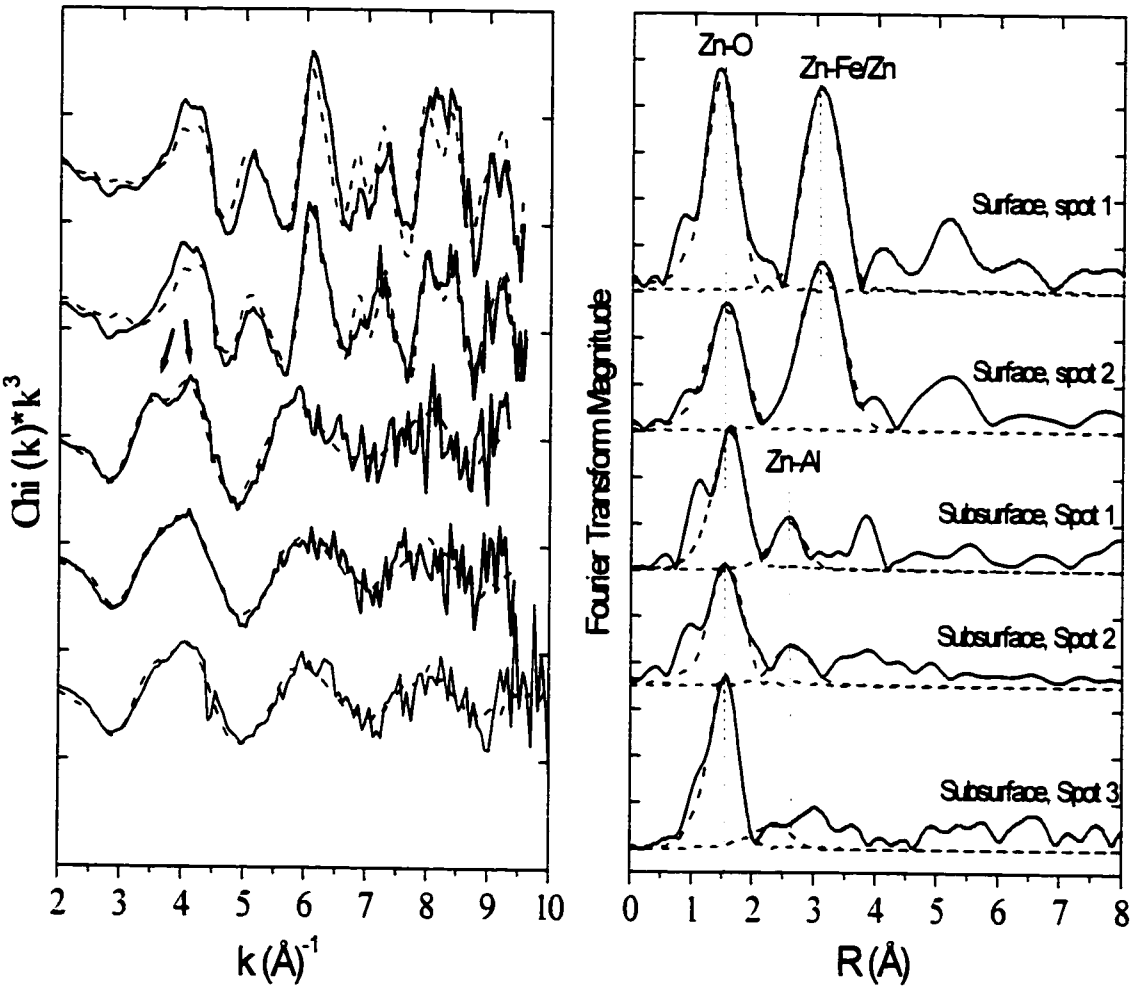

Figure 4.9 Normalized Zn-XAFS chi spectra weighted by k^3 (left panel) and corresponding Fourier transforms (right panel) of surface and subsurface samples using micro-focused XAFS. In the left panel, the solid lines are the raw data and the dotted lines are fit results from linear combinations of chi data. In the right panel, solid lines represent experimental data and dashed lines represent results from non-linear, least squares fitting of individual shells.

These results vary slightly from recent investigations by Manceau et al. (2000a) on Zn-contaminated smelter soils in which XAFS revealed Zn was predominately found in neo-formed Zn-containing phyllosilicates, and to a lesser extent bound to Mn and Fe oxides. Given the less acidic soils in their study (pH > 5.5) and higher Zn concentrations in subsurface soils compared to our soils, it is reasonable that our results are different as these soils are undersaturated with respect to any neo-formed phyllosilicates. However, more experiments need to be performed on the Palmerton soils to completely rule out Zn neo-precipitate formation.

4.4.4 Zinc Desorption Behavior

Figure 4.10 displays the results from the stirred-flow desorption of Zn from the surface and subsurface samples. The top panel displays the desorption data as cumulative total Zn removed from the samples and the bottom panel presents it as the percent Zn desorbed from the sample relative to the total amount present. A clear difference in the amount of Zn removed from each of the samples is observed with nearly 65% of total Zn removed from the subsurface soil and approximately 11% of the Zn removed from the surface litter material after 70 chamber volumes of desorbing solution passed through the samples (approximately 24 h). Moreover, the subsurface sample has a more rapid release of Zn with over 60% of the total Zn removed from the soil after only 5 chamber volumes compared to a more gradual release from the surface material.

Given the presence of Zn in relatively insoluble metal phases (franklinite and sphalerite) in the surface sample, one would not expect much Zn desorption. Zn is most

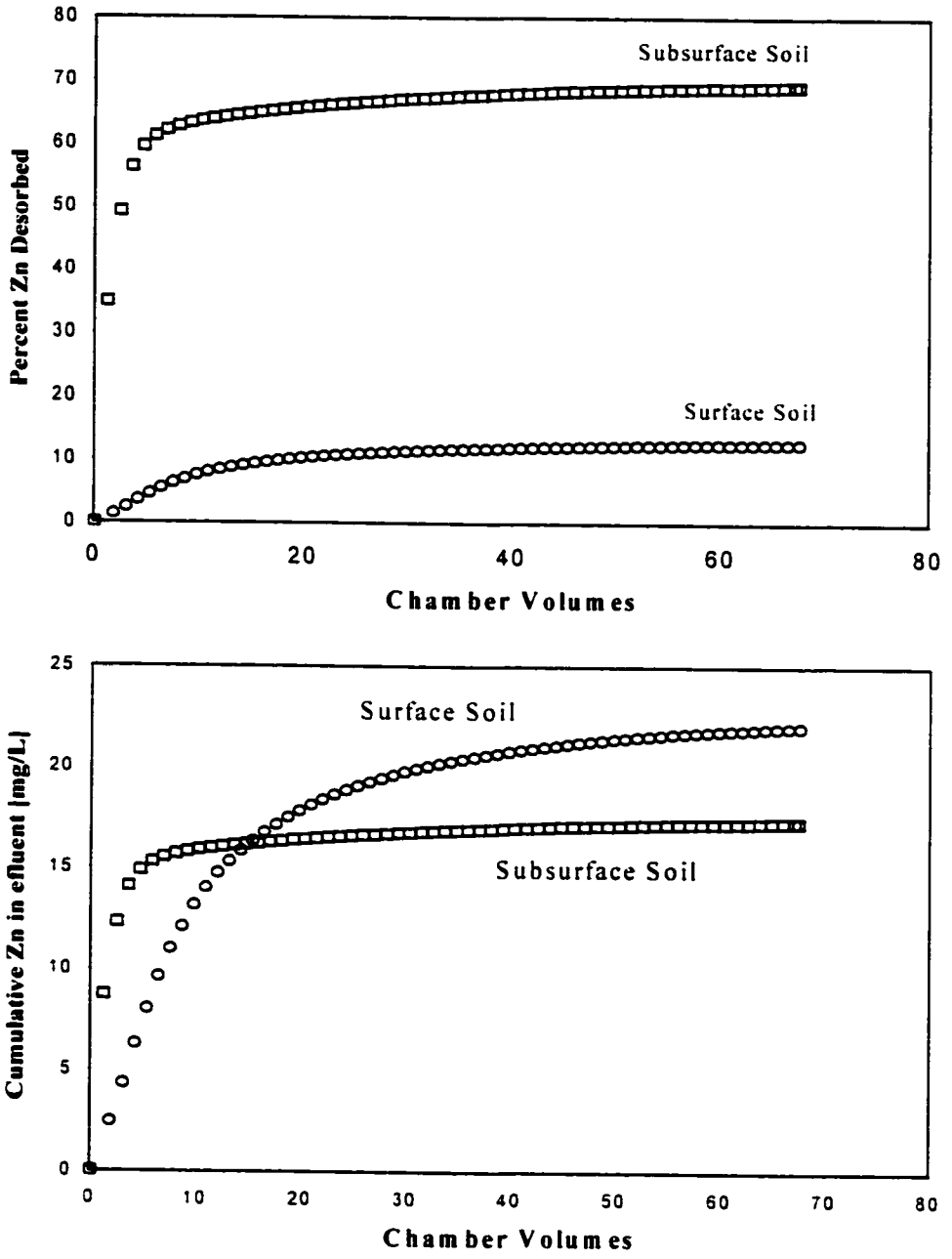

Figure 4.10 Zn desorption from surface and subsurface soil samples. The top panel is displayed as cumulative effluent and the bottom panel as percent Zn desorbed.

likely removed from weaker complexes, such as Zn sorbed to Fe oxide or complexed to organic matter, in the initial stage of Zn release into solution. The plateau reached when 10% total Zn was released indicated the remainder of the Zn was in a more stable form. If any Zn is coming from a solid phase, one would predict Zn is released from sphalerite rather than franklinite since sphalerite is unstable in oxidizing environments and franklinite is quite insoluble (Lindsay, 1979). In addition, some labile Zn may be associated with the organic matter in this sample that was not well detected with from using the XAFS approach.

In the subsurface soil, the Zn is rapidly released initially followed by a slower desorption step. In this case, labile Zn that is adsorbed as a weak adsorption complex (i.e., outer-sphere) is initially removed followed by a slower removal due to the release of Zn bound to Al minerals/oxides and Fe/Mn oxides as inner-sphere complexes. The greater amount of Zn removal from the subsurface soil relative to the surface sample agreed with the spectroscopic results which indicated Zn was not present as a solid phase. However, there is still nearly 30% of Zn remaining in the subsurface soil after the desorption experiments, indicating Zn is in a fairly stable complex.

4.4.5 Environmental Significance

The results of this study show the importance of combining several analytical techniques to accurately determine Zn speciation in soils as no one technique is capable of completely characterizing a system. XAFS spectroscopy was by far the most useful technique to directly identify Zn species. Zinc speciation varies greatly between the surface and subsurface soils, and between small areas within the subsurface sample

itself, an observation made possible using micro-focused synchrotron techniques. The acidic conditions of this site do not favor the immobilization of Zn into a stable phase, as suggested by the presence of outer-sphere complexes from XAFS analysis and significant Zn removal from the subsurface soil. However, a significant portion of Zn does exist in stable complexes as evidenced by inner-sphere complex formation and the fact that 35% of Zn remains bound to the subsurface soil. Increasing the pH of the site may help immobilize Zn. To our knowledge this is the first study that has directly identified Zn species in surface and subsurface soils in the Palmerton area and the results should prove valuable in developing an effective remediation strategy.

4.5 References

Barak, P. and P.A. Helmke. 1993. The chemistry of zinc. pp. 1-13. *In* A.D. Robson (ed.) Zinc in Plants and Soils. Kluwer Academic, Dordrecht, The Netherlands.

Bargar, J.R., G.E. Brown Jr. and G.A. Parks. 1997. Surface complexation of Pb(II) at oxide-water interfaces: II. XAFS and bond-valence determination on mononuclear and polynuclear Pb(II) sorption products and surface functional groups on iron oxides. *Geochim. Cosmochim. Acta* **61:** 2639-2652.

Bertsch, P.M. and D.B. Hunter. 1998. Elucidating fundamental mechanisms in soil and environmental chemistry: The role of advanced analytical spectroscopic, and microscopic methods. pp. 103-122. *In* P.M. Huang, D.L. Sparks and S.A. Boyd (eds.) Future of Soil Chemistry. Soil Sci. Soc. Am., Madison, WI.

Bochatay, L. and P. Persson. 2000. Metal ion coordination at the water-manganite (γ-MnOOH) interface II. An EXAFS study of zinc(II). *J. Colloid Interface Sci* **229:** 593-599.

Bruemmer, G.W., J. Gerth and K.G. Tiller. 1988. Reaction kinetics of the adsorption and desorption of nickel, zinc and cadmium by goethite: I. Adsorption and diffusion of metals. *J. Soil Sci.* **39:** 37-52.

Buchauer, M.J. 1973. Contamination of soil and vegetation near a zinc smelter by zinc, cadmium, copper, and lead. *Environ. Sci. Technol.* **7:** 131-135.

Chaney, R.L. 1993. Zinc phytoxicity. pp. 135-144. *In* A.D. Robson (ed.) Zinc in Soils and Plants. Kluwer Academic Publishers. The Netherlands.

Charlet, L. and A. Manceau. 1992. X-ray absorption spectroscopic study of the sorption of Cr(III) at the oxide-water interface. II. Adsorption, coprecipitation, and surface precipitation on hydrous ferric oxide. *J. Colloid Interface Sci.* **148:** 443-458.

de Groot, A.J. 1995. Metals and sediments: a global perspective. pp. 1-80. *In* H.E. Allen (ed.) Metal Contaminated Aquatic Sediments. Ann Arbor, Chelsea.

Dudka, S. and D.C. Adriano. 1997. Environmental impacts of metal ore mining and processing: a review. *J. Environ. Qual.* **26:** 590-602.

Duff, M.C. et al. 1999. Mineral associations and average oxidation states of sorbed Pu on tuff. *Environ. Sci. Technol.* **33:** 2169-2163.

Effenberger, H., K. Mereiter and J. Zemann. 1981. Crystal structure refinements of magnesite, calcite, rhodochrosite, siderite, and dolomite, with discussion of some aspects of the stereochemistry of calcite type carbonates. *Z. Kristallogr.* **156:** 233-243.

Elgersma, F., J.N. Schinkel and M.P.C. Weijnen. 1995. Improving environmental performance of a primary lead and zinc smelter. pp. 193-235. *In* W. Salomons, U. Förstner and P. Mader (eds.) Heavy Metals: Problems and Solutions. Springer-Verlag, Berlin.

Elzinga, E.J. and D.L. Sparks. 1999. Nickel sorption mechanisms in a pyrophyllite-montmorillonite mixture. *J. Colloid Interface Sci.* **213:** 506-512.

Fendorf, S.E., G.M. Lamble, M.G. Stapleton, M.J. Kelley and D.L. Sparks. 1994. Mechanisms of chromium (III) sorption on silica: 1. Cr(III) surface structure derived by extended x-ray absorption fine structure spectroscopy. *Environ. Sci. Technol.* **28:** 284-289.

Ford, R.G. and D.L. Sparks. 2000. The nature of Zn precipitates formed in the presence of pyrophyllite. *Environ. Sci. Technol.* **34:** 2479-2483.

Gerth, J., G.W. Brümmer and K.G. Tiller. 1992. Retention of Ni, Zn, and Cd by Si-associated goethite. *Z. Pflanzenernähr. Bodenk.* **156:** 123-129.

Hesterberg, D., D.E. Sayers, W. Zhou, G.M. Plummer and W. Robarge. 1997. X-ray absorption spectroscopy of lead and zinc speciation in a contaminated groundwater aquifer. *Environ. Sci. Technol.* **31**.

Huang, C.P. and A. Rhoads. 1989. Adsorption of Zn(II) onto hydrous aluminosilicates. *J. Colloid Interface Sci.* **131:** 289-306.

Hunter, D.B. and P.M. Bertsch. 1998. In situ examination of uranium contaminated soil particles by micro-X-ray absorption and micro-fluorescence spectroscopies. *J. Radioanal. Nucl. Chem.* **234:** 237-242.

Ketterer, M.E., J.H. Lowry, J. Simon Jr., K. Humpries, and M.P. Novotnak. 2001. Lead isotopic and chalcophile element compositions in the environment near a zinc-smelting-secondary zinc recovery facility, Palmerton, Pennsylvania. *Appl. Geochem.* **16:** 207-229.

Kinniburgh, D.G., M.L. Jackson and J.K. Syers. 1976. Adsorption of alkaline earth, transition, and heavy metal cations by hydrous oxide gels of iron and aluminum. *Soil Sci. Soc. Am. J.* **40:** 796-799.

Ladonin, D.V. 1997. Specific adsorption of copper and zinc by some soil minerals. *Eurasian Soil Sci.* **30:** 1478-1485.

Lalo, J. 1988. Pennsylvania's dead mountain. *Am. Forests* **March/April:** 55-69.

Lin, Z. and R.B. Herbert Jr. 1997. Heavy metal retention in secondary precipitates frm a mine rock dump and underlying soil, Dalarna, Sweden. *Environ. Geol.* **33:** 1-12.

Lindsay, W.L. 1979. Chemical Equilibria in Soils. John Wiley and Sons, New York.

Lytle, F.W. et al. 1984. *Nucl. Instrum. Methods Phys. Res.* 542-548.

MacDowell, A.A. et al. 1998. Progress towards sub-micron hard x-ray imaging using elliptically bent mirrors. pp. 137-144. *In* I. McNulty (ed.) X-ray microfocusing: Applications and Techniques.

Manceau, A. et al. 1996. Direct determination of lead speciation in contaminated soils by EXAFS spectroscopy. *Environ. Sci. Technol.* **30:** 1540-1552.

Manceau, A. et al. 2000a. Quantitative Zn speciation in smelter-contaminated soils by EXAFS spectroscopy. *Am. J. Sci.* **300:** 289-343.

Manceau, A. et al. 2000b. Crystal chemistry of trace elements in natural and synthetic goethite. *Geochim. Cosmochim. Acta* **64:** 3643-3661.

McBride, M.B. 1994. Environmental Chemistry of Soils. Oxford University Press, New York.

McKenzie, R.M. 1971. The synthesis of birnessite, cryptomelane, and some other oxides and hydroxides of manganese. *Miner. Mag.* **38:** 493-502.

Melis, P., B. Manunsa, A. Premoli and C. Gessa. 1987. Sulfate-zinc interaction on aluminum hydroxide surfaces. *Z. Pflanzenernahr. Bodenk.* **150:** 99-102.

Metwally, A.I., A.S. Mashhady, A.M. Falatah and M. Reda. 1993. Effect of pH on zinc adsorption and solubility in suspensions of different clays and soils. *Z. Pflanzenernähr. Bodenk.* **156:** 131-135.

Morin, G. et al. 1999. XAFS determination of the chemical form of lead in smelter-contaminated soils and mine tailings: importance of adsorption processes. *Am. Mineral.* **84:** 420-434.

Morris, D.E. et al. 1996. Speciation of uranium in Fernald soils by molecular spectroscopic methods: characterization of untreated soils. *Environ. Sci. Technol.* **30:** 2322-2331.

Murray, J.W. 1975. The interaction of metal ions at the manganese dioxide-solution interface. *Geochim. Cosmochim. Acta* **39:** 505-519.

O'Day, P.A., S.A. Carroll and G.A. Waychunas. 1998. Rock-water interactions controlling zinc, cadmium, and lead concentration in surface waters and sediments, U.S. tri-state mining district. 1. Molecular identification using x-ray absorption spectroscopy. *Environ. Sci. Technol.* **32:** 943-955.

Ostergren, J.D., G.E. Brown Jr., G.A. Parks and T.N. Tingle. 1999. Quantitative speciation of lead in selected mine tailings from Leadville, CO. *Envrion. Sci. Technol.* **33:** 1627-1636.

Ressler, T. 1997. WinXAS: A new software package not only for the analysis of energy-dispersive XAS data. *J. Phys. IV* 7:269-270.

Rose, S. and A. Ghazi. 1998. Experimental study of the stability of metals associated with iron oxyhydroxides precipitated in acid mine drainage. *Environ. Geol.* **36:** 364-370.

Sadiq, M. 1991. Solubility and speciation of zinc in calcareous soils. *Water, Air, Soil Pollut.* **57-58:** 411-421.

Scheckel, K.G. and D.L. Sparks. 2000. Kinetics of the formation and dissolution of Ni precipitates in a gibbsite/amorphous silica mixture. *J. Colloid Interface Sci.* **229:** 222-229.

Scheidegger, A.M., G.M. Lamble and D.L. Sparks. 1997. Spectroscopic evidence for the formation of mixed-cation hydroxide phases upon metal sorption on clays and aluminum oxides. *J. Colloid Interface Sci.* **186:** 118-128.

Scheidegger, A.M., D.G. Strawn, G.M. Lamble and D.L. Sparks. 1998. The kinetics of mixed Ni-Al hydroxide formation on clays and aluminum oxides: a time-resolved XAFS study. *Geochim. Cosmochim. Acta* **62:** 2233-2245.

Schlegel, M., L. Charlet and A. Manceau. 1999. Sorption of metal ions on clay minerals II. Mechanism of Co sorption on hectorite at high and low ionic strength and impact on the sorbent stability. *J. Colloid Interface Sci.* **220:** 392-405.

Schlegel, M.L., A. Manceau and L. Charlet. 1997. EXAFS study of Zn and ZnEDTA sorption at the goethite (α-FeOOH)/water interface. *J. Phys. IV* **7:** 823-824.

Schwertmann, U. and R.M. Cornell. 1991. Iron Oxides in the Laboratory : Preparation and Characterization. Weinheim. New York City.

Spark, K.M., J.D. Wells and B.B. Johnson. 1995. Characterizing trace metal adsorption on kaolinite. *Eur. J. Soil Sci.* **46:** 633-640.

Stahl, R.S. and B.R. James. 1991. Zinc sorption by manganese-oxide-coated sand as a function of pH. *Soil Sci. Soc. Am. J.* **55:** 1291-1294.

Storm, G.L., R.H. Yahner and E.D. Bellis. 1993. Vertebrate abundance and wildlife habitat suitability near the Palmerton zinc smelters, Pennsylvania. *Arch. Envrion. Contam. Toxicol.* **25:** 428-437.

Strawn, D.G., A.M. Scheidegger and D.L. Sparks. 1998. Kinetics and mechanisms of Pb(II) sorption and desorption at the aluminum oxide-water interface. *Environ. Sci. Technol.* **32:** 2596-2601.

Strawn, D.G. and D.L. Sparks. 1998. Effects of soil organic matter on the kinetics and mechanisms of Pb(II) sorption and desorption in soil. *Soil Sci. Soc. Am. J.* **64:** 144-156.

Towle, S.N., J.R. Bargar, G.E. Brown Jr. and G.E. Parks. 1997. Surface precipitation of Co(II)(aq) on Al_2O_3. *J. Colloid Interface Sci.* **187:** 62-82.

Trainor, T.P., G.E. Brown Jr. and G.A. Parks. 2000. Adsorption and precipitation of aqueous Zn(II) on alumina powders. *J. Colloid Interface Sci.* **231:** 359-372.

Venditti, D., J. Berthelin and S. Durécu. 2000. A multidisciplinary approach to assess history, environmental risks, and remediation feasibility of soils contaminated by

metallurgical activities. Part B: direct metal speciation in the solid phase. *Arch. Environ. Contam. Toxicol.* **38:** 421-427.

Webb, S.M., G.G. Leppard and J.-F. Gaillard. 2000. Zinc speciation in a contaminated aquatic environment: characterization of environmental particles by analytical electron microscopy. *Environ. Sci. Technol.* **34:** 1926-1933.

Zabinsky, S.L., J.J. Rehr, A. Ankudinov, R.C. Albers and M.J. Eller. 1995. Multiple-scattering calculations of x-ray absorption spectra. *Phys. Rev. B: Condens. Matter* **52:** 2995-3006.

Zasoski, R.J. and R.G. Burau. 1988. Sorption and sorptive interaction of cadmium and zinc on hydrous manganese oxide. *Soil Sci. Soc. Am. J.* **52:** 81-87.

Chapter 5

SUMMARY AND FUTURE RESEARCH NEEDS

The ever-increasing strain on our environmental resources as a result of anthropogenic processes will provide an infinite amount of research opportunities. Coupled with the rapid advancements in computational chemistry and analytical techniques, the face of environmental geochemical and soil chemical research is undergoing tremendous transformations. The research presented in this dissertation was intended as a step in the direction of applying advanced analytical approaches to better understand metal reactions in soils and on soil constituents. To that end, a range of systems was studied, from the more 'neat' to those that are a bit more 'dirty', indicative of systems found in surface and subsurface environments.

The research findings in this dissertation demonstrated the extreme variability in metal sorption to solid surfaces. The identity of the sorbent phase, pH, reaction time, initial metal concentration, and concentration of solid all had effects on Ni and Zn sorption mechanisms. By employing cutting-edge techniques such as XAFS to study the metal sorption in combination with traditional macroscopic sorption and desorption studies, sorption mechanisms never before identifiable can be directly gleaned. Only by employing XAFS spectroscopy and electron microscopies have researchers been able to conclude that metal precipitate formation is a much more likely mechanism of sorption

over a wide range of reaction conditions than previously thought. To take this one step further this study identified these phases in actual soils under reaction conditions typical in many natural settings.

In addition to precipitate formation occurring when only adsorption is thought likely, the opposite holds true as well. Modeling programs designed to predict the speciation of a metal ion in solution do not always take into account the influence of the sorbent phase in preventing precipitate formation. The study in Chapter 3 indicated this was the case for Zn. It was predicted that ZnO would form over all reaction conditions studied, however, monitoring Zn sorption mechanisms using XAFS indicated no precipitate formation. In contrast, Zn preferred inner-sphere complexation to silica and gibbsite surfaces even as the solution was saturated with respect to ZnO. This example and the case of precipitate formation below the solubility of any likely precipitate phase indicates the complexity that arises in attempting to predict surface complexation in soil and aquatic environments.

There remains a need to use the findings using direct molecular probes to investigate metal sorption phenomena, such as XAFS or TEM investigations, and implement them into current surface complexation and transport models. Specifically, more attention should be put on considering surface precipitate phenomena when designing such models. The results of this study and other similar studies investigating metal sorption behavior on clay minerals and oxides unequivocally indicates that precipitate phenomena is a viable sorption mechanism in soil environments. However, continued research on the exact mechanisms of precipitate formation and the stability of these phases over a range of reaction conditions needs to be determined. The ultimate

goal, which may be realized with the advent of more powerful spectroscopic and microscopic tools, is to identify the multitude of metal complexes in soils and then be able to predict the risk involved to plants and animals with regards to the contaminated site.

The work presented in this dissertation on Zn speciation in smelter-contaminated soils is aimed at determining such risks. By directly identifying Zn species in soils, one is more able to predict the potential for transport, and the eventual risk to humans. Moreover, the identity of the metal species in the soil is directly correlated to the uptake of the metal by plants. My identifying metal species directly, it may be possible to avoid phytoxicity by using plants which are known to be tolerant of the identified metal species. Aside from mammalian and vegetative life there is an entire realm of microorganisms in soil and aquatic environments. In addition to being at risk of contamination in metal-rich soils, the microorganisms may offer a means of remediation by altering the forms of the contaminants. Conversely, a microbe may make contaminants more bioavailable, for instance by reductive dissolution of solid phases, and make a bad situation worse. There remains a nearly untapped area of research incorporating the inorganic component of soils with the living, organic community that is ubiquitous in nearly every soil environment.